UNIVERSIDAD POLITÉCNICA DE MADRID

ESCUELA TÉCNICA SUPERIOR DE INGENIEROS DE CAMINOS, CANALES Y PUERTOS

EFFECTS OF MOVING LOADS ON RAILWAY BRIDGES CONSIDERING THE STRUCTURE OF RAILWAY TRACK

TRABAJO FIN DE MÁSTER

Autor: Ing. Elena Pilar Martínez González
Tutor: Dr. Ing. Caminos Carlos Zanuy Sánchez
Dr. Ing. Caminos Gonzalo Sanz-Diez de Ulzurrun Casals

A mis ángeles

Table of contents

ABSTRACT

A significant increase of the high-speed railway network has been built in Spain and other European countries for the last decades. Due to the complex Spanish orography, several tunnels and bridges are necessary to accommodate the railway layout to the specific site conditions. Already from the first installation of high-speed viaducts, concerns regarding dynamic effects caused by train loads and eventual resonance called the attention of engineers and scientists. As a result, dynamic analyses are typically required at the design stage of railway bridges in order to verify the structural safety, serviceability and passenger comfort. Despite the experience gained for the last years, new challenges have arisen due to the introduction of technological innovations in railway construction. Among them, track types different from the traditional ballasted track are being introduced, including ballastless track systems or slab track.

Ballastless track has been identified as a promising alternative against ballasted track due to the reduced maintenance costs and excellent quality control. Ballastless track has been recently installed in several railway bridges of the new high-speed lines in northern Spain (e.g. new access to Galicia). Due to its practical interest, the main goal of the present TFM is to analyze whether the track structure (i.e. ballasted or ballastless) can play a role in the dynamic performance of railway bridges and the passenger comfort.

As the term ballastless track can include several track types which can affect differently to the whole structural response, the present TFM has covered the analysis of so-called monolithic and independent ballastless track systems, depending on the interaction degree of the track with the bridge girder. The former can be a design consisting of an in-site continuous reinforced concrete slab in which twin-block sleepers are embedded. The later can be implemented as floating precast concrete slabs separated from the bridge girder with an intermediate elastomeric layer or mat. In addition, a reference ballasted track has been also considered in the study.

In the present TFM, the purpose has been to study the influence of the above-mentioned track types on the dynamic behavior of railway bridges under moving loads. The methodology has consisted of numerical simulations including the different elastic components between the track and the bridge. The loads have consisted of a set of moving loads due to the passage of high-speed commercial trains at different velocities. Two types of bridges have been studied, according to the common bridge typologies of the Spanish network, namely a short single-span bridge and a long statically indeterminate bridge.

Comparisons have been carried out in terms of displacements, accelerations and dynamic amplifications at the bridge and the rail. The results have indicated that the short bridge is rather sensitive to dynamic effects caused by moving train loads, especially for speeds over 300 km/h. Moreover, it has been obtained that ballastless track systems can help in reducing accelerations and dynamic amplifications at the bridge with respect to ballasted tracks. In turn, the long multi-span bridge has shown to suffer much less dynamic effects than the short bridge.

RESUMEN

En las últimas décadas se ha experimentado en España y otros países europeos un importante incremento de la red de alta velocidad ferroviaria. Debido a la compleja orografía española, son necesarios múltiples túneles y puentes para adaptar el trazado ferroviario a las condiciones específicas del lugar. Ya desde la primera instalación de viaductos de alta velocidad, la preocupación por los efectos dinámicos de las cargas en movimiento y los eventuales problemas de resonancia fueron el centro de atención de ingenieros y científicos. Por ello, en la fase de diseño de los puentes ferroviarios se suelen exigir análisis dinámicos para verificar la seguridad estructural, el comportamiento en servicio y el confort de los pasajeros. A pesar de la experiencia adquirida en los últimos años, recientemente han surgido nuevos retos debido a la introducción de soluciones innovadoras en la construcción ferroviaria. Entre ellas, se están implantando tipos de infraestructura de vía diferentes de la clásica vía en balasto, incluyendo los sistemas de vía sin balasto o vía en placa.

La vía en placa se ha identificado como una alternativa prometedora frente a la vía en balasto debido a la reducción de los costes de mantenimiento y su excelente control de calidad. Además, la vía en placa se ha instalado recientemente en varios puentes ferroviarios de las nuevas líneas de alta velocidad del norte de España (por ejemplo, el nuevo acceso a Galicia). Debido su interés práctico, el principal objetivo de este TFM ha sido el análisis de la influencia de la estructura de la vía (con o sin balasto) en la respuesta dinámica de puentes ferroviarios y el confort de los pasajeros.

Dado que el término vía en placa puede incluir varios tipos de vía que pueden afectar de forma diferente a la respuesta estructural, el presente TFM ha abordado el estudio de sistemas monolíticos y sistemas independientes, en función del grado de interacción entre la vía y el tablero del puente. El sistema monolítico puede consistir en una losa continua de hormigón armado ejecutada in-situ que embebe a traviesas bi-bloque. Por su parte, un sistema independiente puede estar formado por placas de hormigón prefabricadas, separadas del tablero mediante una capa o manta de material elastomérico. Además, se ha considerado también como referencia a una vía convencional sobre balasto.

En el presente TFM, el objetivo ha sido estudiar la influencia de los sistemas de vía indicados anteriormente en el comportamiento dinámico de puentes ferroviarios bajo cargas en movimiento. La metodología ha consistido en simulaciones numéricas incluyendo de forma realista las diferentes componentes elásticas entre la vía y el puente. Las cargas han consistido en el conjunto de cargas móviles producidas por trenes comerciales a diferentes velocidades. Se han analizado dos tipos de puente habituales en la red española: un puente corto isostático y un puente largo hiperestático.

Se han llevado a cabo comparaciones en términos de desplazamientos, aceleraciones y factores de incremento dinámico. Los resultados muestran que los puentes cortos pueden sufrir efectos dinámicos considerables, especialmente para velocidades superiores a 300 km/h. Además, se ha obtenido que los sistemas de vía en placa pueden ayudar a reducir las aceleraciones y amplificaciones dinámicas con respecto a puentes con vía en balasto. A su vez, los resultados indican que los puentes hiperestáticos desarrollan efectos dinámicos mucho menores que los de los puentes cortos isostáticos.

AGRADECIMIENTOS

El éxito, el fin de este máster, marca de una forma el camino al éxito particular. En estos años he aprendido que el éxito no va asociado al talento innato, aunque en cierto modo es así, pero muchas veces nos olvidamos de lo importante que es contar con las oportunidades para poder triunfar. La gran serie de oportunidades que se me han ofrecido para poder desarrollarme y convertirme en la persona que soy ahora.

La oportunidad de poder formar parte de una de las universidades con más prestigio en el ámbito de ingeniería civil a nivel internacional, y dentro de esta universidad poder hacerlo en la Escuela de Ingenieros de Caminos, Canales y Puertos de Madrid, que es única en muchos aspectos, pero sobre todo es única porque las personas que la forman la dotan de un carácter especial.

Ante las oportunidades brindadas, lo más sabio es agradecerlo y en este caso quiero agradecerle a mi tutor, Carlos Zanuy, haberme descubierto que esta escuela no sólo era donde venir a aprender y examinarme, sino que iba a ser el medio para mi crecimiento personal y profesional, agradecerle que siempre haya confiado en mí y haberme brindado la oportunidad de trabajar en proyectos únicos durante los tres últimos años en los que lo he compaginado con mis estudios. También quiero agradecerle haberme enseñado que no hay peor enemigo en el camino al éxito que uno mismo, y poder aprender de ti directamente la importancia de la confianza y la perseverancia por alcanzar los objetivos que uno quiere. Me has enseñado como buen profesor, como buen tutor y jefe, pero lo más valioso de todo es que me has enseñado como buena persona, gran parte de lo que he logrado es gracias a las oportunidades que me has brindado y desde luego no he desaprovechado.

No sólo es importante tener oportunidades sino saber utilizarlas, por eso cuando Gonzalo Sanz, mi cotutor, volvió a la escuela como profesor, no dudé en aprovechar el momento para aprender de él, y no puedo estarle más que agradecida por su dedicación además de estarlo por sus palabras de ánimo en momentos difíciles y por sus consejos en los de duda.

Creo firmemente que lo más valioso que existe no es otra cosa que el efecto que causamos en las personas que tenemos alrededor y que este efecto viene determinado por los valores y los principios bajo los que actuamos. Estos valores no solo los he recibido a través de la escuela, sino que en casa desde pequeña mis padres han sido mi pilar incondicional y han sido ellos quienes me han inculcado valores como la perseverancia, el trabajo duro, la empatía, el respeto y el compañerismo. Mamá y papá, gracias por haberme dado las herramientas necesarias para construirme como persona y alcanzar cada uno de mis objetivos. También a mi familia que siempre ha estado a mi lado y que es lo más importante que tengo.

A lo largo de todos estos años, mi vida se ha centrado en estudiar y quizás en algunos momentos las relaciones sociales han sido más difíciles por eso, quiero darles las gracias a mis amigos porque me han apoyado siempre y me han dado la mano cuando tenía vértigo, por las horas de estudio compartidas y sobre todo por las que se invertían en cuidarnos.
Por último, a todos aquellos que me han acompañado a lo largo de estos años y que se han alegrado por mí cada vez que he conseguido alcanzar mis metas.

Notation

Latin Capital Letters

A	Area
C_{crit}	Critical damping coefficient
C^*	Damping coefficient of the equivalent single DOF system
COG_b	Centre of gravity (distance from the bottom fibber)
COG_t	Centre of gravity (distance from the top fibber)
E	Modulus of elasticity
E_c	Modulus of elasticity of concrete
E_s	Modulus of elasticity of steel
F_i	Forces
I	Inertia
$G(\lambda)$	Dynamic signature
K^*	Stiffness of the equivalent single DOF system
L	Span length of the structure.
L_{ter}	Length of the lateral embankment in the model
M^*	Mass of the equivalent single DOF system
P_i	Loads
V	Speed of the train

Latin letters

$a(x)$	Modal form
a'	First derivative of a
a''	Second derivative of a
F	Excitation frequency
f_0	Natural frequency
h	Height
m	Mass per unit length
$q(t)$	Periodic external load
q_0	Initial external load
$q^*(t)$	Periodic external load with sinusoidal shape
v	Displacement
$\dot{v}$	Velocity
$\ddot{v}$	Acceleration
$v(t)$	Displacement of the generalized coordinate
v_{dyn}	Maximum vertical dynamic displacement
v_{stat}	Maximum vertical static displacement
x	Distance
y	Vertical displacement
$\dot{y}$	Vertical velocity

$\ddot{y}$	Vertical acceleration

Greeks capital letters

Ω	Angular velocity of the excitation
Φ	Impact envelope coefficient

Greeks letters

δ	Vertical displacement
δ_{sta}	Vertical displacement due to static loads
ρ	Density
ξ	Damping ratio
φ	Phase angle
ω	Damped angular velocity
ω_0	Undamped natural angular velocity
1+φ'	Impact coefficient for real trains
ν	Poisson Ratio

Acronyms

AV	Alta velocidad
CA	Cement-Asphalt
DAF	Dynamic amplification factor
DOF	Degree-of-freedom
FEM	Finite element method
HP	Hormigón pretensado
HS	High speed
HSLM	High Speed Load Model
IAPF	Instrucción sobre las acciones a considerar en el proyecto de puentes de ferrocarril
TFM	Master Thesis (from Spanish Trabajo Fin de Máster)
SLS	Serviceability Limit State
UIC	Union Internationale des Chemins de Fer
ULS	Ultimate Limit State

Table index

Figure index

Chapter 1

Introduction

1.1. Motivation

A significant increase of the high-speed railway network has been built in Spain for the last decades. Due to the complex Spanish orography, has several tunnels and bridges are necessary to accommodate the railway layout to the specific site conditions. Already from the first installation of high-speed viaducts, serious concerns regarding dynamic effects of moving loads and eventual resonance problems were focus of engineers and scientists. As a result, dynamic analyses are typically required at the design stage of railway bridges in order to verify the structural safety, serviceability and passenger comfort (ACHE 2015). Despite the experience gained for the last years, new challenges have recently arisen due to the introduction of innovative solutions in railway construction. Among them, track infrastructure types different from the classic ballasted track (in which the rails are fastened to the sleepers resting on a ballast layer) are being introduced, including ballastless tracks (or slab track).

In particular, ballastless track has been identified as a promising alternative against ballasted track due to the reduced maintenance costs and excellent quality control (Esveld 2001). Ballastless track has been recently implemented in several railway bridges of the new high-speed lines in northern Spain (e.g. new access to Galicia). Due to the practical interest, it is convenient to analyze whether the track structure (i.e. ballasted or ballastless) can play a role in the structural performance of railway bridges and the passenger comfort.

Therefore, comprehensive structural analyses including dynamic studies are necessary. Though many formulations and long experience regarding dynamic effects on bridges with ballasted track already exists (Dominguez Barbero 2001), the same is not for ballastless track. It is necessary to understand the dynamic effects in such cases. Specific comprehensive studies have not been carried out so far.

The term ballastless track includes several track types which can affect differently to the whole structural response. For example, there are ballastless track systems built on-site as a continuous reinforced concrete slab in which precast sleepers are embedded. There are also ballastless track designs consisting of floating precast slabs to which the rails are directly fastened. The structural performance can be different depending on the bridge-track interaction degree, as it can range from monolithic to fully independent, which includes the installation of intermediate elastic layers or mats.

In the present TFM, the influence of the track type on the dynamic behavior of railway bridges under moving loads is studied. The analysis of the structural response has been done with numerical simulations that include the behavior if the components of the track and the bridge. The effect of train passage at different velocities has been included with a set of moving loads, which represent real commercial trains defined in the existing designed codes (IAPF 2007). Comparisons are carried out for different track structures, including a reference ballasted track and different types of ballastless tracks depending on the track-bridge interaction degree.

Though the TFM includes a study of the typology of railway bridges typical of Spanish high-speed lines, a detailed practical application dealing with a short bridge is included as case study due to its highest sensitivity to dynamic effects caused by moving loads.

1.2. Objectives

In the present TFM, it is discussed how the track type can influence the dynamic structural behavior of railway bridges under the moving loads of high speed trains. In particular, the objectives of the present TFM are as follows:

- To approach the problem of dynamic effects caused by HS trains in railway bridges with ballasted and ballastless track, in order to understan the posible influence of the track typology on the dynamic performance of the bridges. The most relevant dynamic results will be analyzed according to common comercial trains operating on the Spanish high speed network.

- To propose a numerical methodology to compare the dynamic behavior between HS bridges with ballasted or ballastless track, taking into account different parameters that influence the structural behavior such as the speed of high speed trains and the characteristics of the bridges, including short single-span bridges and long hyperestatic bridges, considering the span lengths and the properties of the bridge section.

- To establish practical conclusions which would allow to make relevant decisions on the type of track that could be installed in bridges of the high-speed network, and report on possible lines of research.

1.3. Work methodology and organization

The present Master's thesis (TFM) deals with the analysis of dynamic effects produced by high-speed trains in railway bridges, taking into account the typology and layer morphology of the track infrastructure (ballasted or ballastless track). In order to complete the TFM, a comprehensive numerical work has been carried out. The employed methodology has dealt with the finite element simulation of the track-bridge interaction under moving train loads. A large number of models has been programmed in Ansys 15 software, a general finite element software which has required programming in APDL language all the input models, solver specifications and post-processing tools. The Ansys software is available in the Department of Continuum Mechanics and Structures of the ETSICCP. The main challenge of the numerical simulations is to clearly understand the effects of each component of the track avoiding the black-box approach. To introduce the employed methodology it is important to define the conditioning aspects dealt with in the present TFM.

First of all, a study of the typical bridge typologies of the Spanish railway lines has been carried out in order to define the mechanical properties of the bridges object of the numerical analysis. The mechanical properties are those which characterize the bridge cross-section (inertia, area, position of the centroid). From a parametric analysis of different existing bridges, some simplified expressions are used to characterize the mechanical properties of railway bridges as a function of the span length.

Secondly, different track structure types are studied. As a reference, a ballasted track system is simulated including the rails, the fastening system, the sleepers and the ballast layer on the bridge girder. Then, two different types of ballastless track systems are studied including a monolithic solution and an independent system. Numerical simulations include the different elastic layers of each system and its damping abilities, which have shown to be relevant by previous researchers (Goicolea et al. 2012).

The effect of moving loads is analyzed considering different train types and running velocities. Due to the fact that dynamic effects are typically produced by high-speed (passenger) trains at velocities higher than 220 km/h, commercial high-speed trains common in Spanish networks (Talgo and AVE) have been simulated as sequence of axle loads.

The present TFM is divided into six chapters. Chapter 1 presents an introduction to the TFM, including the main objectives and general description of the methodology. Chapter 2 includes a brief but comprehensive state-of-the-art review of existing researches and engineering works dealing with the TFM subject. Chapter 3 is intended to describe the details of the numerical models used for the dynamic analysis of railway bridges subjected to moving loads in the high-speed range. Chapter 4 shows the results obtained in the different cases of the finite element models. The first issue is to establish the limits that the IAPF standard dictates in relation to vertical displacements and accelerations in the deck of railroad bridges. The influence of the type of track on the most important results obtained previously, determining the dynamic response of bridges, is discussed and developed in Chapter 5. Such results are the dynamic amplification factor (DAF) and the acceleration at the midspan of the bridge.

The last chapter of the present document, Chapter 6, contains the main conclusions reached after a thorough analysis of the results and the future research lines are highlighted. As in other research works, the results of the present TFM lead to interesting concluding remarks, which are detailed in Section 6.2. Also like all researches, the results open the gate for further detailed analyses and other lines for future works.

Chapter 2

Problem statement

2.1. Introduction to moving loads

The dynamic response of a beam structure subjected to time-dependent loads can be well understood with a simplification of the problem to a single degree-of-freedom (DOF) system or a mass-spring-damper model, as represented in Figure 1. The corresponding dynamic equation of motion is as follows:

$$M^*\ddot{v}(t)+C^*\dot{v}(t)+K^*v(t)=-q^*(t) \tag{1}$$

where M^*, C^* and K^* are the mass, damping coefficient and stiffness of the equivalent single DOF system, which can be calculated from the structural properties:

$$M^*=\int_0^L m(x)\left[a(x)\right]^2 dx \tag{2}$$

$$K^*=\int_0^L EI(x)\left[a''(x)\right]^2 dx \tag{3}$$

$$C^*=\xi\cdot C_{crit}=\xi\cdot 2M^*\omega_0 \tag{4}$$

$$\omega_0=2\pi f_0=\sqrt{\frac{K^*}{M^*}} \tag{5}$$

In turn, $v(t)$ in Eq. (1) is the displacement of the generalized coordinate which governs the modal form $a(x)$. Typically, $v(t)$ is the displacement of the midspan section in the case of a simply supported beam vibrating according to the first vibration mode, with a natural frequency of f_0 according to Eq. (5).

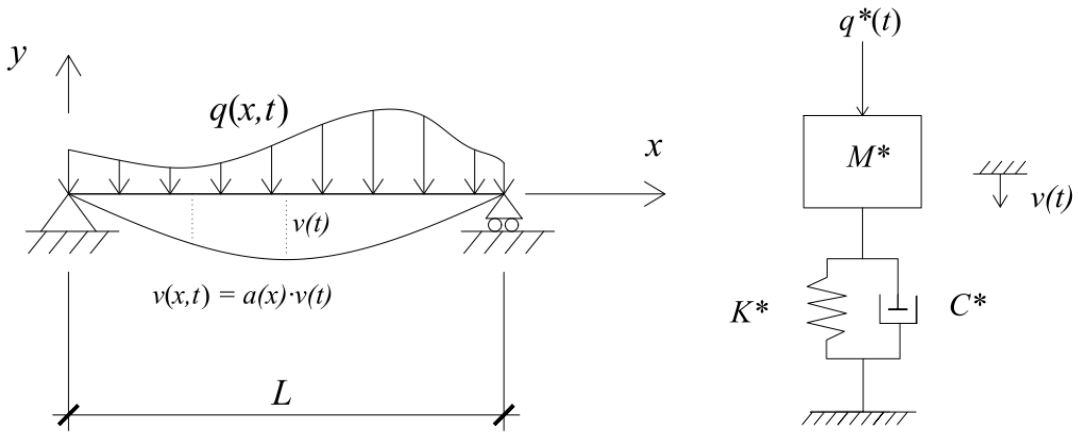

Figure 1. Equivalence of a simply supported beam to a single DOF system.

A detailed study of the dynamic equation of motion and its equivalence with a single DOF system can be found in well known handbooks of Dynamics (Chopra 2007, Humar 2005, Clough & Penzien 2010). Accordingly, the general solution of Eq. (1) consists of two components, a transient one and a steady-state one. In the case of a periodic external load with a sinusoidal shape ($q^*(t) = q_0 \sin(\Omega t)$), the general solution of Eq. (1) is as follows:

$$v(t) = A \cdot e^{-\xi\omega_0 t} \sin(\omega t + \varphi) + H \sin(\Omega t + \Psi) \tag{6}$$

where A and φ can be determined with the initial conditions.

In Eq. (6), the first component is the transient part of the solution, which vanishes in a relatively short period of time due to the effect of damping. The second component of Eq. (6) is the steady-state solution, which is present as long as the external load is applied. Factors H and Ψ can be analytically determined directly from the parameters defining the external load (Chopra 2007). Due to its significant interest for the present work, factor H is reproduced next:

$$H = \frac{q_0 / K^*}{\sqrt{\left[1 - \left(\frac{\Omega}{\omega_0}\right)^2\right]^2 + 4\xi^2 \left(\frac{\Omega}{\omega_0}\right)^2}} \tag{7}$$

As the numerator of Eq. (7) is the static response of the beam subjected to a load q_0, it is clear that the amplification of the structural response due to dynamic effects can be expressed by a dynamic amplification factor (DAF) as follows:

$$DAF = \frac{1}{\sqrt{\left[1 - \left(\frac{\Omega}{\omega_0}\right)^2\right]^2 + 4\xi^2 \left(\frac{\Omega}{\omega_0}\right)^2}} \approx \frac{1}{\left|1 - \left(\frac{\Omega}{\omega_0}\right)^2\right|} \tag{8}$$

According to the previous equation, the DAF can be rather large when the frequency of the external load ($f = \Omega/2\pi$) approaches the natural frequency of the structure (f_0). Such a phenomenon is known as resonance. The presence of damping (ξ) affects positively the structural response by decreasing the dynamic amplification. A classical overview of the beneficial effect of damping on the DAF is represented in Figure 2.

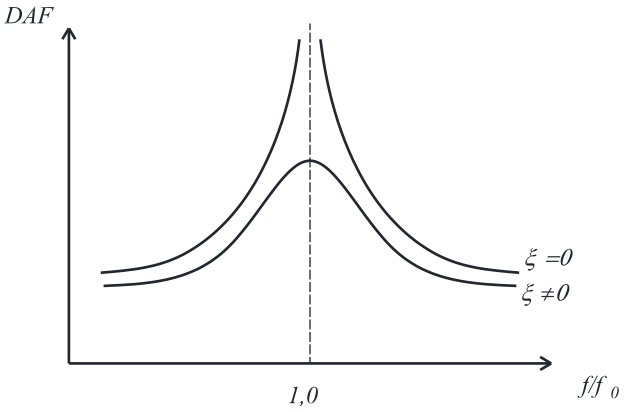

Figure 2. Amplitude of the steady-state solution as a function of the damping coefficient.

As it can be understood, the real response of railway bridges and other structures is more complex than the previously explained one, and the response cannot be in many cases reduced to a single DOF system. In such cases, more than one vibration mode is excited, and the response should be treated as the superposition of several vibration modes. The different approaches to solve the dynamic problem in such conditions are dealt with in the following clauses of this chapter.

The main topic dealt with in the present Master's thesis is the impact phenomenon due to moving loads on railway bridges, the eventual resonance produced by train loads and the basic concepts that govern dynamic behavior, including those arising from the different types of trains, those related to the bridge themselves and the likely influence of the track structure.

Starting with the introduction to dynamic impact and resonance, it is necessary to make a major emphasis on moving loads, which are one of the most important loads in railway bridge design. Moving loads are different from the periodic loads mentioned above, but it will be later observed that the combination of moving loads in a train sequence can take advantage of many of the concepts explained in the previous analysis of a single DOF system.

First of all, it is necessary to study how a single moving load affects the dynamic response of the structure to this solicitation. In order to understand the phenomenon, a first discussion is presented from the solution of a dynamic analysis carried out by Goicolea (2007) for short span (i.e. less than 40 m) statically determinate (isostatic) bridges, for a moving load of 195 kN under different speeds, in particular 220 km/h and 360 km/h. The reason for these speeds will be explained later, as they are not randomly chosen.

In the example of Figure 3, according to Goicolea (2007), the span of the bridge is 15 m, with a moving isolated load of 195 kN and the speeds mentioned above.

A first discussion is done in terms of the vertical displacement suffered by the bridge at the midspan. Figure 3 shows the vertical displacement that the structure suffers at midspan since the load enters the bridge until the load leaves the bridge, at a speed of 220 and 360 km/h, represented by red and green curves, respectively. At a time of 0.12 s, a maximum displacement of -3.0 mm is produced by the moving load at 360 km/h, which decreases thereafter due to the damping effect. When the load moves at 220 km/h, the highest displacement is -2.8 mm, which occurs at 0.15 s after the load has entered the bridge. In addition, the static displacement is also plotted in the figure, which is -1.9 mm. Therefore, the dynamic amplification factor is 1.6 and 1.5 for speeds of 360 and 220 km/h, respectively. This example shows that the velocity can affect the structural response even for single moving loads. An additional and more significant dynamic amplification can be obtained when the applied load is not single, but a set of subsequent loads which moves periodically, as dealt with in the following sub-chapter.

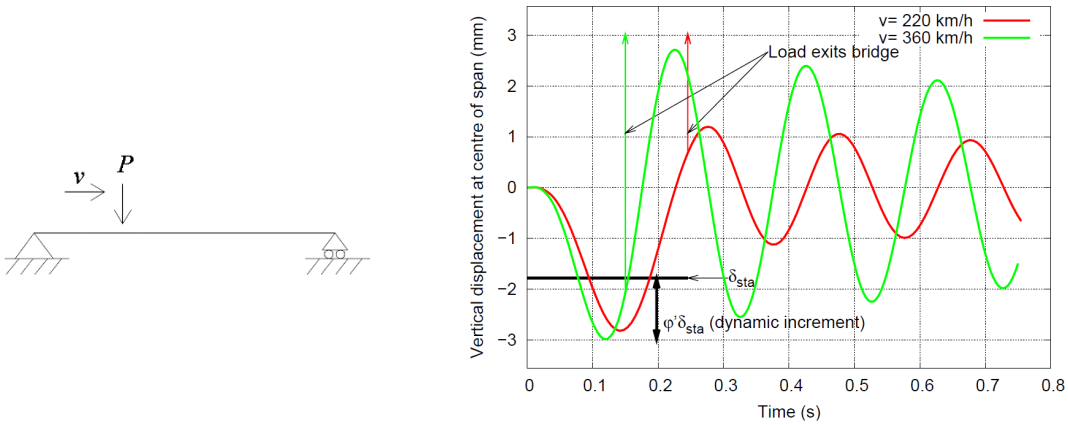

Figure 3. Dynamic response of a short-span isostatic bridge (L = 15 m) under an isolated moving load (P = 195 kN) at 220 km/h and 360 km/h, Goicolea (2007)

2.2. Dynamics in railway bridges

Railway bridges are in fact subjected to the subsequent actions of the axle loads passing at the speed of the trains, rather to isolated moving loads which do not affect to each other. As shown in Figure 4, the action of a train consists of the passing of consecutive loads moving at a speed V. The spacing between the loads and the speed at which they are moving are jointly responsible, to a more or lesser degree, for the dynamic amplification of all the loads with respect to the response of the structure when the loads are applied quasi-statically.

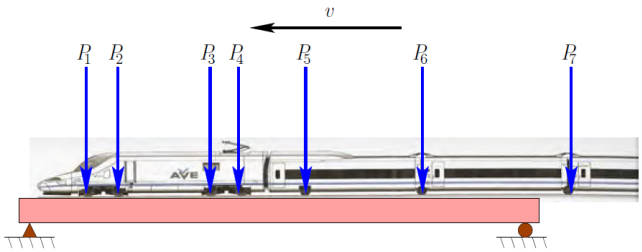

Figure 4. Moving train loads

To exemplarize show the effect of the velocity of train loads, Figure 5a) represents the deflection at midspan on an isostatic bridge of 15 m length due to the passage of a TALGO HS train. Please note that in the graphics the static response due to the application of the UIC-71 train load model is also plotted.

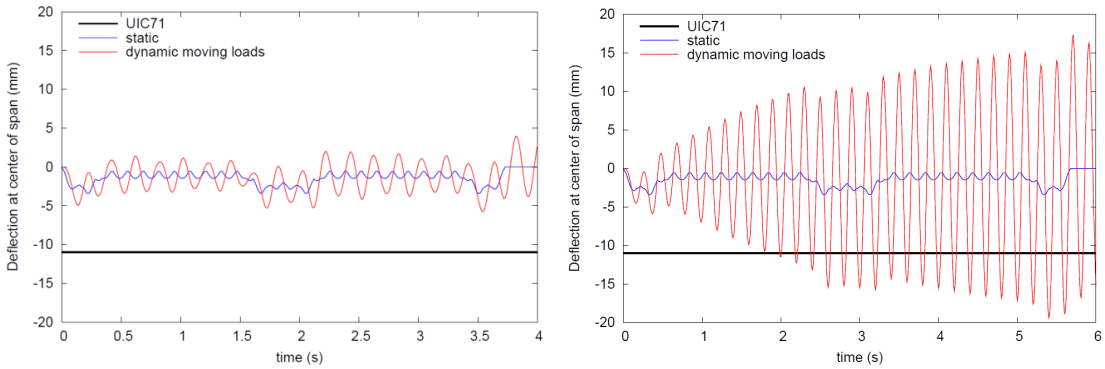

Figure 5. a) Talgo HS; $V = 360$ km/h; b) Talgo HS; $V = 220$ km/h; according to Goicolea (2007).

The red line above represents how the effects of the moving loads are amplified with respect to the static response, which is represented by the blue line. At a speed of 360 km/h, the difference between dynamic and static effects is rather moderate. If the speed is reduced from 360 km/h to 220 km/h the dynamic response changes significantly as shown in Figure 5b) where a dynamic amplification of the order of more than 5 times higher than the static response is obtained. This phenomenon is named resonance and is due to the fact that the relationship between the separation of the axes of the loads and the velocity causes the frequency of the load to approximate the structure's natural frequency, which in this case is around 5 Hz.

Resonance itself is the most damaging phenomenon due to the dynamic loads that a structure can be subjected to and, as it has been shown in the example, it may not occur at the highest speeds but at those speeds where the combination of speed and bogies separation makes the frequency of the load approximately equal to the natural frequency of the structure; in summary, the oscillation amplitude increases with each cycle due to this resonant effect.

Until a few years ago, the phenomenon of resonance was not taken into account in the design of railway bridges, and its effects were assumed by the margins provided by the safety coefficients in the design of the railway structure. With the extension of high-speed lines in many countries like Spain, the need to consider this effect arose. However, it was not until 2002 that this concept was included in the EN 1991-2: EUROCODE 1 calculation standards (CEN 2002) and later in the Spanish IAPF (Ministerio de Fomento 2007), to take into account the dynamic effects in the calculation of railway bridges.

2.3. Calculation Methods

2.3.1. Numerical and analytical methodologies

To analyze the dynamic effects on railway bridges due to the passage of trains, the most general procedure is to integrate the full structural response over time. The loading scheme is characterized by a set of moving loads separated according to the distance between the vehicle axes and the distribution of the bogies. To clarify the scheme, the loads and the velocity are exemplarily represented in Figure 6 by F_i and v, respectively.

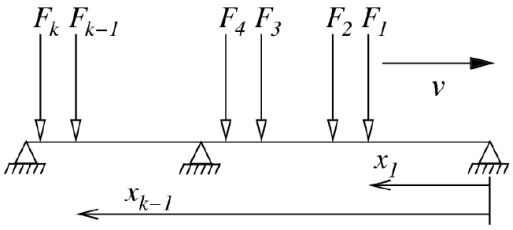

Figure 6. Scheme of moving train loads.

The advantage of the direct time integration is that it can be used for any case, even when there is a situation with resonance or not, leading to very fine results thanks to the current powerful software tools based on the Finite Element Method (FEM). The direct time integration method requires to solve, in each time step, a dynamic system of equations of motion for all the degrees of freedom of the FEM mesh:

$$\mathbf{M}\cdot\ddot{\mathbf{v}}(t)+\mathbf{C}\cdot\dot{\mathbf{v}}(t)+\mathbf{K}\cdot\mathbf{v}(t)=\mathbf{f}(t) \tag{9}$$

An easier and faster solution can be found with the help of modal analysis. Actually, modal analysis in railway bridges is considered one of the most effective procedures to solve the problem, because the eventual difficulties of the full integration (computational cost) can be reduced by just focusing on the most significant vibration modes. Then, a short system of uncoupled equations of motion is derived, which can be easily integrated. Only a few modes (typically 5 or even less) are necessary to be considered instead of the total degrees of freedom of a general model like Eq. (9). Moreover, the reduced system can be integrated manually in some simple cases and an analytical solution can be found.

Analytical and FEM approaches differ from each other in that the first can provide the solution through algebraic equations for simplified or single DOF systems (similar to those discussed in Section 2.1), while the second can be used to obtain a numerical solution of a large system of equations with several degrees of freedom. Besides the finite element mesh, a time discretization is required to achieve an integration of the solution over time.

A significant topic when dealing with the dynamic behaviour of railway bridges is the interaction between the train vehicle and the structure. The dynamic calculation of the interaction problem involves the integration of the dynamic equations in time, including in the FEM the components of the vehicle, i.e. the mass, stiffness and dampers of the train.

At this point, it is essential to take into account that the vehicle also vibrates due to its own suspension. In these interaction models, both the primary and secondary suspension modes have to be considered (Figure 7): primary suspension refers to the stiffness and damping per axle (K_p, C_p), while secondary suspension involves several additional terms, which are listed in Table 1 for the sake of simplicity.

Wheel axle	Nominal mass	(m_w)
Bogie	Stiffness and damping	(K_s,C_s)
	Inertia, Length and mass	(J_B,L_B,M_B)
Vehicle	Mass and Inertia	(J,M)
Vehicle geometry	Length	(L)
	Distance between GC of vehicle and pivots	(d_{Bd},d_{Bt})
	Distance between bogie axis	(d_{eB})

Table 1. Secondary suspensions of train vehicles.

Complete vehicle models are not always necessary. It is possible to perform the dynamic calculation through simplified models that allow obtaining the same results using an easier procedure. This simplified calculation method assumes that the interaction between each axis is completely independent from the others, which actually means that there is no interaction between the axis of a vehicle (an independent axis is plotted in Figure 7b). The secondary suspensions are reduced to the nominal value of mass per axle plus the proportional mass of the vehicle, which in turn is equal to the proportional bogie mass.

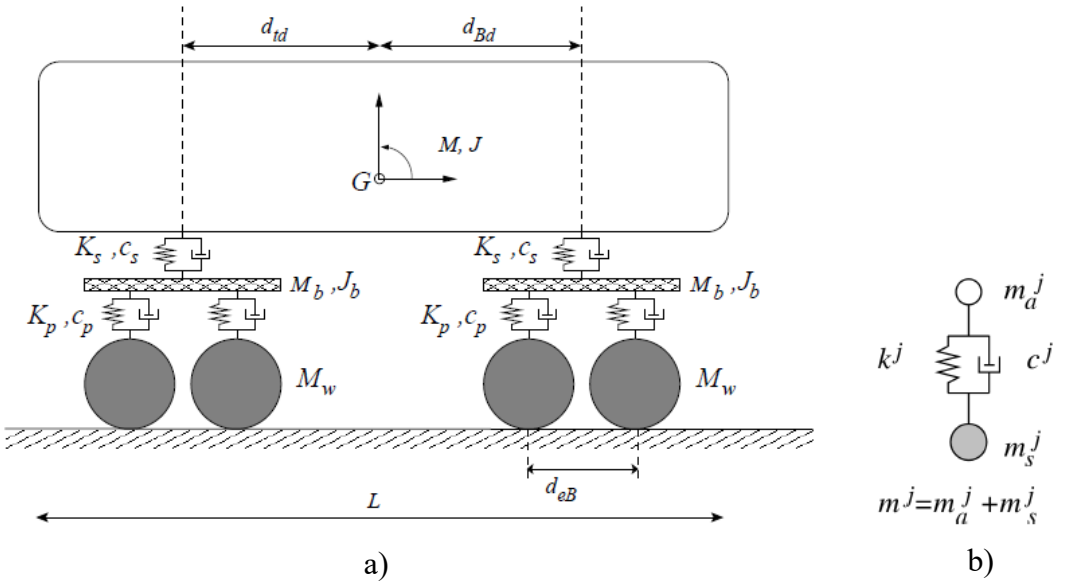

Figure 7. a) Complete vehicle model; b) simplified model; Dominguez Barbero (2001)

The vehicle-bridge interaction often results in a positive reduction of the bridge response with respect to no-interaction models due to the beneficial effect of the mechanisms that facilitate the dissipation of energy, called dampers, or those that exchange energy, suspensions.

When there is no resonance or in statically indeterminate bridges, interaction effects are not as significant as those that can occur under resonance or in short span bridges, between 15 and 30 m. Therefore, neglecting the vehicle-structure interaction is typically on the safe side as no-interaction models provide conservative results.

Apart from the possibility to perform a dynamic analysis requiring the solution of each particular problem, some simplified models have been proposed to estimate the dynamic effects due to train loads without completing the time-dependent analysis. Among them, the most extended procedure is based on the estimation of the dynamic amplification factor (DAF) through simplified formulations valid only in specific cases. It is for example the case of the impact coefficient Φ that can be used for speeds under 220 km/h according to IAPF (which for high-speed calculations is obviously not enough):

$$\Phi = \max\left(\varphi' + \varphi'' + 1\right) \tag{10}$$

In Eq. (10), a first term φ' includes the train effects over an ideal track without irregularities and a second one φ'' includes the track irregularities. This formulation is based on ballasted track on the bridge. In the case of slab track, no general cases have been studied and there are no formulations even for speeds under 220 km/h. This is one of the reasons which justifies the present TFM.

2.3.2. Design standards and recommendations

Nowadays, different design standards and codes of practice provide the requirements and recommendations to design railway bridges considering the dynamic effects due to moving loads. In Spain, the current IAPF standard (Ministerio de Fomento 2007) has been a significant step forward with respect to its previous versions from 1975, which did not offer great contributions as far as dynamic actions on bridges are concerned. Currently, the standard includes the evaluation methods for the dynamic effects and the vehicle-bridge interaction.

As a summary, the methods included in this standard to perform a dynamic analysis are as listed in Table 2. As it can be observed, for speeds smaller than the high-speed domain, simplified models based on dynamic amplification coefficients can be used. For cases sensitive to resonance in the high-speed domain, specific dynamic analysis has to be performed.

Impact increase factor methods	General methods
B.2.1: Impact envelope coefficient (Φ); $V < 220$ km/h	B.2.4: Dynamic analysis with moving loads
B.2.2: Impact coefficient for real trains (1+φ'); $V < 220$ km/h	B.2.5: Dynamic signature $G(\lambda)$. Isostatic bridges.
*The application range of this methods does not include the resonance phenomenon	B.2.6: Dynamic analysis with vehicle-structure interaction.

Table 2. IAPF (2007). Dynamic calculation methods

In addition to the recommendations regarding the calculation method, IAPF also includes the train types (refer to Section 2.6) and the limits of displacements and accelerations that should not be overcome in order to ensure the correct serviceability of the structure and the comfort of the users.

The Eurocodes 0 (EN 1990-A1) and 1 (EN 1991-2) contain the main research outcomes of the UIC (1979) and ERRI (2002) about dynamic loads on railway bridges, although the new versions of the Eurocodes separate the actions of the specifications for ULS and SLS. It must be also mentioned the report UIC 776-1R, UIC (1979) that compiles the work of the UIC-71 train loads and the associated impact coefficients for the consideration of dynamic forces, which has been the design basis of railway bridges for the last decades. The above mentioned standards provide the guidelines to consider the dynamic effects in railway bridges, which will be considered in the present TFM.

2.4. Track infrastructure

2.4.1. Types of track

The influence of the track infrastructure on the dynamic effect of moving loads on bridges deserves specific research as ballastless track systems have been implemented on bridges very recently. A clear example is the first Spanish application of precast slab track system for the bridges of the high-speed accesses to Galicia and the new Pajares Pass, constructed simultaneously between 2020 and 2021 (Figure 8). Nowadays it is possible to find several articles and investigations on the dynamic analysis of train loads on railway bridges, but they mainly deal with ballasted track. Existing works on ballastless track are mostly for embankments. General and comprehensive studies and results on the influence of the track type for bridges are difficult to find, unless specific or particular projects such as for example those of the applications in Galicia and Pajares.

Figure 8. Prefabricated slab track system VP by AFTRAV on railway viaduct. Source: https://magazine.mafex.es/sistema-via-en-placa-vp/

Generally speaking, a track infrastructure can be of two main types, ballasted or ballastless track (the later also known as slab track).

The purpose of this TFM is to look for general results depending on the track-structure interaction against dynamic loads, and thus to determine in which cases the use of ballastless or ballasted track can be more appropriate. The use of each type of track depends on the needs of the design, since there are advantages and disadvantages in both types, which will be discussed later in this document. Before defining each of them, it is important to summarize shortly the historical application of both systems.

Since the beginning of the railway history, ballasted track has been the most commonly used system. Railway track construction has evolved over a historical period of 150 years since the first railway track was introduced as a set of wooden sleepers relying on a ballast bed. For much of this period, the ballasted track system has consisted of certain components including rails, fastenings, sleepers, ballast and subgrade. The sleepers were primarily made of wood, but concrete was progressively introduced and nowadays concrete sleepers are mostly employed due to their excellent durability and structural performance, for both passenger and freight traffic lines. Concrete sleepers can be monoblock prestressed or twin-block reinforced elements.

First applications of ballastless track systems were initially in tunnels and later on embankments, which has allowed new possibilities for railway infrastructures. In the last 20 years, the use of concrete slab track systems for transit, regional and high-speed railway applications has been increasing. Basically, a slab track is a concrete plate or slab laid on a sub-base on a prepared subgrade. The rails can be fastened directly to the concrete slab or can be laid on concrete blocks. Slab track for passenger service operations can incorporate additional requirements to mitigate noise and vibration, including intermediate elastic layers such as mats or pads. A newer type of ballastless track, which has been developed in the Netherlands, has rails embedded in a trough in the slab and surrounded by an elastomeric material.

The move towards the implementation of slab track in railway infrastructure instead of ballasted track is due to its advantages in some aspects, but to obtain some conclusions it is necessary to define the track types with clarity. Ballasted track is the type of track in which the rail rests on the sleepers (through the pad of the fastening system), which in turn rely on a bed of ballast. The sleepers are responsible for ensuring the track gauge and are part of the superstructure together with the rails and pads. Also, they are in charge of transmitting the loads to the ballast layer, which is the infrastructure of the track that sometimes has a sub-ballast layer. In Figure 9 below, it is possible to observe the configuration of this kind of track.

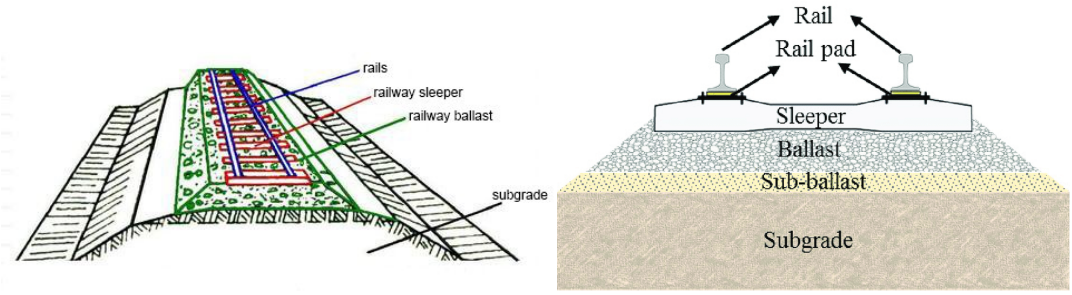

Figure 9. Ballasted track cross section, according to Barkhordari, et al. (2019).

Ballasted track has some particular characteristics that have made it the most used system. Today, most of railroads for freight and passenger traffic in the world are carried over conventional ballasted track due to advantages like the easy and cost-effective way to construct the track, the high elasticity, simple maintainability, huge capacity to drain the water due to its porosity and shape, and also the large lateral and longitudinal stability to conserve the track gauge, taking advantage of the high frictional resistance to lateral sleepers movements.

In spite of the fact that ballasted track has relatively lower construction costs comparing to ballastless track, it requires frequent conservation tasks such as tamping. Therefore, slab track is experiencing increasing use for high-speed lines, principally in Japan, China and Europe. It is necessary to remark that so far the most frequent use of slab track has been for passenger train operations in urban areas, in stations where special components to reduce noise and vibrations can be additionally required, as well as in applications to reduce the long term costs and maintenance of the track (for example in tunnels).

The main drawback of ballastless track is the initial construction and installation costs. Other advantages can be however considered, like its life-cycle cost lower than the one of the ballasted track, its easy and practical maintenance, for example fasteners direct installation, giving at meantime the necessary strength and durability. Therefore, the use of slab track provides in general some advantages like the reduced maintenance requirements coupled with longer service life than ballasted track (around 10-20 years of the ballast and 40 years of the sleepers), as well as the higher structural stability.

Different criteria can be used to classify ballastless track systems. Concrete slab track types can be classified in four groups according to Michas (2012):

Cast-in-place systems	Jointed plain or reinforced concrete slabs/ continuous reinforced concrete slabs
Sleeper-embedded systems	Block- or full sleepers embedded in a concrete slab placed on a concrete base, eventually with rubber boots
Two-slab layer systems	Precast concrete slab placed on a concrete base separated with asphaltic or elastomeric layer
Embedded-rail systems (ERS)	Rail embedded in elastomeric material

Table 3. Concrete slab track systems. *(Michas 2012)*

Other criteria to classify the slab track can be based on the longitudinal continuity of the rail-supporting slab (continuous or discrete) or regarding the connection between the slab track and the lower supporting layers (leading to either a monolithic or an independent structural behaviour). According to the longitudinal continuity of the concrete slab which supports the rails, the following ballastless track systems which will be useful for the present TFM can be considered:

- Discrete rail support (short precast concrete slabs):
    - Shinkansen (prefabricated slabs, see Figure 10).
    - VP Aftrav (prestressed, see Figure 8).
    - Porr (reinforced).

- Continuous rail support (long plain or reinforced concrete slab built on site, typically with embedded twin-block sleepers):
    - Rheda (reinforced).
    - Bx Aftrav (reinforced).

Figure 10. Cross and transversal section of concrete slab track. Esveld (2001)

According to the layer structure and the interlayer connection, different cross-sections of ballastless track can be considered, as represented in Figure 11a)-d) in comparison with a conventional ballasted track (Figure 11e). If a precast concrete slab is used (Figure 11a-c), it is necessary to introduce a cement-asphalt (CA) mortar or filling layer between the concrete slab and the supporting layer so that full surface contact is achieved. If the frictional capacity between the mortar and the concrete is not enough to transfer the horizontal forces, additional connecting dowels can be used between the CA mortar and the concrete slab (Figure 11c). In other cases, concrete stoppers can be provided between the mortar and the slab. If the concrete slab is constructed on site (e.g. Figure 11d, with embedded twin-block sleepers), a filling mortar layer is not typically required as the concrete slab is poured directly on the supporting layer and full contact is achieved.

In addition to the schemes plotted in Figure 11, the cross-section can incorporate a resilient layer below the concrete slab to isolate the bending behavior or reduce the transmission of vibrations to the ground. In railway technology, a resilient layer is typically referred to describe elastic or elastomeric materials with long-term durability.

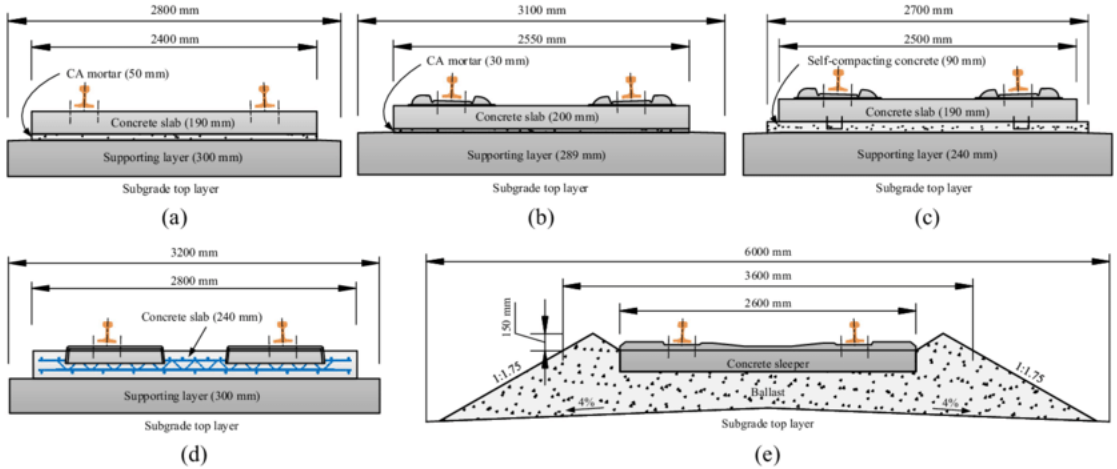

Figure 11. Cross sections of different track types according to Zhai, et al. (2020): a)-b) Slab track with prefabricated concrete slab independent from the lower layers; c) Slab track with concrete slab connected to mortar layer; d) Slab track with bi-block sleepers embedded in a concrete slab supported on lower layers; e) Ballasted track with sleepers.

As a final thought, in bridges it makes sense to study the possibility of installing ballastless track systems because of its fast installation (especially in case of precast slabs) and the simple maintenance, which contrasts with the frequency of maintenance (tamping) and repairing works involving railway traffic interruptions of ballasted track. The total dead load on the bridge girder can be also reduced with respect to ballasted track due to the absence of the ballast layer. Therefore, the advantages offered by the slab track are adequate compared with the constant maintenance of the ballasted track in this type of structure.

2.4.2. Track mechanics

As the main objective of this TFM is the analysis of the dynamic effects that occur on the bridge structure due to train loads considering the influence of the track type, it is necessary to carry out a research on the already existing studies and investigations in the literature to find out how far they have gone on the issue.
It must be said that most of the existing comparative studies on the dynamic performance of ballasted or ballastless track systems have been done for embankment applications and not for bridges.

The conventional structural model to study the track on ballast makes use of springs and dampers to reproduce the transmission of loads through the track components, due to the fact that all elements are elastic within the service load domain. If a general cross-section of a ballasted track as the one represented in Figure 12 is considered, a numerical model with the scheme of Figure 13 can be employed. The rail acts as a beam, which by means of the fastenings (springs and dampers) transmits the moving train loads to the sleeper (point mass) and finally to the foundation subgrade through the ballast layer (springs and dampers), as it is shown in Figure 13, where the train has been also represented by springs and dampers.

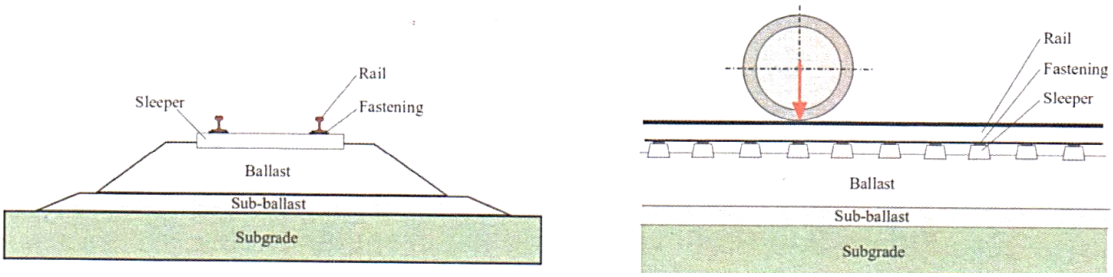

Figure 12. Cross- and longitudinal section of ballasted track. Goicolea et al. (2007)

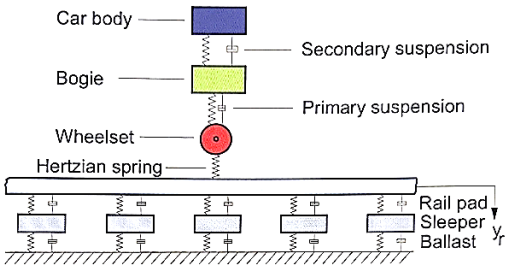

Figure 13. Elastic model used in ballasted track, Esveld (2001)

The sources of dynamic effects on track systems on embankments or earth works are due to the moving loads and the irregularities of the rails or the wheels. The irregularities can be classified according to the wave length, as follows:

- Irregularities D1: from 3 to 25 m wave length. Short wave geometry associated with transverse and vertical forces, automatic, tamping actions, and exceedances due to local defects.
- Irregularities D2: from 25 to 70 m wave length. Associated with car body accelerations at medium speeds
- Irregularities D3: from 70 to 120 m. Associated with car body accelerations at high speeds.

In high-speed lines, irregularities D3 are not allowed by the standards, specifically by NAV 7-10.7 in Spain (ADIF 2021).

Some researchers like Goicolea et al. (2007) have made an exahustive dynamic analysis on the effects of the irregularities taking into account the type of track, ballasted or slab track, for tracks on embankments. Some results are summarized in Figure 14-Figure 15 in terms of the dynamic amplification factor (DAF) of the reaction under the rail pads. The analysis of the DAF has focused on the high-speed range from 200 to 360 km/h. It must be noted that the load has been modelled as a signle axis, like in Figure 7b. In the analysis, the irregularities D1 and D2 have been subdivided into 3 groups.

According to Figure 14, in case of ballasted track, the dominant irregularity of type D1 which provides the maximum DAF always occurs for wave lengths between 10 and 18 m (D1-2), regardless of the speed of the train. DAF values up to 1.24 can be found for speeds of 360 km/h. However, for irregularity type D2 the maximum DAF is not always reached at the same wavelenght, but it depends on the speed of the train. For velocities from 200 to 280 km/h the worst wave length values are between 33-51 m approximately (D2-2). When the speed increases up to 300 km/h the worst value of the wavelength oscilates from 15 to 33 m (D2-1); finally, from 320 to 360 km/h the worst values for the wavelength are the highest ones, from 51 to 70 m approximately (D2-3). The envelope in Figure 14 represents the curve that includes all the maximum dynamic amplification factors in order to always cover the worst situation. The highest DAF of 2.4 is found for speeds of 200 and 240 km/h.

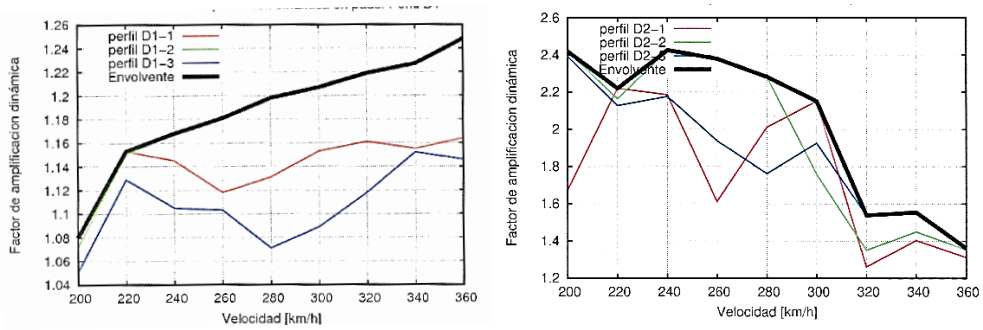

Figure 14. Dynamic amplification envelope. Irregularities D1 (left) and D2 (right) in ballasted track on embakment. Goicolea et al. (2007).

The same analysis is done for slab tracks on embankment in Figure 15. For irregularities D1, the maximum DAF from 200 to 260 km/h occurs with wave lengths from 3 to 10 m (D1-1), while when the train runs at speeds between 260 and 340 km/h, the maximum DAF is obtained with wave lengths of 18-25 m (D1-3). With the maximum velocities, the lowest wave lengths achieve the maximum value of DAF. The largest DAF of 1.24-1.32 is obtained for the highest speed of 360 km/h.

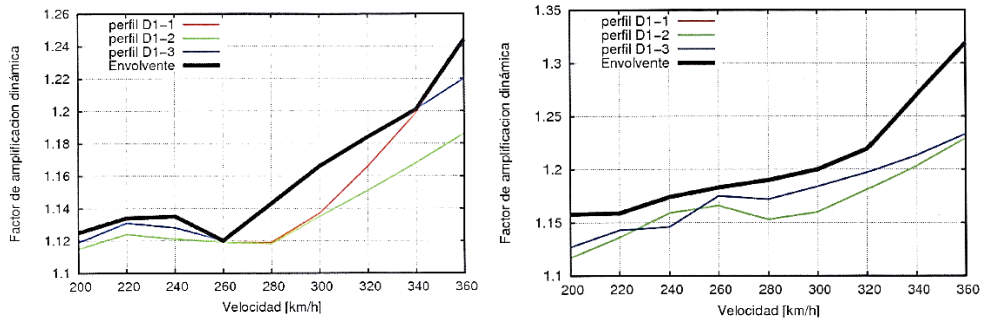

Figure 15. Dynamic amplification envelope. Irregularities D1 on the slab (left) and at the wheel-rail contact (right), in slab track on embankment. Goicolea et al. (2007).

Thanks to this study, it is easier to understand the behaviour of slab and ballasted track under dynamic loads, and the results that can be deduced from Figure 14 and Figure 15 are that when the moderate wavelengths exist (D2), dynamic loads transmitted to the ballast bed or to the sleepers increase so much that even the DAF can be in some cases higher than 2. Depending on the track, the highest DAF found at the wheel-rail contact is as listed in Table 4. It can be concluded that for embankment applications, the use of slab track provides a better load distribution than ballasted track, thereby reducing the pressure on unconfined soil layers and the subgrade.

Track	DAF D1 irregularities	DAF D2 irregularities
Ballasted	1.33	2.81
Ballastless (Rheda)	1.32	1.66
Ballastless (Aftrav)	1.32	1.70

Table 4. Summary of DAF on embankments depending on the irregularities, according to Goicolea et al. (2007)

To conclude this subchapter, it is important to highlight the existing milestones and the research needs. For railway tracks on embankments, dynamic effect studies have been carried out in detail, being able to relate and find quantitative differences between the dynamic performance of ballasted or ballastless track, showing the advantages and disadvantages of each type of track in this type of structure. Not only has the type of track been studied in the analysis, but also the irregularities of the rail. However, no similar general studies are available for bridges in order to compare the possible differences between ballasted and slab track. This TFM aims to analyze the behaviour of the structure (bridge) under dynamic loads depending of the track type.

2.5. Review of structural types of Spanish railway bridges

As this TFM aims at modelling the dynamic behaviour of railway bridges including the track infrastructure, it is convenient to briefly summarize the most employed bridge typologies in Spanish railway lines.

To understand the development of the typology of the railway bridges it is necessary to go back over thirty years. In Spain, the first high-speed lines were built between 1992 and 2004. The first one was the AVE Madrid-Seville line and then the Madrid-Barcelona and Madrid-Valencia high-speed lines. They were constructed on ballasted track in all stretches with the exception of some tunnels where slab track was used. The bridges of these lines have a ballasted track on the girder and they are double track, which means that both directions run on the same girder, leading to the typical 14 m wide box cross-section of Figure 16 (top). That is the dominant case of the first Spanish high-speed lines, where only in some tunnels and urban zones the track was built on slab track.

The criteria for the design of a railway line and the choice of the track's cross-section on embankment, tunnel or viaduct are twofold: orography and safety criteria. When the orography is not very complicated, most of the track can be designed on embankment, with the exception of stretches of plateaus and mountainous areas where tunnels need to be built. The safety criterion is also very important in railway design. In case of tunnels, the eventuality of an accident in the track of one direction affects the track of the other direction if both tracks are installed in a single tunnel. Moreover, a fire event would also affect the service of both tracks. The increase of safety and security standards in the last years thus recommends the construction of one tunnel per track so that accidental events occurring in one track or direction do not affect the other, so that the likelihood of service interruption is much smaller.

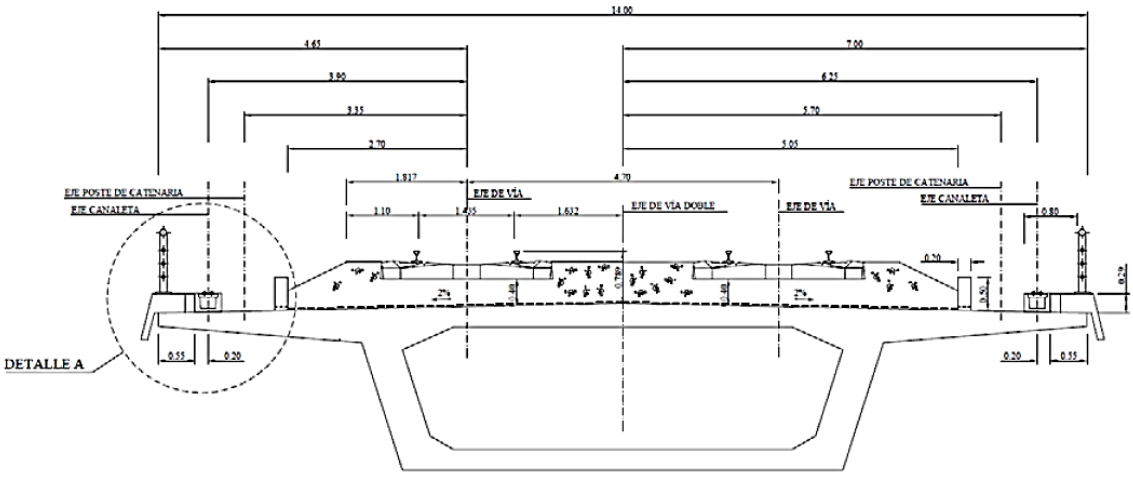

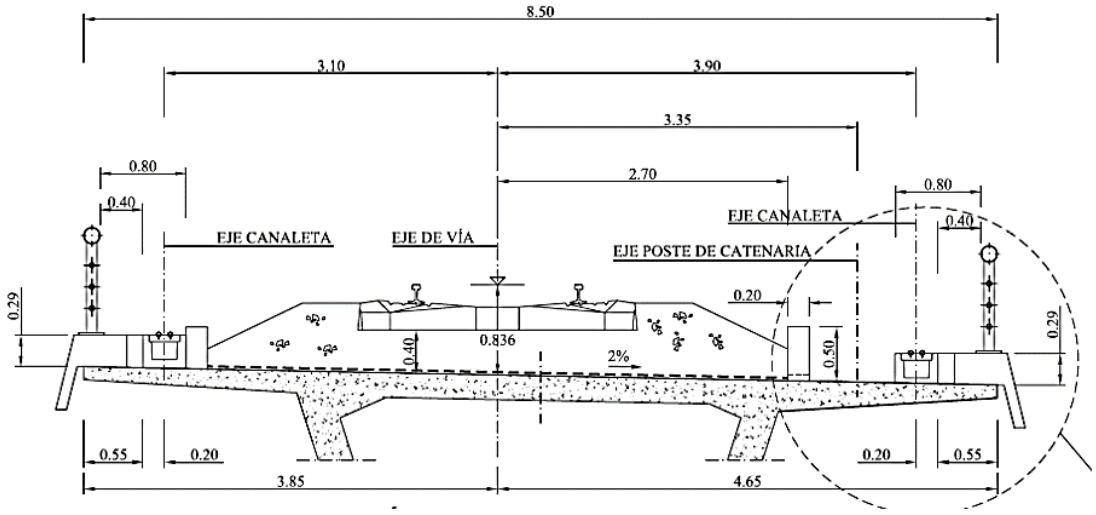

Figure 16. Cross-section for double track (top) and simple track (bottom). INECO 2018

The consideration of the former orography and safety criteria can lead to the usefulness of constructing the railway bridges in independent structures, i.e. one girder per track. In such a case, the railway bridge only carries one track rather than the two tracks. As it is shown in Figure 16, the 14 m wide cross-section for double track is modified to a 8.5 m wide cross-section for simple track. In both cases, the box section typically rests on piles and abutments using pot supports.

From the first installation of the Madrid-Seville line until today, the construction needs of high-speed lines have evolved. The lines that have been built recently or those which are in the process of being built run over regions of complex orography, in which most of the line can require successive tunnel-viaduct sections, as in the Pajares Pass or in the Madrid-Galicia line. This is the main reason that has lead to the separation of the track in tunnels and viaducts, from double to single track. Each direction runs through independent but parallel viaducts and tunnels. In addition, this is related to the previously mentioned evolution in safety criteria.

Not only have the new lines led to the change from double to single track structures, but also the installation of slab track has become very convenient because of the profusion of tunnels. Moreover, the installation of slab track in tunnels and the subsequent presence of viaducts (tunnel-viaduct-tunnel sequence) has made it convenient to use slab track also on the bridges. Thereby the need of transitions between ballasted and ballastless types of track is interestingly reduced. Furthermore, the technological development of slab track has made it competitive to offer the same level of service as the ballasted track.

In order to analyze the structural types of the bridges installed in the most recent high-speed lines in Spain, the main characteristics of some of them are summarized in Table 5. The main characteristics listed in Table 5 are the span length distribution, if it is hyperstatic or isostatic, and the cross-section. In the majority of the cases the cross-section is a box girder of 8.50 m width with a single slab track. It is important to remark that most of these examples are bridges of the new high-speed access to Galicia and the Pajares Pass. Also, it is important to remark that all sections were constructed with the VP prefabricated slab track system by AFTRAV (Figure 8), which consists of 5.1 m long prestressed concrete slabs supported on an elastomeric layer.

Name	Characteristics	Cross Section
Felgueira	<u>Bridge:</u> Hyperstatic, Three spans L_1=L_3=24.00 m; L_2=49.00 m Box section (b=8.50 m)	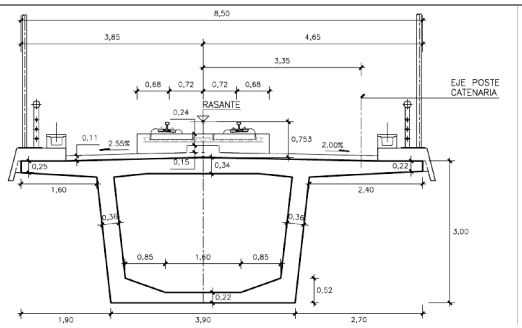
Huerna	<u>Bridge:</u> Isostatic L_1= 40.00 m Double precast U-section with on-site concrete top slab (b=9.50 m)	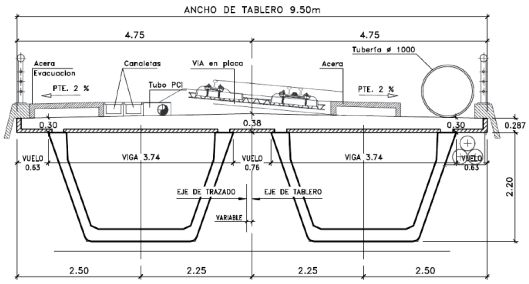
Leira	<u>Bridge:</u> Hyperstatic, Four spans L_2=L_3=60.00m; L_1=L_4=36.00m Box section (b=8.50 m)	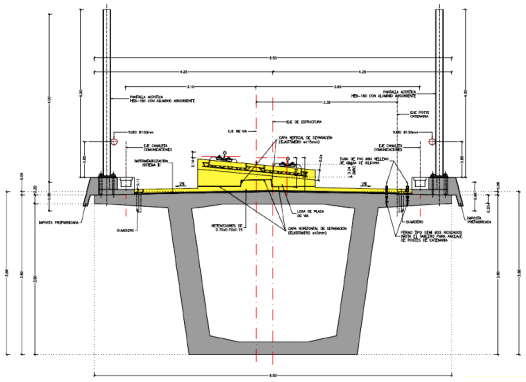
Os Portos	<u>Bridge:</u> Hyperstatic, Six spans L_1=L_6=25.00 m; L_2=L_3=L_4=L_5=44.00 m Box section (b=8.50 m)	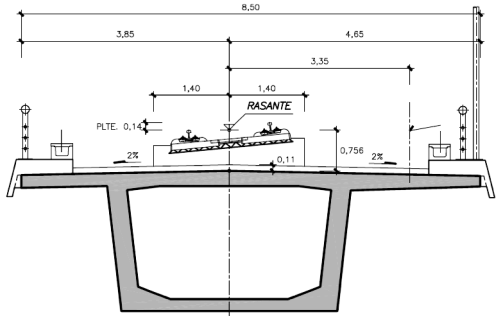

Pedregales	<u>Bridge:</u> Hyperstatic, Eighteen spans L_1=47.00 m; L_{17}=50.00 m; L_{18}=40.00 m From L_2 to L_{16}=55.00 m Box section (b=8.50 m)	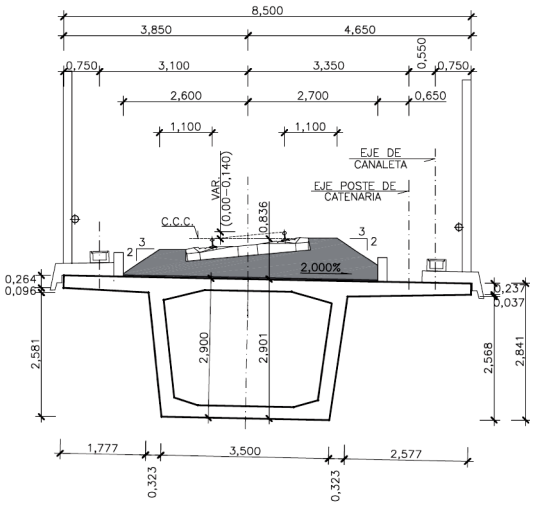
Pedro	<u>Bridge:</u> Hyperstatic, Six spans L_1=L_6=30.00 m; L_2=L_5=50.00 m; L_3=L_4=60.00 m; Box section (b=8.50 m)	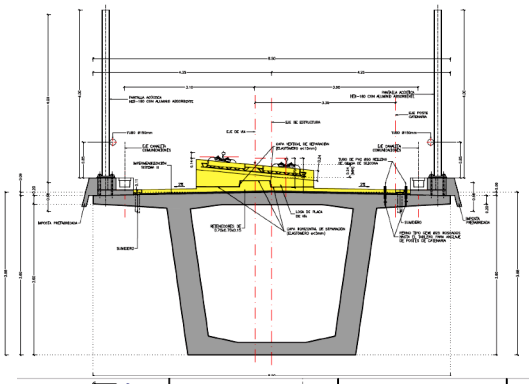
Porto	<u>Bridge:</u> Hyperstatic, Three spans L_1=L_3=26.00 m; L_2=38.00 m Box section (b=8.50 m)	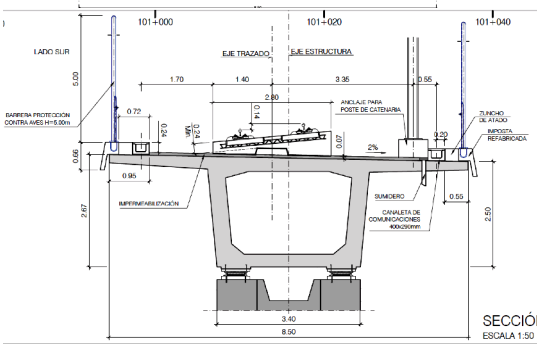
Teixeiras	<u>Bridge:</u> Hyperstatic, Nine spans L_1=42.00 m; L_2=58.00 m From L_3 to L_7=65.00 m L_8=49.00 m; L_9=35.00 m Box section (b=8.50 m)	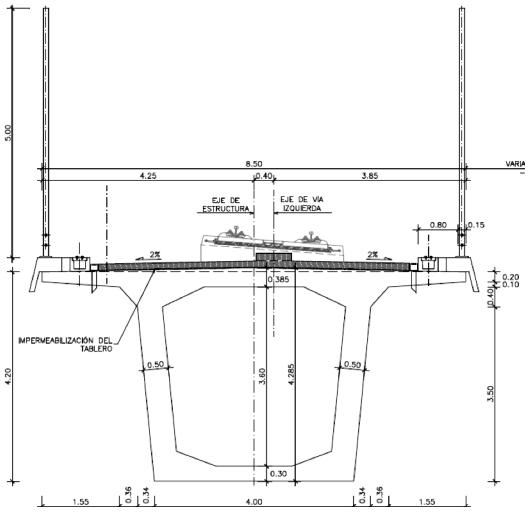

Tuela	<u>Bridge:</u> Hyperstatic, Six spans L_1==36.00 m; L_2=L_6=44.00 m L_3=L_4=L_5=55.00 m; Box section (b=8.50 m)	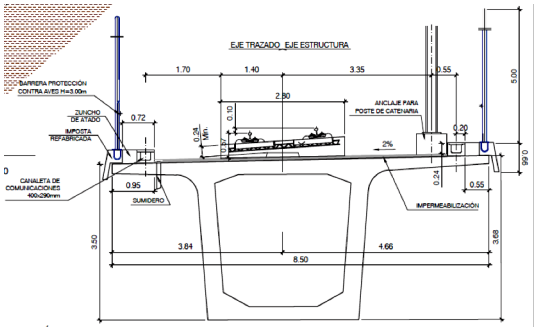
Vilavella	<u>Bridge:</u> Hyperstatic, Five spans L_1=L_5=23.00 m; L_3=44.00 m; L_2=L_4=29.00 m Box section (b=8.50 m)	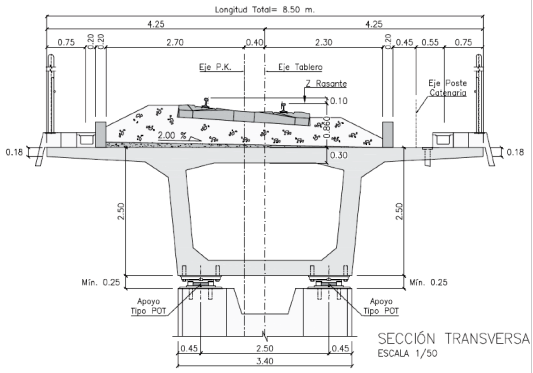

Table 5. Railway bridges: Characteristics and cross section. In all cases, the VP precast slab track system by AFTRAV was finally installed.

The analysis of the cross-sections allows calculating the mechanical properties of the above single-track bridges as a function of the span length. Such a study is very interesting since most of the existing formulations for the mechanical properties of bridges are based on double-track girders. To resume the mechanical properties of the cross-section of single-slab track railway bridges, Martín de Soto Aláez (2020) presented in his TFM a regression analysis which is shown in the graphics below:

- Figure 17: Height (m) over Span Length (m); Position of the centre of gravity (m) over Span Length (m).

- Figure 18: Area (m^2) over Span Length (m); Inertia (m^4) over Span Length (m).

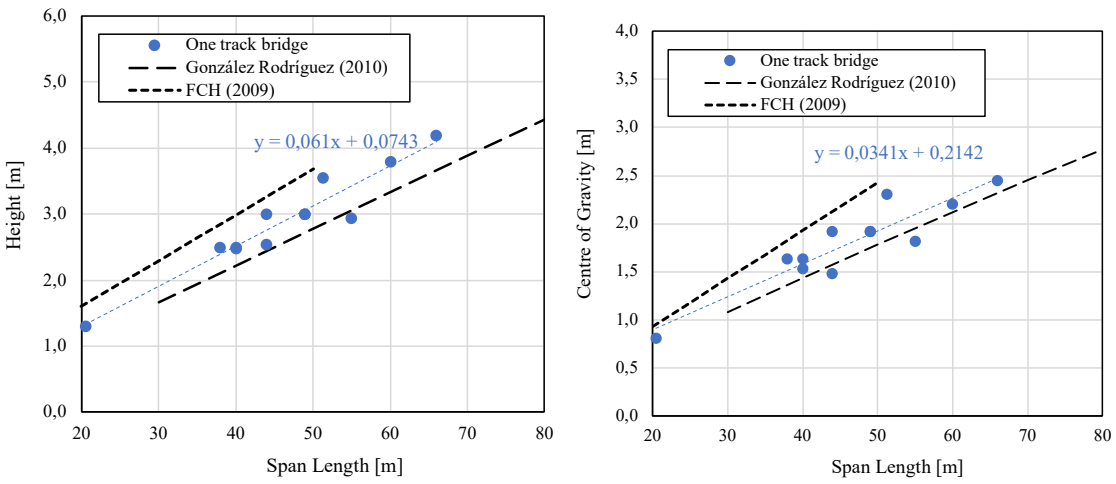

Figure 17. Mechanical Properties of Railway Bridges: Height and Distance of Centre of Gravity from the section's bottom.

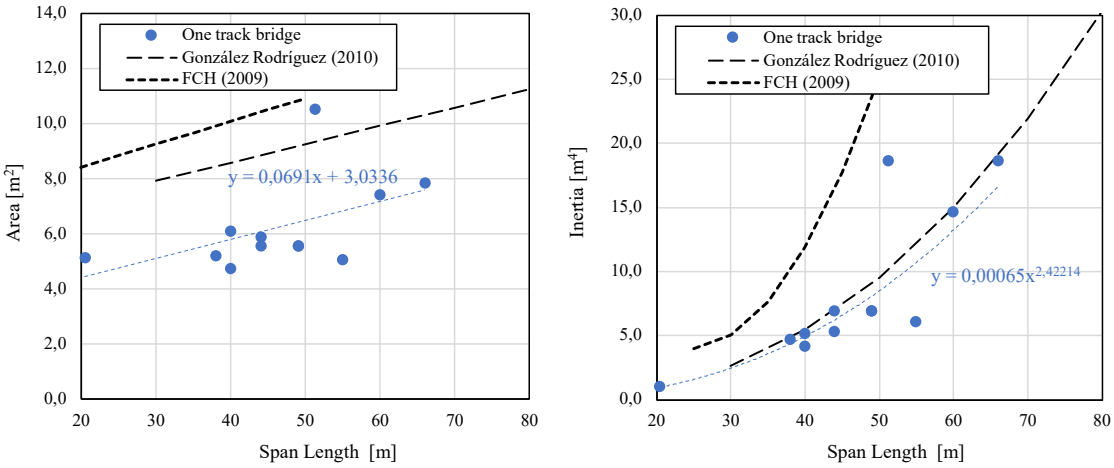

Figure 18. Mechanical Properties of Railway Bridges: Area and Inertia.

In Figure 17 and Figure 18 three different curves are shown. One of them (blue lines and points) makes reference to the least-squares fitting for single-track bridges according to Martín de Soto Aláez (2020), the two others make reference to existing formulations for double-track bridges. The difference between them is that FCH (2006) obtained formulations for the mechanical properties of the isostatic bridges on the Madrid-Sevilla, Madrid-Málaga and Madrid-Barcelona lines, while González Rodríguez (2010) studied both isostatic and hyperstatyc bridges with double track.

To sum up, the equations that will be used for the calculation of the mechanical properties in this TFM are the following ones according to Martín de Soto Aláez (2020) for slab track cases, L being the span length in m:

Height (m)	$h = 0.061L + 0.074$	(11)
Centre of Gravity (m)	$yG = 0.0341L + 0.214$	(12)
Area (m^2)	$A = 0.0619L + 3.033$	(13)
Inertia (m^4)	$I = 0.00065L^{2.42}$	(14)

2.6. High-speed trains

The train loads considered in the dynamic analysis of railway bridges must include the real distribution of moving loads and their velocity. In Spain, IAPF (2007) requires the consideration of the dynamic effects of all train types than can run over the line of each studied bridge. A detailed description of train types is given in Appendix C of IAPF (2007). Basically, train types can be classified as real trains and envelope HSLM trains.

In Europe, HS trains must guarantee the interoperability in all lines that conform the trans-European rail infrastructure. So, all trains and their speeds must be accounted for in the dynamic design. That has made necessary to define the so-called HSLM envelope trains referred to in Appendix C.1 of the IAPF (2007) in agreement with Eurocode 1 (UNE-EN 1991-2).

Such standards classify the HSLM for all European lines according to the non-constant length between the bogies in two train families, named Universal Dynamic Train-A (valid for multi- or single-span bridges with span length longer than 7.0 m) and Universal Dynamic Train-B (valid for single-span bridges shorter than 7.0 m). Both families guarantee envelope results of dynamic effects produced for all trains according to the interoperability request. The definition of Train-A and -B can be found in Figure 19 (Table 6) and Figure 20, respectively.

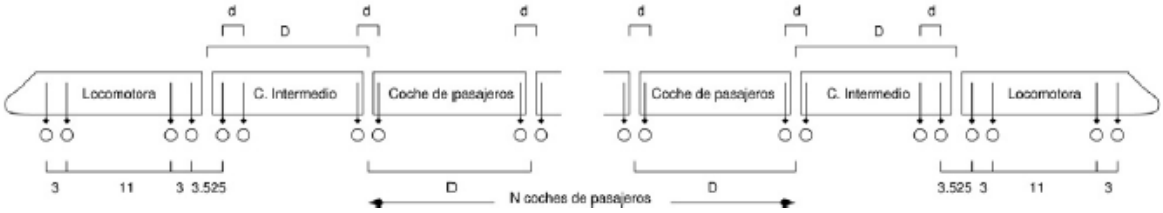

Figure 19. Universal Dynamic Train-A according to IAPF (2007)

Tren	*Número de coches de pasajeros N*	*Longitud del coche D* [m]	*Distancia entre ejes de un bogie d* [m]	*Carga nominal por eje P* [kN]
A1	18	18	2,0	170
A2	17	19	3,5	200
A3	16	20	2,0	180
A4	15	21	3,0	190
A5	14	22	2,0	170
A6	13	23	2,0	180
A7	13	24	2,0	190
A8	12	25	2,5	190
A9	11	26	2,0	210
A10	11	27	2,0	210

Table 6. Definition of distances and loads in Universal Dynamic Train-A

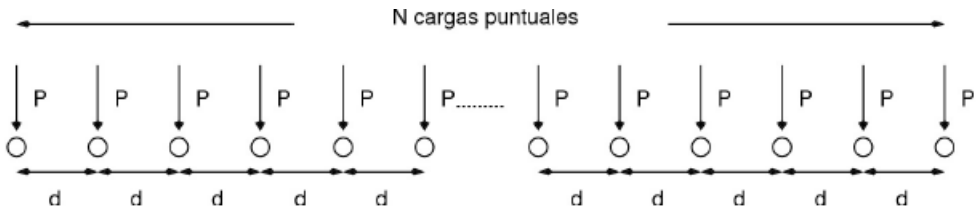

Figure 20. Universal Dynamic Train-B according to IAPF (2007)

Besides HSML envelopes, real trains for high-speed calculations are defined in Appendix C.2 of the IAPF. A detailed description of the axle loads and the separation between them, as given in IAPF, is reproduced in the following figures for articulated, conventional and regular trains. Additionally, lower-speed conventional trains (V < 220 km/h) are defined in Appendix C.3 of the IAPF, which are the basis of the heavy envelope UIC-71 train typically used in static design.

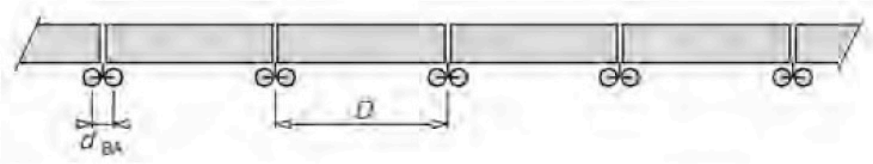

Articulados: Thalys, AVE-S101 y Eurostar.

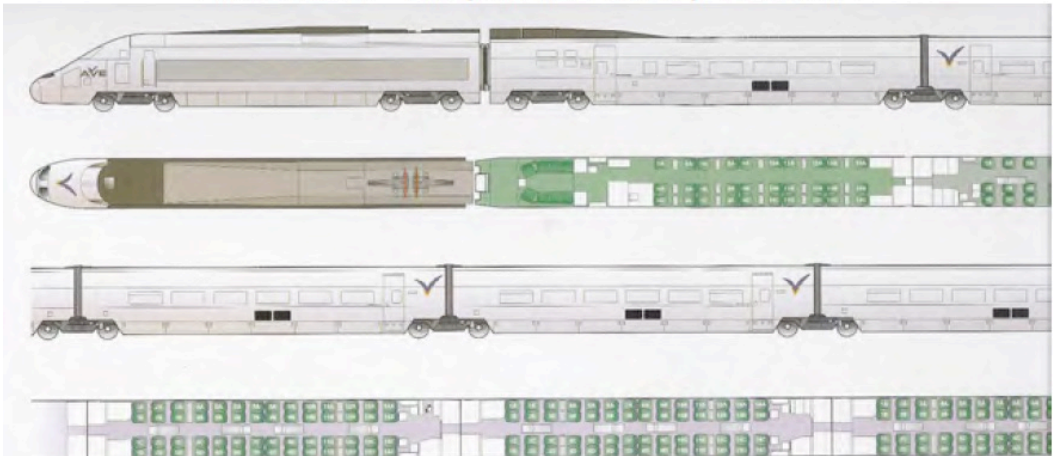

Figure 21. Thalys, AVE and Eurostar scheme according to Goicolea (2011)

l_k^a	F^b	l_k^a	F^b
0,000	170,0	200,190	170,0
3,000	170,0	203,190	170,0
14,000	170,0	214,190	170,0
17,000	170,0	217,190	170,0
20,275	163,0	220,465	163,0
23,275	163,0	223,465	163,0
38,975	170,0	239,165	170,0
41,975	170,0	242,165	170,0
57,675	170,0	257,865	170,0
60,675	170,0	260,865	170,0
76,375	170,0	276,565	170,0
79,375	170,0	279,565	170,0
95,075	170,0	295,265	170,0
98,075	170,0	298,265	170,0
113,775	170,0	313,965	170,0
116,775	170,0	316,965	170,0
132,475	170,0	332,665	170,0
135,475	170,0	335,665	170,0
151,175	170,0	351,365	170,0
154,175	170,0	354,365	170,0
169,875	163,0	370,065	163,0
172,875	163,0	373,065	163,0
176,150	170,0	376,340	170,0
179,150	170,0	379,340	170,0
190,150	170,0	390,340	170,0
193,150	170,0	393,340	170,0

l_k^a	F^b	l_k^a	F^b
0,00	172,1	200,15	172,1
3,00	172,1	203,15	172,1
14,00	170,7	214,15	170,7
17,00	170,7	217,15	170,7
20,28	131,6	220,43	131,6
23,28	131,6	223,43	131,6
38,98	161,9	239,13	161,9
41,98	161,9	242,13	161,9
57,68	169,2	257,83	169,2
60,68	169,2	260,83	169,2
76,38	167,9	276,53	167,9
79,38	167,9	279,53	167,9
95,08	160,5	295,23	160,5
98,08	160,5	298,23	160,5
113,78	167,9	313,93	167,9
116,78	167,9	316,93	167,9
132,48	169,2	332,63	169,2
135,48	169,2	335,63	169,2
151,18	161,9	351,33	161,9
154,18	161,9	354,33	161,9
169,88	131,6	370,03	131,6
172,88	131,6	373,03	131,6
176,16	170,7	376,31	170,7
179,16	170,7	379,31	170,7
190,16	172,1	390,31	172,1
193,16	172,1	393,31	172,1

l_k^a	F^b	l_k^a	F^b
0,000	170,0	195,095	170,0
3,000	170,0	198,095	170,0
14,000	170,0	213,795	170,0
17,000	170,0	216,795	170,0
20,275	170,0	232,495	170,0
23,275	170,0	235,495	170,0
38,975	170,0	251,195	170,0
41,975	170,0	254,195	170,0
57,675	170,0	269,895	170,0
60,675	170,0	272,895	170,0
76,375	170,0	288,595	170,0
79,375	170,0	291,595	170,0
95,075	170,0	307,295	170,0
98,075	170,0	310,295	170,0
113,775	170,0	325,995	170,0
116,775	170,0	328,995	170,0
132,475	170,0	344,695	170,0
135,475	170,0	347,695	170,0
151,175	170,0	363,395	170,0
154,175	170,0	366,395	170,0
169,875	170,0	369,670	170,0
172,875	170,0	372,670	170,0
188,575	170,0	383,670	170,0
191,575	170,0	386,670	170,0

Table 7. Head distance [m] and axle load [kN] for the train composition. From left to right: Thalys, AVE and Eurostar data

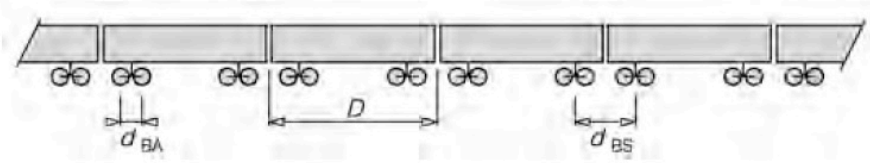

Convencionales: Ice2, AVE-S103, Etr-y, Virgin.

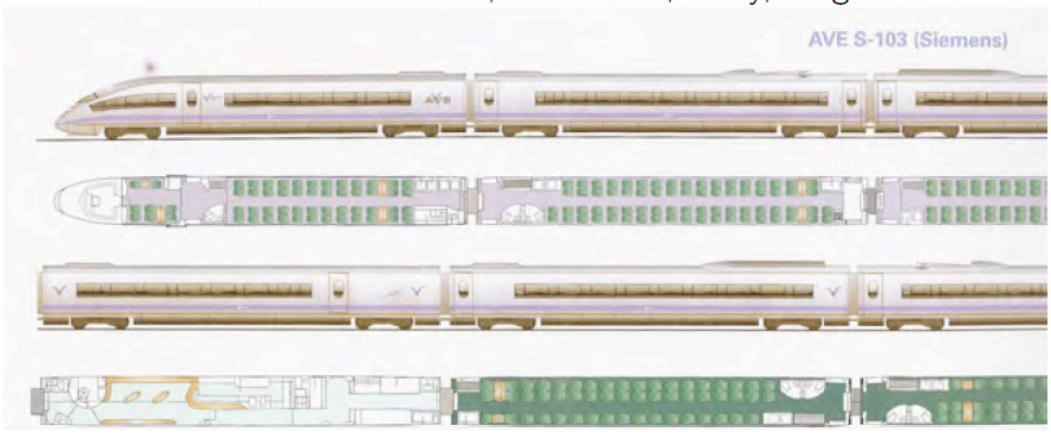

Figure 22. ICE2, AVE-S103, Etr-y and Virgin Scheme according to Goicolea (2011)

l_k^a	F^b	l_k^a	F^b
0,00	195,0	177,71	112,0
3,00	195,0	180,21	112,0
11,46	195,0	196,71	112,0
14,46	195,0	199,21	112,0
19,31	112,0	204,11	112,0
21,81	112,0	206,61	112,0
38,31	112,0	223,11	112,0
40,81	112,0	225,61	112,0
45,71	112,0	230,51	112,0
48,21	112,0	233,01	112,0
64,71	112,0	249,51	112,0
67,21	112,0	252,01	112,0
72,11	112,0	256,91	112,0
74,61	112,0	259,41	112,0
91,11	112,0	275,91	112,0
93,61	112,0	278,41	112,0
98,51	112,0	283,31	112,0
101,01	112,0	285,81	112,0
117,51	112,0	302,31	112,0
120,01	112,0	304,81	112,0
124,91	112,0	309,71	112,0
127,41	112,0	312,21	112,0
143,91	112,0	328,71	112,0
146,41	112,0	331,21	112,0
151,31	112,0	336,06	195,0
153,81	112,0	339,06	195,0
170,31	112,0	347,52	195,0
172,81	112,0	350,52	195,0

l_k^a	F^b	l_k^a	F^b
0,00	187,0	149,90	120,0
3,00	187,0	152,90	120,0
12,00	187,0	168,90	120,0
15,00	187,0	171,90	120,0
19,40	120,0	176,00	120,0
22,40	120,0	179,00	120,0
38,40	120,0	195,00	120,0
41,40	120,0	198,00	120,0
45,50	120,0	202,10	120,0
48,50	120,0	205,10	120,0
64,50	120,0	221,10	120,0
67,50	120,0	224,10	120,0
71,60	120,0	228,20	120,0
74,60	120,0	231,20	120,0
90,60	120,0	247,20	120,0
93,60	120,0	250,20	120,0
97,70	120,0	254,30	120,0
100,70	120,0	257,30	120,0
116,70	120,0	273,30	120,0
119,70	120,0	276,30	120,0
123,80	120,0	280,70	187,0
126,80	120,0	283,70	187,0
142,80	120,0	292,70	187,0
145,80	120,0	295,70	187,0

l_k^a	F^b	l_k^a	F^b
0,00	170,0	136,50	170,0
2,70	170,0	139,20	170,0
17,00	170,0	143,40	170,0
19,70	170,0	146,10	170,0
23,90	170,0	160,40	170,0
26,60	170,0	163,10	170,0
40,90	170,0	167,30	170,0
43,60	170,0	170,00	170,0
47,80	170,0	184,30	170,0
50,50	170,0	187,00	170,0
64,80	170,0	191,20	170,0
67,50	170,0	193,90	170,0
71,70	170,0	208,20	170,0
74,40	170,0	210,90	170,0
88,70	170,0	215,10	170,0
91,40	170,0	217,80	170,0
95,60	170,0	232,10	170,0
98,30	170,0	234,80	170,0
112,60	170,0	239,00	170,0
115,30	170,0	241,70	170,0
119,50	170,0	256,00	170,0
122,20	170,0	258,70	170,0

Table 8. Head distance [m] and axle load [kN] for the train composition. From left to right: ICE2, Etr-y and Virgin data

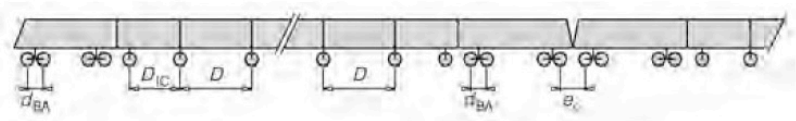

Regulares: AVE-S102 (TALGO).

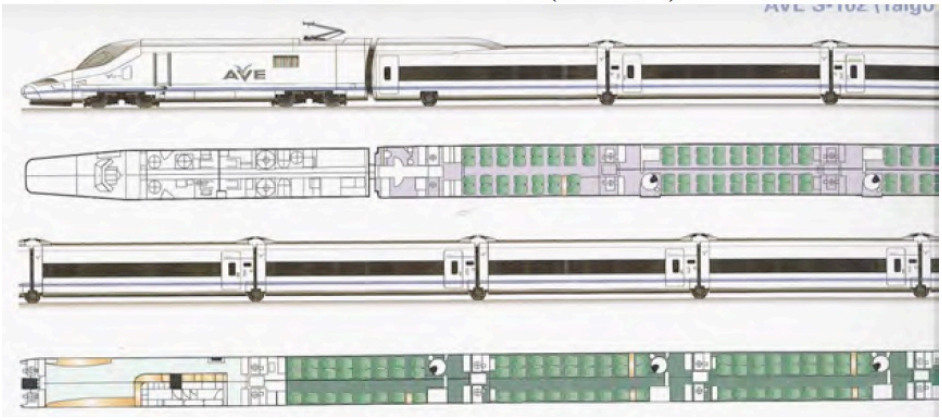

Figure 23. AVE-S102 (TALGO) according to Goicolea (2011)

l_k [a]	F [b]	l_k [a]	F [b]
0,00	170,0	183,49	170,0
2,65	170,0	186,14	170,0
11,00	170,0	194,49	170,0
13,65	170,0	197,14	170,0
19,13	170,0	202,62	170,0
28,10	170,0	211,59	170,0
41,24	170,0	224,73	170,0
54,38	170,0	237,87	170,0
67,52	170,0	251,01	170,0
80,66	170,0	264,15	170,0
93,80	170,0	277,29	170,0
106,94	170,0	290,43	170,0
120,08	170,0	303,57	170,0
133,22	170,0	316,71	170,0
146,36	170,0	329,85	170,0
155,33	170,0	338,82	170,0
160,80	170,0	344,29	170,0
163,45	170,0	346,94	170,0
171,80	170,0	355,29	170,0
174,45	170,0	357,94	170,0

Table 9. Head distance [m] and axle load [kN] for the train composition. TALGO data

Chapter 3

Methodology. Model description

3.1. Introduction

The present Chapter is intended to describe the details of the numerical models employed for the dynamic analysis of railway bridges subjected to moving loads within the high-speed domain. Among the possible methodologies available for the solution of the dynamic problem discussed in Chapter 2, the one employed in this TFM has been the finite element method (FEM) with full time integration in order to obtain the time-dependent dynamic response of the structure against moving train loads. The analysis is focused on vertical dynamic effects without torsion nor lateral effects, i.e. it is assumed that the vertical train loads have no lateral eccentricity with respect to the axis of the bridge. This is consistent with the single-track bridge typologies where ballastless track systems have been installed in Spain, as studied in Section 2.5

Due to the fact that a key element of the TFM is the influence of the track type, three track typologies have been studied, namely a reference ballasted track and two types of ballastless track, depending on the connection of the track with the bridge structure: monolithic (i.e. the slab track is rigidly joined to the bridge girder) and independent (i.e. an intermediate resilient layer is considered to be placed between the slab track and the bridge girder). In order to consider the train loads, the moving load model consisting of separated loads passing the structure at the train velocity has been chosen, rather than more sophisticated vehicle-track interaction models described in Chapter 2 (moving mass-spring-dampers). This type of load model leads to conservative results, as discussed in Chapter 2.

Two types of bridges have been studied: a single-span statically determinate one and a three-span statically indeterminate one. Moreover, two types of trains have been considered (Talgo and AVE). In all cases, the objective of the model is to provide results in terms of vertical deflections and accelerations so that a comparison of the influence of the track type can be performed.

In Section 3.2, the general aspects of the numerical methodology are explained. In Sections 3.3 and 3.4, a comprehensive description of the models for ballasted and ballastless track systems is given, respectively.

3.2. Methodology

In order to develop the present work, it is necessary to carry out a complete study of the effect of both single and complete train loads on the bridge, which has required the use of the finite element method (FEM). The calculation sequence has started from the lowest simplicity (single moving point load passing over a single-span beam without explicit consideration of the track components) to the most complex compositions of both the configuration of the track-structure interaction and the full sequence of train load. Modelling is carried out with ANSYS version 15.0 (ANSYS 2013), a finite element software which has been employed using linear-elastic analysis with full time integration. A two-dimensional model of the structure and the external loads has been completed for all the cases and parametric analyses. The input computational models have been programmed by this TFM's author in a parametric way in order to ease the completion of the parametric studies.

Two-dimensional modelling with full integration in time requires solving the dynamic equations of motion (eq. (9)) at each node of the model, so that a precise time-dependent solution can be obtained and exported at desired locations of the structure and superstructure. As commented above, the model is not a vehicle-track-structure interaction analysis, but a track-interaction model with the vehicle action introduced directly as the sequence of axle forces given by the (IAPF 2007). The components of the track, the structure and the interaction between them are modelled in this work. The irregularities of the rail have not been included in the models, as such defects are supposed to be rather small in highly-maintained railway lines and its eventual effect can then be added to the model results by other formulations (e.g. the φ'' factor referred to in Section 2.3).

In the different solved cases, the exported results are the vertical displacements, whose second derivatives are the accelerations suffered by the elements when they are subjected to moving loads under different conditions. The obtention of these accelerations in the structure is essential to check if the comfort requirements of the design standards are fulfilled. A longitudinal overview of the models is represented in Figure 24, where it can be noted that the rails and the bridge are connected through a set of springs and dampers defining the components of the track. The length of the model is longer than the bridge because a length of L_{ter} (50 m) of the track on lateral embankments is modeled at both sides of the bridge. The detailed cross-sections of the track-bridge models are explained in Sections 3.3 and 3.4. In general, all the components of the track and the bridge structure are modeled with beams, springs and dampers with the help of the ANSYS capabilities.

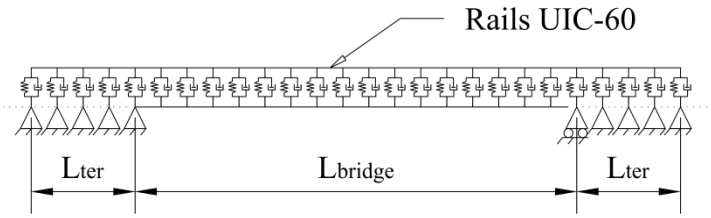

Figure 24. Longitudinal scheme of the numerical model (case of sinlge-span bridge)

For the purpose of the study, the rail and the bridge have been modelled with BEAM3 elements (2D Euler beam contained in the XY-plane). Such a beam is a 2-node uniaxial element with three degrees of freedom at each node (displacements in the x and y axes, and rotation in z), which can be subjected to axial forces, shear forces (though shear strains are neglected) and bending moments. It is defined by its mechanical properties (real constants in ANSYS): area, inertia, height and centroid position, and by the material that composes the beam: modulus of elasticity, Poisson's coefficient, damping ratio and density.

In each model hereafter, the particular components of each track type are defined through COMBIN14 and LINK1 elements, and in some cases MASS23 elements are also required:

COMBIN14 is a longitudinal spring-damper element with optional torsional stiffness (not used in the present work). In the longitudinal axis it contains both a uniaxial spring and a damper with allowed tensile and compressive forces in which there are two degrees of freedom at each node: translations in the x and y-axis. The element as a whole has no mass per se and it is fully defined by the damping coefficient and the spring stiffness constant.

Elements of type LINK1 refer to uniaxial springs or two-dimensional bars. It is an element that can be subjected to axial compressive and tensile forces with two degrees of freedom at each node: translations in the x- and y-axis. It is defined with two real constants that depend on the area of the section and its initial deformation (which throughout the present calculation process will be taken as zero corresponding to the rest state when no loads act on the structure). In addition, the required material properties are its modulus of elasticity, Poisson's ratio, damping ratio and density.

Finally, MASS21 type elements have been used to model the sleepers as single masses concentrated at one node. This element can have up to six degrees of freedom, but only three are allowed in the present two-dimensional calculations: translations in the x- and y-axis and rotations in the z-axis. The element is defined at a single node with a concentrated mass component.

Particular values of the parameters of the elements defined above (mechanical and material properties) depend on the case being studied, which will be described in more detail in Sections 3.3 and 3.4. Depending on the type of track and its configuration, it is necessary to add or subtract elements to the model.

All models have in common that BEAM3 elements are used for the rails and the bridge. The properties of the rail are those of two UIC-60 steel rails according to ADIF standard (2021).

It must be noted that the rail has been modelled along a length longer than the length of the bridge at both sides (Figure 24), in order to simulate the possible influence of the circulation of the train on the lateral embankments before entering and after leaving the bridge. Therefore, the BEAM3 elements of the rail are extended an additional length of L_{ter} = 50 m at each end. To simplify the model, the rails are located along a horizontal line positioned at the COG of the rail UIC-60.

Depending on the type of bridge (number of spans and their lengths), the mechanical properties of the BEAM3 beam type elements are different. In the present Master's thesis, only one-track bridges with 8.5 m top width section (as represented in Figure 16) have been studied because it is the dominant typology of the bridges where ballastless track systems have been recently installed in Spain. To establish the mechanical properties of the bridges, equations (11)-(14) by Martín de Soto Aláez (2020) previously defined in Section 2.5 of this document are used. For the modelling of the bridges, it has been taken into account whether they are short or long. The short bridges are considered to be isostatic with a span of up to 40 m, while long bridges are those with hyperstatic, continuous beams and with lengths of more than 40 m in some of the spans. In this TFM the bridge boundary conditions (simple supports) are located at the extremes of the span in the isostatic case and also at the intermediate piles positions in the hyperstatic cases. The constrains block the vertical displacement and, only at one the ends, the horizontal displacement, simulating the effect of a fixed abutment. In all calculations the material used for the bridge is Prestressed Concrete HP40. It must be remarked that the density of the bridge has been increased in the model with respect to the concrete density in order to include the mass of non-structural elements (catenary, barriers, ballast retainer and parapets, in total of 13.70 t/m). The length of the beam elements in the mesh has been equal to the longitudinal spacing between rail seats (0.60 m for ballasted track and 0.65 m for ballastless tracks).

The connection between the rail and the bridge (or embankment in the end zones) is modelled with mass, spring and damper elements depending on the type of track as discussed above and is detailed in Sections 3.3 and 3.4 for each case.

The loading type has been analysed in steps of increasing complexity. First of all, the passage of a single moving point load of 225 kN has been studied, representing an isolated axle of a train which is forced to pass at different speeds between 200 and 360 km/h along the model. In the next step of further complexity, the calculations have then been performed with the passage of two different high-speed trains operating in Spanish networks and defined in the IAPF (2007) standard. Such trains are the Talgo (Figure 23 and Table 9) and the AVE-S101 (Figure 21 and Table 7). All cases are solved for each type of track, with each train passing at speeds from 200 to 360 km/h. The train velocity defines the time discretization of the model in order to complete the full time integration. The axle loads are subsequently applied and removed in the nodes of the rails as a function of the velocity (Figure 25). The time step for the integration is adapted by ANSYS as a function of the convergence requirements, depending on the normal, minimum and maximum time steps defined by the user (in the present Master's thesis, the normal, minimum and maximum time have been set to 0.003, 0.001 and 0.01 s). An additional final time step has been considered in the numerical model after the train leaves the bridge in order to simulate the free vibration decay of the unloaded structure (the time of this step has been 0.2 times the train needs to cross the bridge).

All the input files defining the finite element mesh, material and element properties, loading sequence and train loads definition have been programmed by this work's author as no prepared routines are available in ANSYS. According to the previous explanations, the bridge model is able to simulate a large number of cases, which can be finally classified according to four main variables, defined in Table 10:

Variables	Values
Speed	from 200 to 360 km/h (increments of 10 km/h)
Span Length	Short (Isostatic, 20 m span length) or Long (Hyperstatic, 40 + 60 + 40 m span length)
Track Structure	Ballasted track, Monolithic slab track or Independent slab track.
HS Train	AVE-S101 or TALGO

Table 10. Variables of modelling

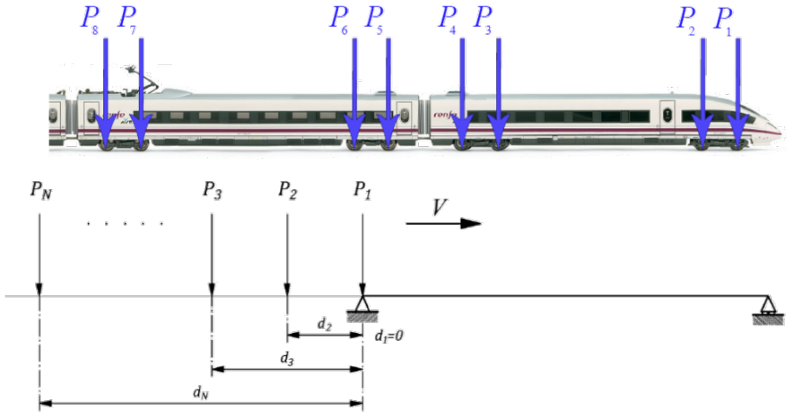

Figure 25. Train of loads crossing the bridge. Courtesy of Dr. J.M. Soria.

3.3. Description of model with ballasted track

One of the main variables to be studied with the model is the type of track structure. The first track type is the ballasted track. The studied cross-section is depicted in Figure 26. Note that the drawing of the bridge cross-section is illustrative, and the slight non-symmetric position of the track with respect to the vertical axis is because many real bridges typically have a very large curvature in plant which does not affect the vertical behavior studied here. Therefore, in the model it is assumed that the position of the track is centered with respect to the bridge, i.e. the load has no eccentricity and, thus, there is no torsion. The components of the cross-section are modeled in ANSYS according to the scheme of Figure 27. The corresponding values of material and mechanical properties are listed in Table 11.

To model this case, the components of the track from the top to the bottom begin with the UIC-60 rails (2 rails for a track), which, as previously mentioned in Section 3.2, is a linear-elastic steel beam common for all studied cases, modelled with BEAM3 elements. Then there are the fasteners, which join the rail to the sleepers, spaced every 0.60 m in longitudinal direction. The fastening system is introduced as a linear spring-damper COMBIN14 element.

Its properties (stiffness and damping coefficient) correspond to those defined in the CEDEX Monograph by Goicolea et al. (2007). It is worth mentioning that the dynamic vertical stiffness of the fasteners (governed by the rail pads) of ballasted tracks is considerably higher than that of ballastless track systems (150 kN/mm and 50 kN/mm, respectively).

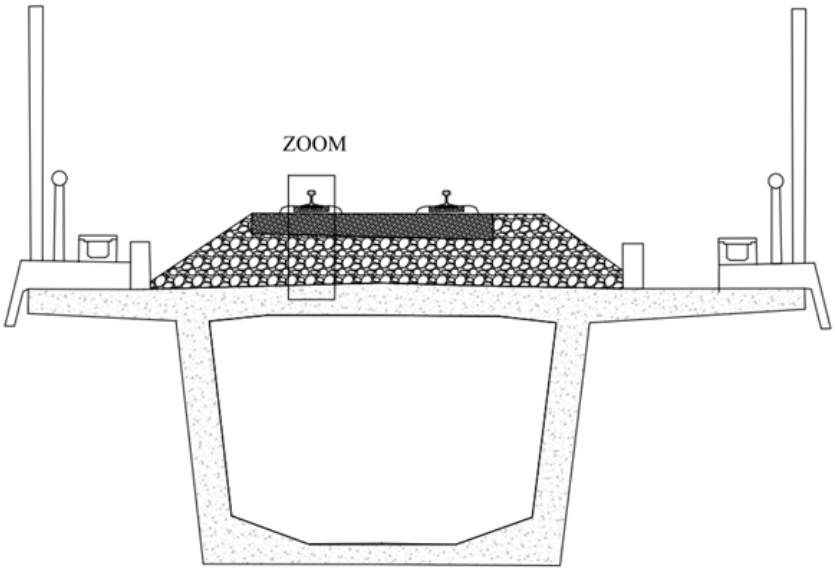

Figure 26. Bridge cross-section with ballasted track

Furthermore, in this ballasted track model, the sleepers are defined as point masses (MASS23) concentrated at the position of their centroid. The ballast layer of 0.5 m height is defined by linear spring LINK1 elements whose properties are taken from the same reference as the fastenings. Also this LINK1 includes the mass and the damping of the ballast layer. It should be noted that the damping of this model, as well as the successive ones, are introduced through the Rayleigh beta coefficient (alpha coefficient is equal to 0).

The material of the bridge girder will also be the same concrete, a HP-40, with increased density to include the mass of non-structural components.

As it can be observed in Figure 27, the legend indicates the centroids of the structural elements and track components, where the nodes of the model are located. The scheme on the left shows a sketch of the cross-section from the rail to the bridge, where all the layers and components that make up the model are defined, while on the right-hand side of the figure, the finite elements involved in the model can be observed, making reference to each of the components of the cross-section.

In order to verify the goodness of the track-bridge interaction model, a first simplified model without explicit modelling of the track components has been simulated for the case of a single-span bridge under a single moving load of 225 kN. In this model, only the bridge girder (including the mass of all the components of the track) has been modelled with BEAM3 elements.

The results have been compared to those of the full track-bridge interaction model in order to check that the more complex model makes sense and, therefore, it can be used with confidence for all the other cases. Such comparisons are explained in Section 4.3.1.

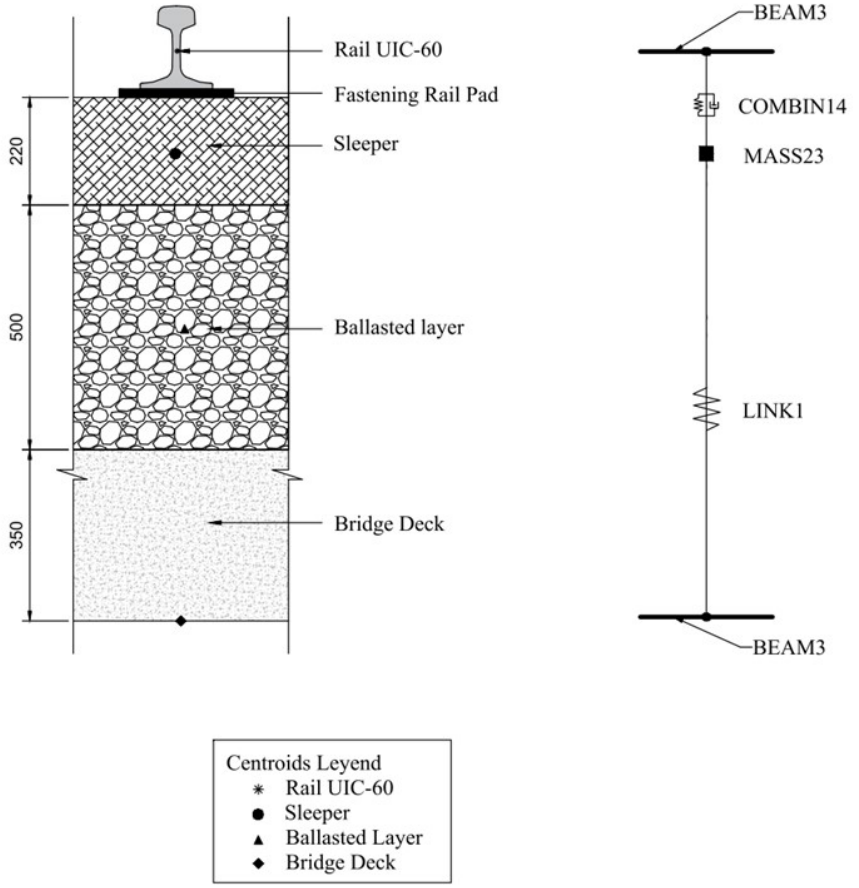

Figure 27. Ballasted scheme for modelling (note that the distance of 350 mm from the top of the girder to its centroid in this figure is only orientative).

Components of modelling	Element	Material	Properties
Rail UIC-60	BEAM3	Steel E_s = 2x10^8 kN/m^2, ν = 0.3, ρ = 7.85 t/m^3	A = 76.7 cm^2; I = 3038cm^4; COG_i = 8.09 cm; h = 172 mm
Fastening rail pad	COMBIN14		K = 150 kN/mm; C = 15 kNs/m
Sleeper	MASS21	M = 357.5 kg	-
Ballast layer	LINK1	ρ = 1.8 t/m^3	Bedding modulus c = 0.2 N/mm^3; C = 12.3 kNs/m/rail seat
Bridge deck	BEAM3	Concrete E_c = 37.1 GPa; ρ = 2.5 t/m^3 (plus the mass of non-structural elements); ν = 0.2	A, I, h, COG acc. to Martín de Soto Aláez (2020), eqs. (11) to (14); ξ = 2%

Table 11. Ballasted track model. Elements, materials and properties values

3.4. Description of model with ballastless track

The second part of the study has to do with the consideration of ballastless track (Figure 28). Within the ballastless track systems, two cases have been studied: a first one in which the slab track system is monolithically joined to the bridge, and a second one in which the slab track system is independent to the bridge, with an intermediate elastomeric layer between them. In both cases, the ballast layer of Section 3.3 is replaced with a concrete slab and a layer of mortar underneath it.

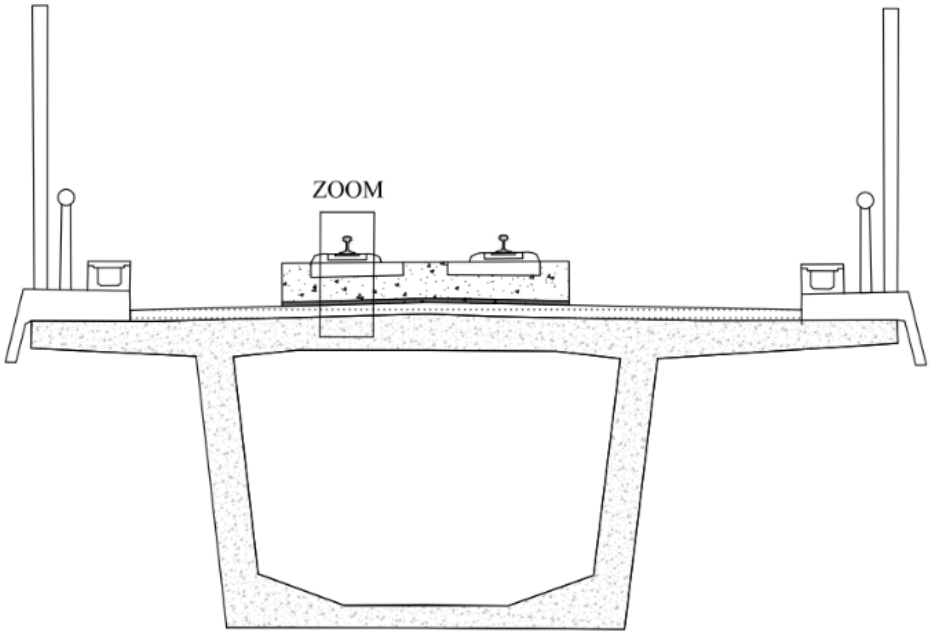

Figure 28. Bridge Cross section with slab track

It should be noted that slab track models are designed in both cases taking into account that the slab and the mortar or concrete layer are infinitely rigid in vertical direction and with no damping.

3.4.1. Monolithic slab track

This first type of ballastless track is considered to behave monolithically with the bridge girder, which means that the components of the track are joined rigidly to the top side of the bridge. This can be achieved by surface roughness, connecting shear keys, dowels or stoppers. This ballastless track system can be achieved either with prefabricated slabs supported on a lower cementitious base or mortar layer (Figure 11c) or with a continuous concrete slab on a mortar base (Figure 11d). The last situation is the most typical, and it is for example the case of the Rheda system or the Bx-AFTRAV system, both with embedded twin-block sleepers in the concrete slab. For the present work, the cross-section with the components shown in Figure 29 has been considered. The ballastless track consists of a 0.20 m height concrete slab supported on a mortar or cement-based layer of 0.15 m thickness. The width of the slab and the mortar is 3.60 m.

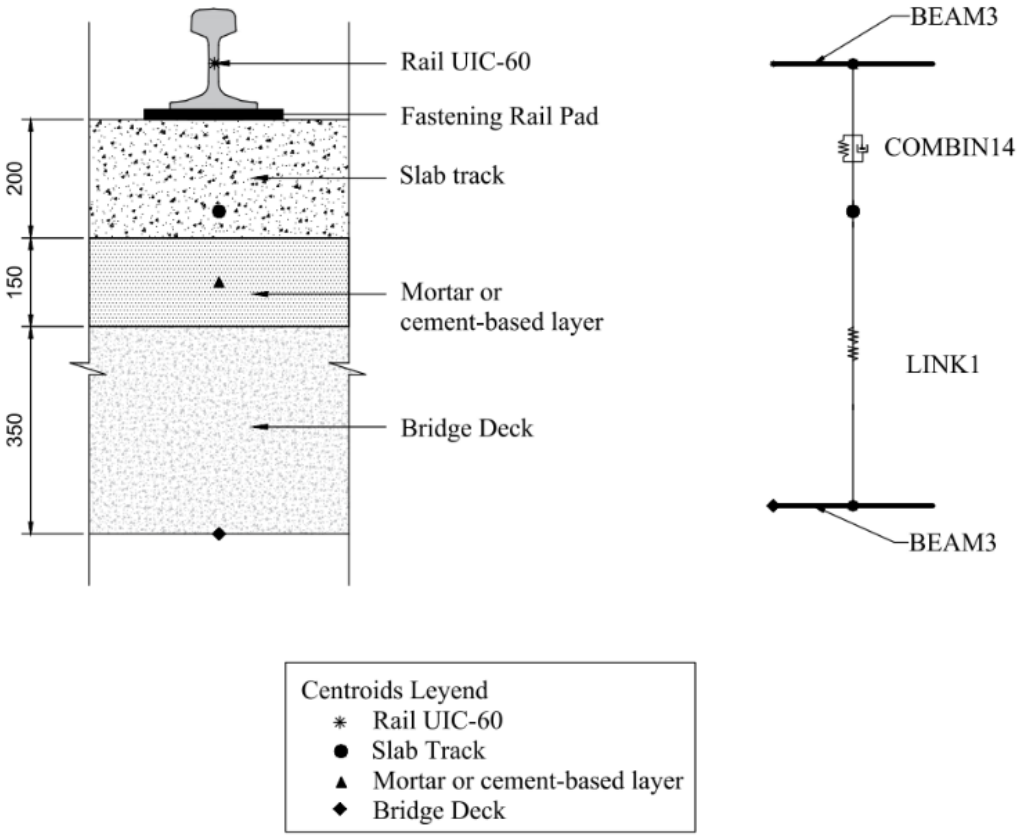

Figure 29. Monolithic slab track scheme for modelling (note that the distance of 350 mm from the top of the girder to its centroid in this figure is only orientative)

In the legend of Figure 29 the centroids of the structural elements and components of the track are shown again as nodes. The longitudinal distance between rail seats is 0.65 m. At the right of Figure 29, the finite elements used in the ANSYS 15.0 model are represented. The UIC-60 rails defined as BEAM3 elements are connected to the concrete slab by the COMBIN14 elements representing the fastening system. It is again noted that the vertical dynamic stiffness of the fastenings in ballastless track systems is smaller than that of ballasted tracks (refer to the parameters in Table 12). It should be also noted that, as mentioned above in Section 3.2, the properties of the rail and the fasteners refer to the set of two per section, concentrated at the centre of gravity of the fasteners.

Underneath, the connection with the bridge is made through a LINK1 element that represents simultaneously the concrete slab and the mortar or cement layer. It has infinite vertical stiffness and includes the mass of the two layers with no damping.

In the following Table 12, the values of the material and real structural properties of the elements are listed.

Components of modelling	Element	Material	Properties
Rail UIC-60	BEAM3	Steel E_s = 2 x 10^8 kN/m^2, ν = 0.3 ρ = 7.85 t/m^3	A = 76.7 cm^2; I = 3038 cm^4; COG_i = 8.09 cm; h = 172 mm
Fastening	COMBIN14		K = 50 kN/mm; C = 15 kNs/m
Slab track and mortar/cement based layer	LINK1	ρ = 2.5 t/m^3 $E = \infty$	-
Bridge Deck	BEAM3	Concrete E_c = 37.1 GPa; ρ = 2.5 t/m3 (plus the mass of non-structural elements); ν = 0.2	A, I, h, COG acc. to Martín de Soto Aláez (2020), eqs. (11) to (14); ξ = 2%

Table 12. Monolithic Slab Track Model. Elements, materials and properties values

3.4.2. Independent slab track

The last studied case is the independent slab track, which differs from the monolithic slab track in the fact that a resilient layer is introduced between the concrete layer and the mortar or cement base. Such a resilient layer can be achieved with a CA or elastomeric material and it is intended to isolate the behaviour of the concrete slab from the behaviour of the bridge. In this ballastless track system, the top concrete slab tends to work as a floating slab on an elastic foundation. It is a track type used for vibration mitigation in urban or sensitive zones because the elastic layer is of great importance as a damper for the loads that are introduced into the system. Figure 11a-b in section 2.4.1 shows an example of this type of track.

The components of the cross-section of the independent slab track system studied here are represented in Figure 30. It should be noted that the nodes for connection of the elements are once again made at the centroids of the real structural elements. The model is almost identical to the previous one (Figure 29), but a COMBIN14 spring-damper element divides the LINK1 element to represent this intermediate elastomeric layer between the concrete slab and the mortar/cement-based layer. The sketch of the scheme of the finite elements reproducing the real structural elements and components of the track can be seen in the right hand-side of Figure 30. The width of the concrete slab and mortar layer have been 2.50 m in this case.

The list of elements, their materials and structural properties are defined in Table 13. It must be mentioned that the case studied here is an extreme situation regarding the elasticity of the resilient layer in order to analyse how its flexibility can affect the dynamic behaviour of the bridge and the track. A significantly low bedding modulus and a high damping ratio have been therefore considered. The Spanish VP system by AFTRAV (Figure 8) or the Austrian Porr system are intermediate situations between this case and the monolithic one explained in Section 3.4.1, because they have an elastomeric layer under the precast concrete slabs but not as flexible as considered here.

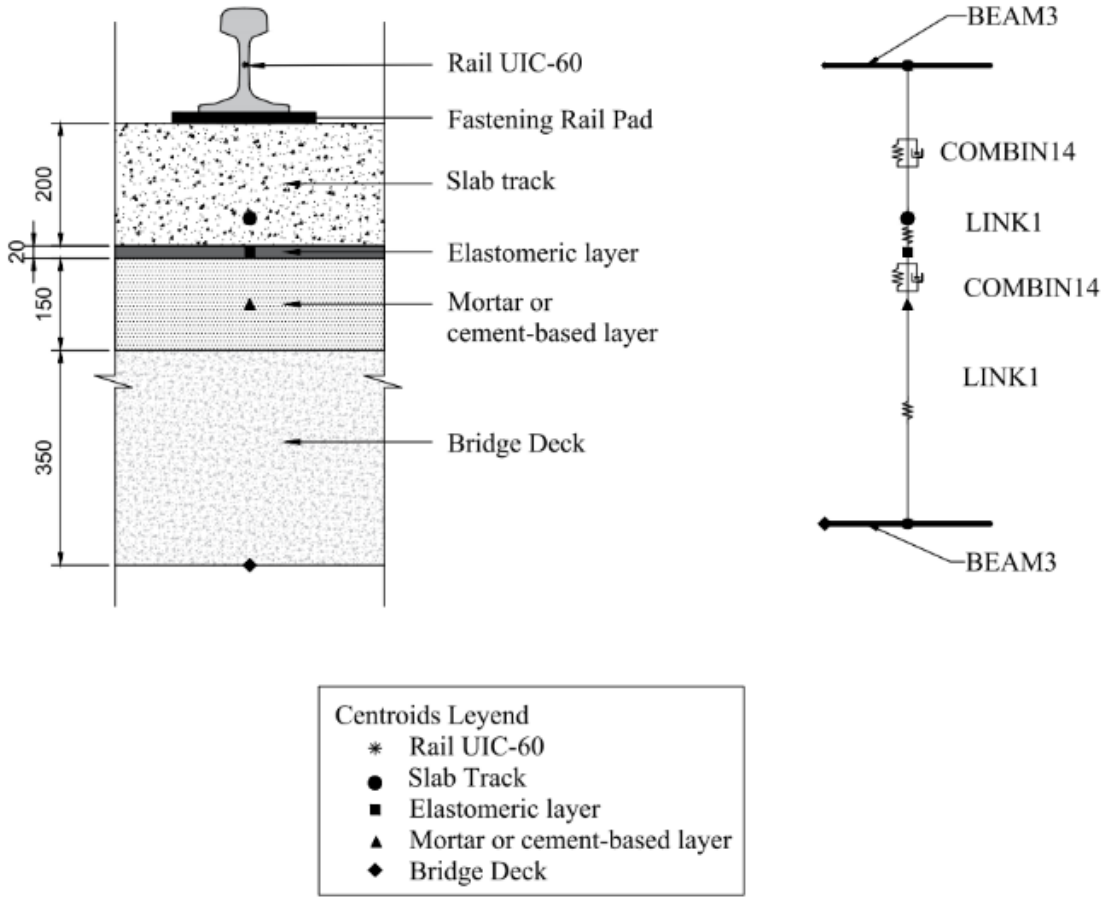

Figure 30. Independent slab track scheme for modelling (note that the distance of 350 mm from the top of the girder to its centroid in this figure is only orientative).

Components of modelling	Element	Material	Properties
Rail UIC-60	BEAM3	Steel E_s = 2x10^8 kN/m^2, ν = 0.3, ρ = 7.85 t/m3	A = 76.7 cm^2; I = 3038 cm^4; COG_i = 8.09 cm; h = 172 mm
Fastening Rail Pad	COMBIN14		K = 50 kN/mm; C = 15 kNs/m
Slab Track	LINK1	E = ∞ ρ = 2.5 t/m^3	-
Elastomeric layer	COMBIN14	-	Bedding modulus, c = 0.015 N/mm^3; ξ = 15%
Mortar or cement-based layer	LINK1	E = ∞ ρ = 2.5 t/m^3	--
Bridge Deck	BEAM3	Concrete E_c = 37.1 GPa; ρ = 2.5 t/m3 (plus the mass of non-structural elements); ν = 0.2	A, I, h, COG acc. to Martín de Soto Aláez (2020), eqs. (11) to (14); ξ = 2%

Table 13. Independent Slab Track Model. Elements, materials and properties values

Chapter 4

Study of cases

4.1. Introduction

In this Chapter, the main results obtained in the different cases simulated with the finite element model are presented. First, the governing limits for deflections and accelerations imposed by the standard IAPF (2007) are highlighted so that they can be used as reference to understand the eventual comfort or serviceability problems produced by the moving loads in the studied bridges. Then, the results are presented in terms of vertical deflections and accelerations for the different simulations.

4.2. Limits of deflections and accelerations

According to the IAPF (2007), bridges must be designed in such a way that they fulfil two main requirements under dynamic loads, the vertical displacement and the vertical acceleration, both at the bridge deck.

The vertical displacement limit imposed by the standard, controlled at the bridge deck and not at the rail, must be less than the span length divided by 600 (L/600). This condition is found in Section 4.2.1.1.3 of the standard.

For accelerations, the IAPF defines a range of values depending on the type of track: for ballasted tracks the acceleration must be limited to 0.35g, where g is the value of gravity taken as g = 10 m/s^2 in this study. Furthermore, for slab track structures, the maximum acceleration to which the bridge deck may be subjected is 0.5g; both values are defined in Section 4.2.1.1.1 of the aforementioned standard.

Additionally, the IAPF also specifies the limit values of maximum accelerations in the train, which must be less than a comfort value for the passengers (Section 4.2.1.2 of IAPF). The verification of this condition implies modelling the complete train, which is not the subject of this study and, actually in the drafting of projects neither. But it has to be noted that the maximum vertical displacement limit (L/600) is taken here as the dominant criterion in the design of railway bridges as it is more restrictive.

In the following Table 14, a brief summary of the previously specified values as well as few remarks to clarify their use are listed.

Parameter	Limit	Notes
Vertical Deflection	$< L/600$	Always in bridge deck
Acceleration	0.35g	Ballasted track limits in bridge deck
	0.50g	Ballastless track limits in bridge deck

Table 14. Maximum values for vertical deflection and acceleration according to IAPF (2007).

4.3. Effect of a single moving load

The first dynamic analysis has consisted on the study of the effect of a moving point load of 225 kN at speeds between 200 and 360 km/h over the short bridge (L = 20 m), with the three track typologies defined in Section 3.2.

4.3.1. Bridge without explicit model of the track

As explained in Chapter 3, a first simplified analysis has been performed without consideration of the track-bridge interaction. This simple case has been solved to have a reference to understand whether the more complex track-bridge interaction models are correct. The solved case has been the short bridge (20 m single span) subjected to a single moving point load of 225 kN at speeds in the range of 200-360 km/h. In this model, only the bridge is simulated with finite elements (BEAM3), including the mass of all the components of the track, but without considering the structural modeling of them (rails, fasteners, sleepers, ballast).

Before the analysis of the effect of the load, a modal analysis has been completed to extract the natural frequencies and the modes of the structure. The first 5 modes are plotted in Figure 31 and listed in Table 15. The first natural frequency is 5.1 Hz. Note that the first, second, fourth and fifth modes correspond to vertical vibrations, while the third mode is a horizontal one (axial deformation of the bridge) and it is therefore not included in the figure.

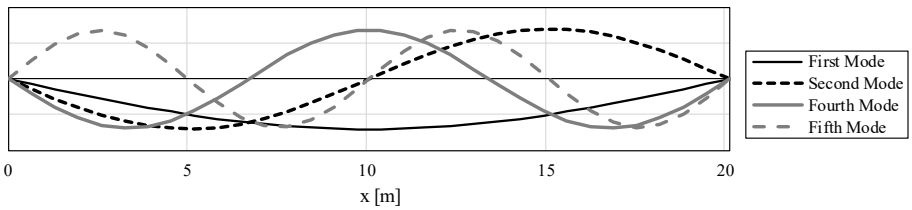

Figure 31. First vertical vibration modes of the bridge without explicit model of the track.

Mode	Frequency (Hz)
1	5.12
2	20.35
3	35.75
4	45.22
5	79.04

Table 15. List of first five frequencies of the bridge model without explicit model of the track.

Next, the results produced by the single moving load of 225 kN have been obtained with the full-time numerical integration method. Figure 32 shows such results in two graphs, on the left the vertical displacements and on the right the vertical accelerations at the midspan of the bridge when the moving point load crosses the bridge. In both graphs the results obtained for speeds of 200 and 360 km/h are plotted.

As it can be seen, the response of the bridge is formed by an initial stationary phase corresponding to the time during which the load is over the bridge and then by a phase of free or transient vibrations in which the response dissipates due to the damping. It is also observed that the mode that governs the response is mainly the first vertical mode. As for the influence of the speed, the graphs show that both deflection and acceleration are higher for 360 than for 200 km/h.

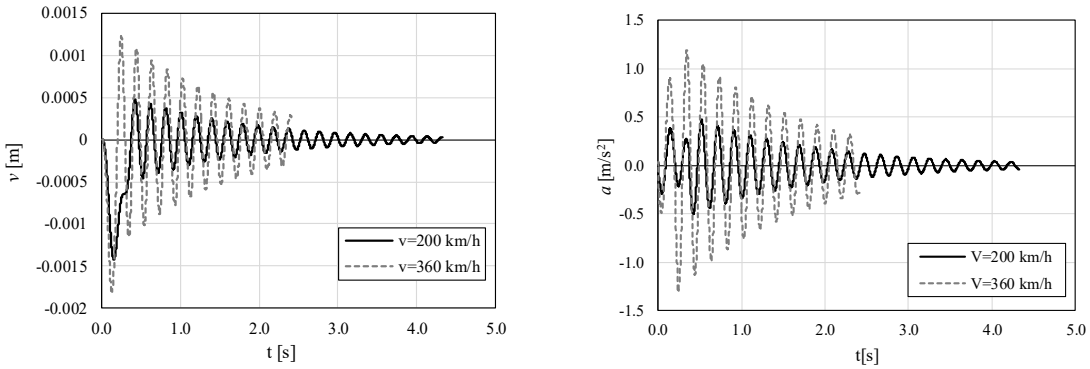

(a) (b)

Figure 32. Results at midspan for V = 200 km/h and 360 km/h. Short bridge, ballasted track (without track-structure interaction), moving point load: (a) Bridge displacement; (b) Bridge acceleration.

4.3.2. Bridge with ballasted track

In this case, the track-bridge interaction is explicitly included in the finite element model, as described in Section 3.3. Accordingly, the first vibration modes are obtained again: the first ones extracted from the analysis are shown in Figure 33, which correspond to vertical vibration modes of the bridge.

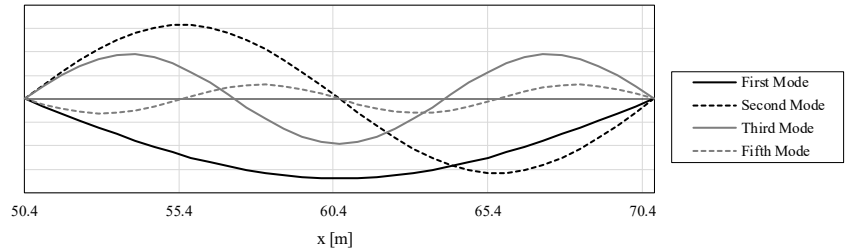

Figure 33. First vertical vibration modes of the bridge model with ballasted track.

Besides the vibration modes corresponding to the bridge, the frequencies and modes of vibration of the track are also provided by this model which includes track-bridge interaction. The first ten frequencies are shown in Table 16.

The first five modes are the same as those explained previously in Section 4.3.1, which are the modes of the bridge, while the next five are those of the track.

The comparison between the frequencies of Table 16 with those of Table 15. indicates how the explicit inclusion of the ballasted track in the model slightly reduces the values of the bridge frequencies: the frequency of the first vertical vibration mode is reduced from 5.1 Hz in the case of beam without explicit track consideration to 4.9 Hz with the introduction of the ballasted track in the model; the second decreases from 20.3 Hz to 19.0 Hz, and so on).

Figure 34 shows the vibration modes corresponding to the track, including the part on the left lateral embankment (corresponding to $x < 50$ m), the bridge ($50 < x < 70$ m) and finally the right lateral embankment ($x > 70$ m).

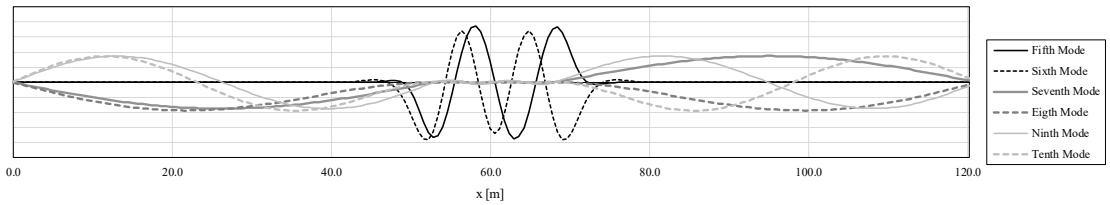

Figure 34. First vertical vibration modes of the rail from the model of ballasted track.

Table 16 includes all the vibration modes. It is necessary to emphasize that neither in Figure 33 nor in Figure 34 the fourth vibration mode is represented, because it corresponds to the horizontal mode that is outside the study (it is not excited by train loads). It has to be noted that modes with a frequency higher than 30 Hz normally have a very small contribution to the total response of the bridge (IAPF even specifies that modes higher than 30 Hz can be neglected for the calculation of accelerations). Nevertheless, a track-structure interaction analysis can excite higher modes and that is why full time integration has been used in this TFM for the solution of the simulations.

Mode	Frequency (Hz)
1	4.91
2	18.99
3	35.48
4	39.10
5	41.47
6	42.95
7	43.32
8	43.32
9	43.32
10	43.32

Table 16. List of first ten frequencies of the bridge model with ballasted track.

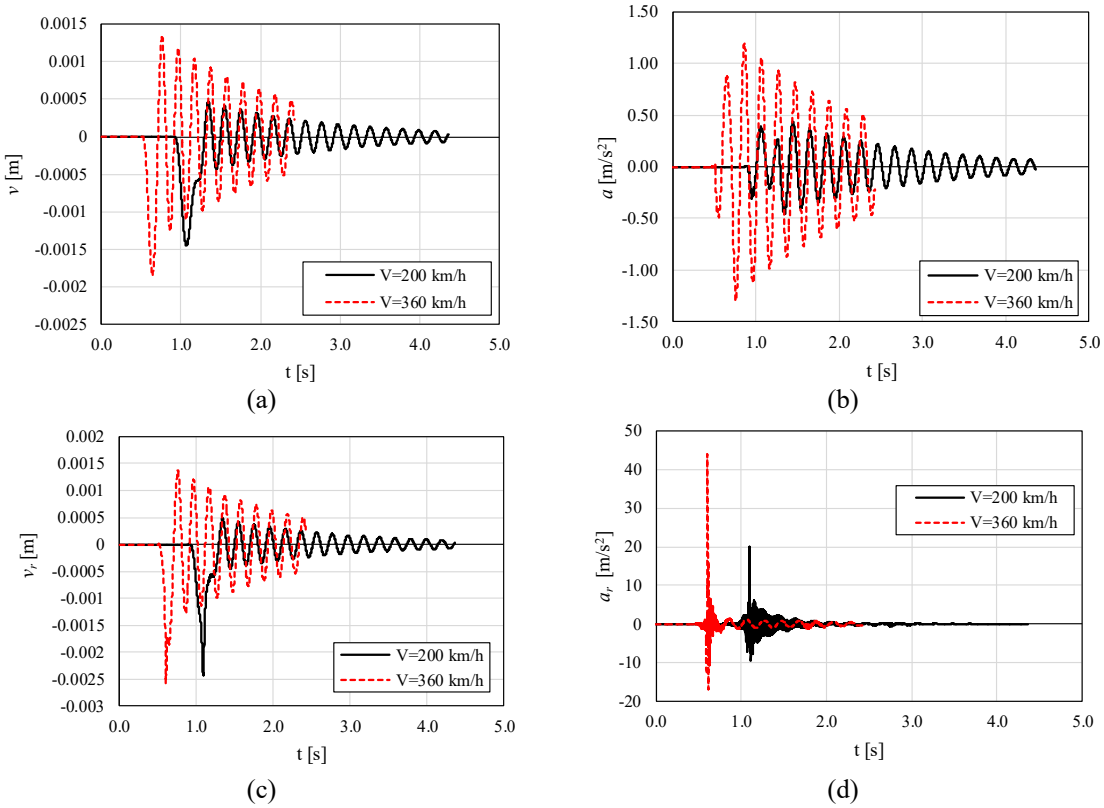

Figure 35. Results at midspan for $V = 200$ km/h and 360 km/h. Short bridge, ballasted track, moving point load: (a) Bridge displacement; (b) Bridge acceleration; (c) Rail displacement; (d) Rail acceleration.

In contrast to section 4.3.1 where the track is not explicitly modeled, now the results for the track are available in addition to those for the bridge. Figure 35 shows the values of vertical displacements and accelerations over time at speeds 200 and 360 km/h at the center of the span. It can be seen that the values at the bridge (Figure 35a-b) correspond perfectly with those obtained in Figure 32a-b with the model without explicitly considering the modeling of the track. Therefore, it can be concluded that the results make sense and that the track-bridge interaction model can be used with guarantees to extract results.

The graphs in Figure 35 show a first peak corresponding to the effect of the moving load and then the dissipation by damping in the free vibration phase. The maximum vertical acceleration on the bridge depends on the speed, being more critical for 360 km/h with a value of 1.29 m/s^2, while for 200 km/h the maximum value is 0.46 m/s^2. Also, the vertical displacement on the deck of the bridge for both speeds is -1.80 mm and -1.48 mm.

Regarding the results at the rail, it is observed that the maximum deflections are similar for both velocities, unlike the acceleration that are 44.1 m/s^2 and 19.9 m/s^2, for 360 and 200 km/h respectively, which means a difference between bridge and rail of approximately 1/3 at the peaks. Also, the vertical displacements on the rail are -1.36 mm and -0.48 mm for 360 km/h and 200 km/h, respectively, and they are almost the same as in the deck of the bridge. To better see the results of the acceleration in the rail, Figure 36 shows a zoom of the first second (period which covers the time when the load enters the bridge, and when the maximum peak occurs) where the peaks are shown.

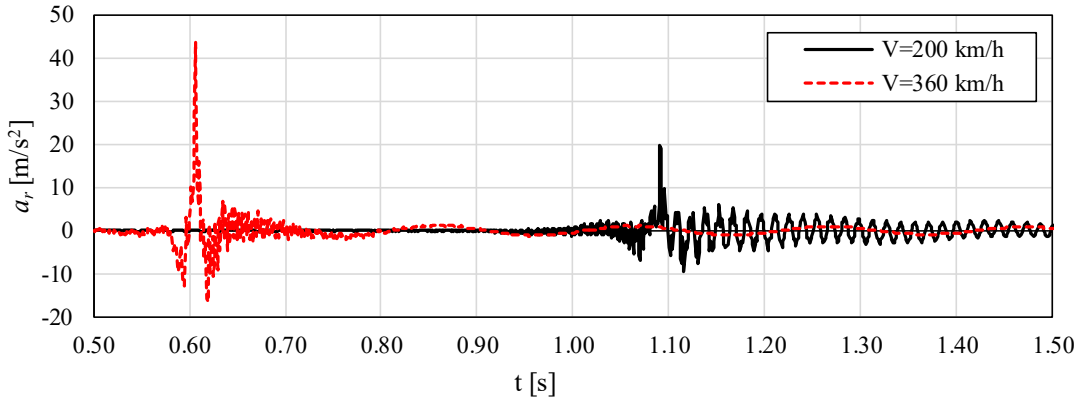

Figure 36. Detail of midspan accelerations at the rails for V = 200 km/h and 360 km/h. Short bridge, ballasted track, moving point load.

Vertical displacements obtained at midspan are plotted in Figure 37 as a function of speed. The vertical deflection on the bridge increases with the speed, while on the rail it has a maximum value at a speed of 280 km/h. Taking into account that the span considered in the numerical model is 20.15 m, the established limit of maximum deflection (IAPF limit for comfort control) of $L/600$ = 0.0334 m. It is observed that it is not exceeded and that both the bridge and the rail meet the requirement of the standard (although it should be emphasized that the limit must be checked only on the bridge).

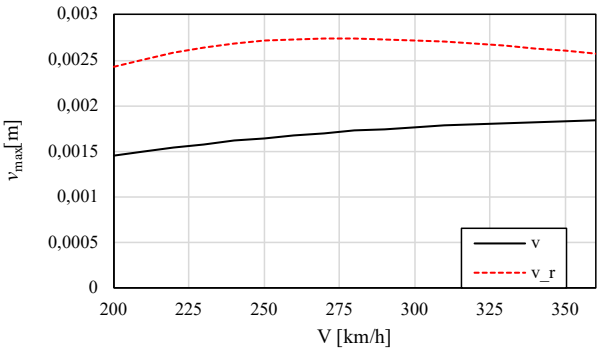

Figure 37. Influence of speed on the midspan delflection. Short bridge, ballasted track, moving point load.

The dynamic effects can be analyzed with the DAF, shown in Figure 38, which has been calculated by dividing the maximum vertical dynamic deflections obtained at speeds in the range between 200 and 360 km/h and the maximum static vertical displacement calculated as $PL^3/48EI$, which is the one that occurs when the load is located at the center of the span of the simply supported beam. According to Figure 38, the DAF is increasing with speed, between 1.30 for 200 km/h and 1.65 for 360 km/h.

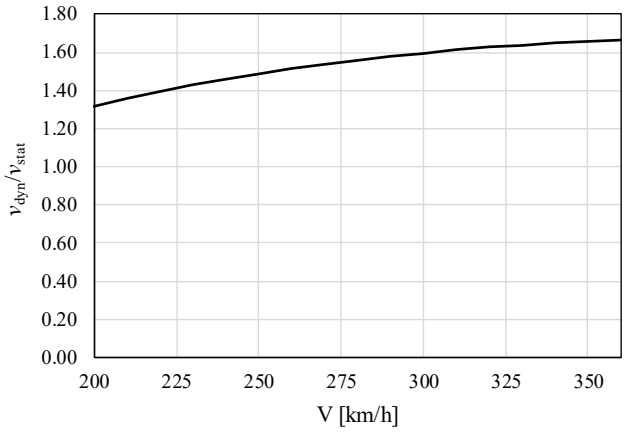

Figure 38. Dynamic increase factor (DAF) of the short bridge, ballasted track, moving point load.

The graph of Figure 39 shows on the left the accelerations occurring both on the rail and on the bridge at speeds from 200 to 360 km/h. In addition, the limit of 0.35g is represented as the most restrictive for all track types. When the values of the track and bridge are plotted together, those of the bridge cannot be well appreciated as they are much lower than those of the track, so a detailed representation is shown in Figure 39 (right), where only the limit established by the standard and the values of the maximum acceleration that the bridge undergoes with the passage of the moving load at each of the speeds are represented. At both the bridge and the rail, the maximum acceleration increases with the speed. The maximum values, in both cases for the speed of 360 km/h, are 1.3 and 44.1 m/s^2, respectively.

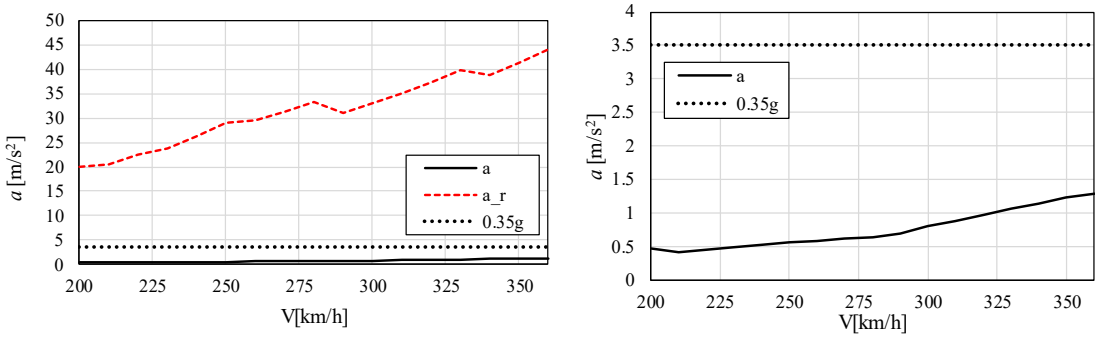

Figure 39. Influence of speed on the midspan acceleration. Short bridge, ballasted track, moving point load.

4.3.3. Bridge with ballastless track

In this sub-clause, the results obtained with the two ballastless track systems are analyzed. As mentioned above, the serviceability and comfort limits established by the standard for ballastless track are less restrictive than for ballasted track. Therefore, the latter will be the safe-side requirement that is represented in the graphs throughout this sub-clause (0.35g for accelerations).

4.3.3.1. Monolithic slab track

The first result is the representation of vibration modes and the list of natural frequencies obtained with the model, which are detailed in Figure 40 and Figure 41, and listed in Table 17. The use of monolithic slab track causes the natural frequencies to increase slightly with respect to those of the ballasted track. For example, the first frequency increases from 4.9 Hz to 5.6 Hz, and the second from 19.0 Hz to 22.3 Hz.
This result may be due to the stiffening effect of the monolithic slab track, as well as a slight reduction of the mass on the bridge when the ballast is replaced by the slab track layers.

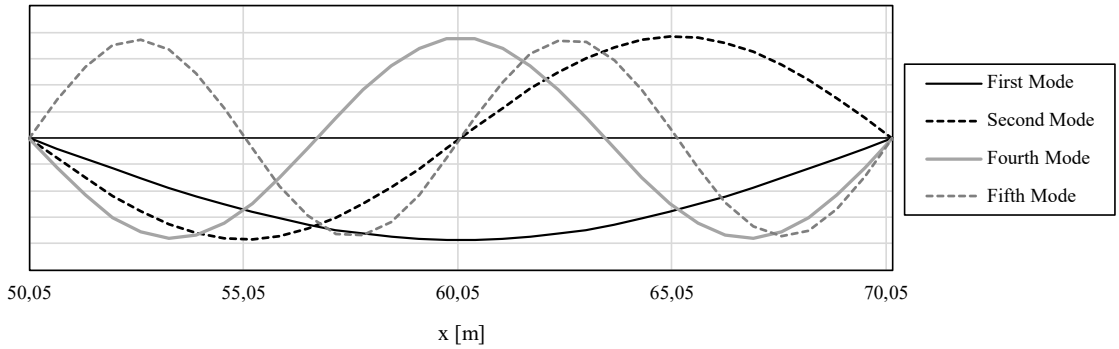

Figure 40. First vertical vibration modes of the bridge model with monolithic ballastless track.

Figure 41 shows the vibration modes corresponding to the track, including the part on the left lateral embankment (corresponding to $x < 50$ m), the bridge ($50 < x < 70$ m) and finally the right lateral embankment ($x > 70$ m). An additional detail including the representation of the track and the bridge is plotted in Figure 42.

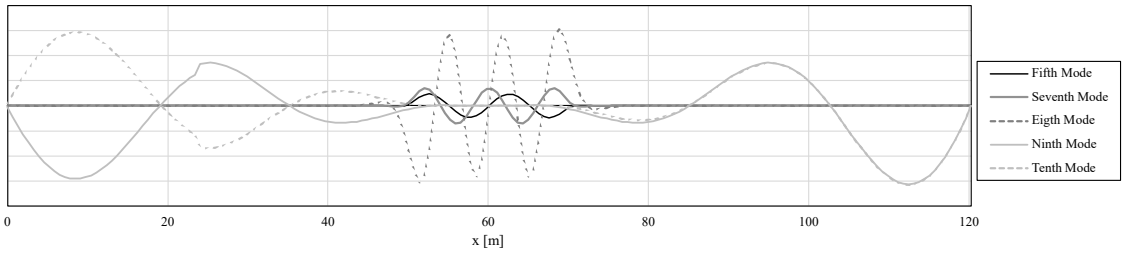

Figure 41. First vertical vibration modes of the rail from the model with monolithic ballastless track.

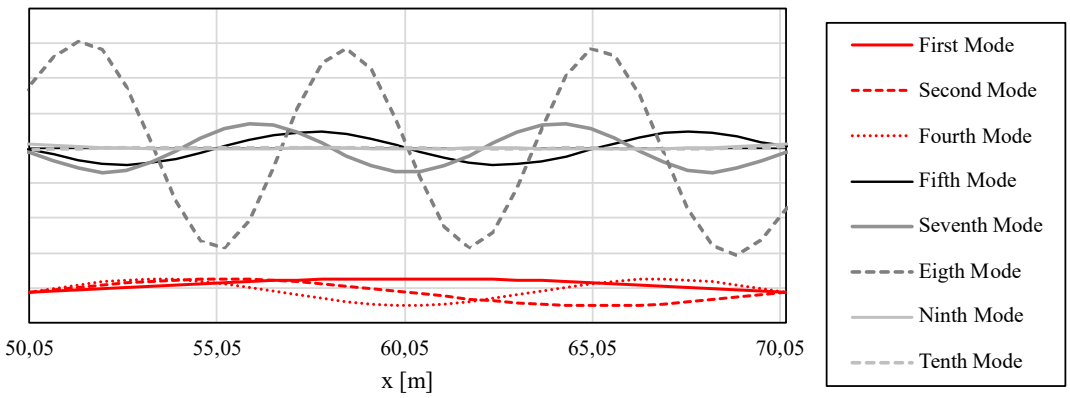

Figure 42. First vertical vibration modes on the rail and bridge deck with monolithic ballastless track.

Table 17 includes all the vibration modes. It is necessary to emphasize that neither in Figure 40 nor in Figure 41 the third and sixth vibration modes are represented, because both correspond to the horizontal modes that are outside the study (they are not excited by train loads). As already mentioned before, it must be noted that modes with a frequency higher than 30 Hz normally have a very small contribution to the total response of the bridge and IAPF even specifies that modes higher than 30 Hz can be neglected for the calculation of accelerations. Nevertheless, a track-structure interaction analysis can excite higher modes and that is why full time integration has been used in this TFM for the solution of the simulations.

Mode	Frequency (Hz)
1	5.61
2	22.30
3	41.63
4	49.63
5	86.92
6	124.97
7	133.06
8	178.52
9	179.69
10	179.69

Table 17. List of first ten frequencies of the bridge model with monolithic ballastless track.

In a completely analogous way to what was done for the ballasted track in section 4.3.2, the different results have been obtained: vertical displacements and accelerations at midspan as a function of time (Figure 43 and detail of accelerations in Figure 44), vertical displacements and DAF as a function of speed (Figure 45), and accelerations as a function of speed (Figure 46).

In overall, it can be concluded that the monolithic slab track model indicates a slight reduction of the dynamic effects on the bridge observable by the slightly smaller DAF, with respect to the previously analyzed case with ballastless track. With respect to the rail, somewhat higher accelerations are obtained with the monolithic ballastless track than with the ballasted track.

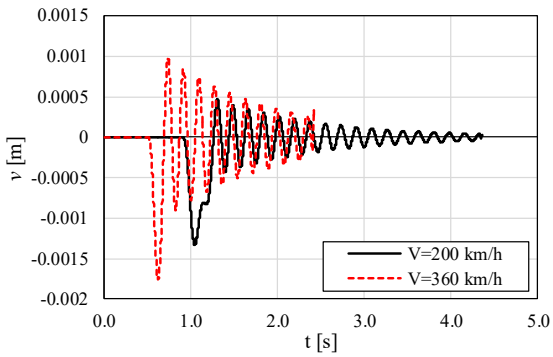

(a)

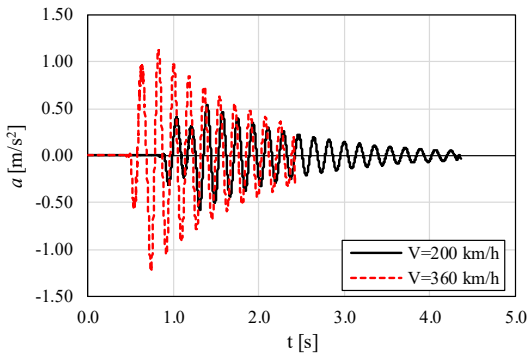

(b)

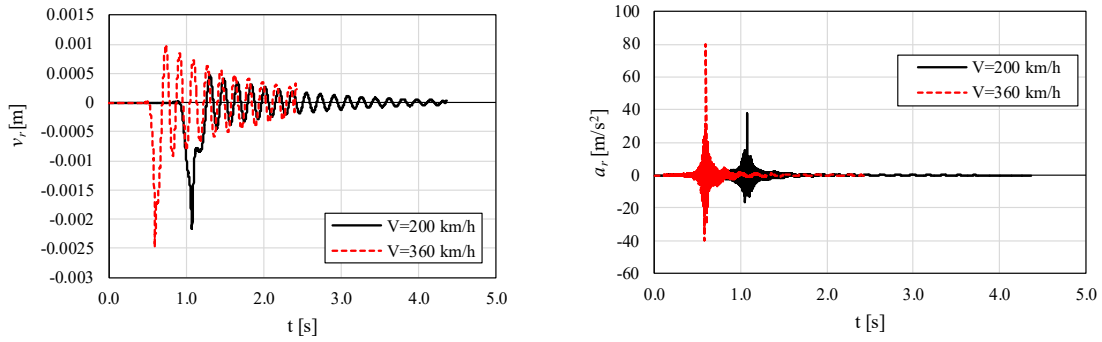

(c) (d)

Figure 43. Results at midspan for V = 200 km/h and 360 km/h. Short bridge, monolithic ballastless track, moving point load: (a) Bridge displacement; (b) Bridge acceleration; (c) Rail displacement; (d) Rail acceleration.

The results for the track are available in addition to those for the bridge in Figure 43, in terms of the vertical displacements and accelerations over time at speeds 200 and 360 km/h at midspan. Results on the bridge deck and on the rail can be seen in Figure 43a-b and c-d, respectively. In Figure 43, the first peak in all graphs represents the effect of the moving load at the time that enters on the bridge and the subsequent dissipation and damping that occurs once the load is on the embankment, corresponding to the free vibration phase. The maximum vertical acceleration on the bridge depends on the speed, being more critical for 360 km/h with a value of -1.23 m/s^2, while for 200 km/h the maximum value is 0.58 m/s^2 and the maximum vertical displacements on the deck of the bridge are -1.76 mm and -1.33 mm for both speeds, respectively.

When analyzing the results at the rail, it is observed that the maximum deflections are similar for both speeds, while the acceleration are 79.85 and 37.77 m/s^2, for 360 and 200 km/h, respectively, which means a difference between bridge and rail of approximately 1/3 at the peaks. To better see the result of the acceleration in the rail, Figure 44 shows a zoom of the period of time which covers the peaks.

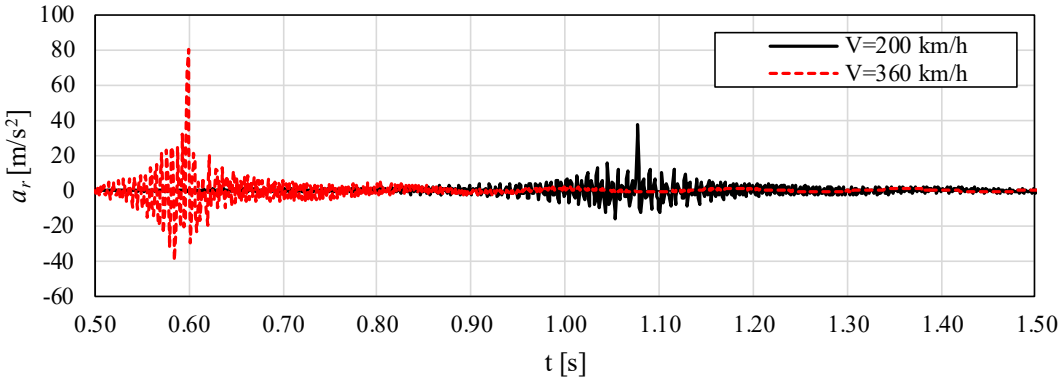

Figure 44. Detail of midspan accelerations at the rails for V = 200 km/h and 360 km/h. Short bridge, monolithic ballastless track, moving point load.

In Figure 45a the vertical displacement is represented as a function of the speed. As it can be seen, the vertical displacement at the bridge deck increases with the speed.

Also, the maximum values of the vertical displacement in the rail and the deck of the bridge occur at a different speed: for the rail the peak is found for 275 km/h, while for the deck, the maximum occurs for 360 km/h. Considering the length of the bridge (L = 20.15 m), the established limit of maximum deflection according to IAPF is $L/600$ = 0.0334 m. It is observed that neither the rail and the bridge exceed such a limit at any velocity, which means that also the rail and the bridge meet the requirement of the standard.

The DAF used to analyze the dynamic effects is shown in Figure 45b. It has been calculated as the relation between the maximum vertical dynamic displacement (in the speed range between 200 and 360 km/h) and the maximum static vertical displacement, calculated as $PL^3/48EI$ when the load is placed at midspan. The DAF increases with the speed, with values from 1.2 to 1.6 at 200 km/h and 360 km/h, respectively.

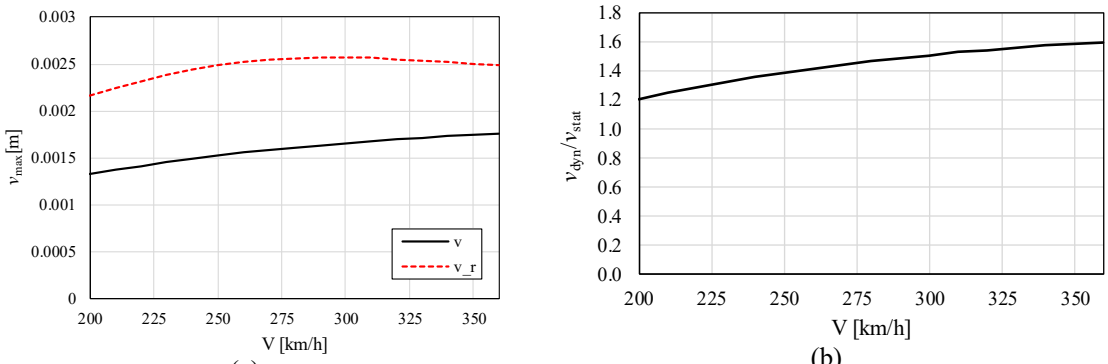

Figure 45. Influence of speed on the (a) midspan deflection and (b) DAF. Short bridge, monolithic ballastless track, moving point load.

The two graphs of Figure 46 show the accelerations occurring at speeds from 200 to 360 km/h. The left one (Figure 46a) represents the results for the rail and the bridge deck, and on the right one (Figure 46b), a zoom is made to easily observe the results on the bridge. The limit of the IAPF (0.35g) is represented in both graphs because it is the most restrictive value for all track types. To sum up, the maximum acceleration at both the bridge and the rail increases with the speed and occurs at the speed of 360 km/h, being the values of 1.23 and 79.85 m/s^2, respectively.

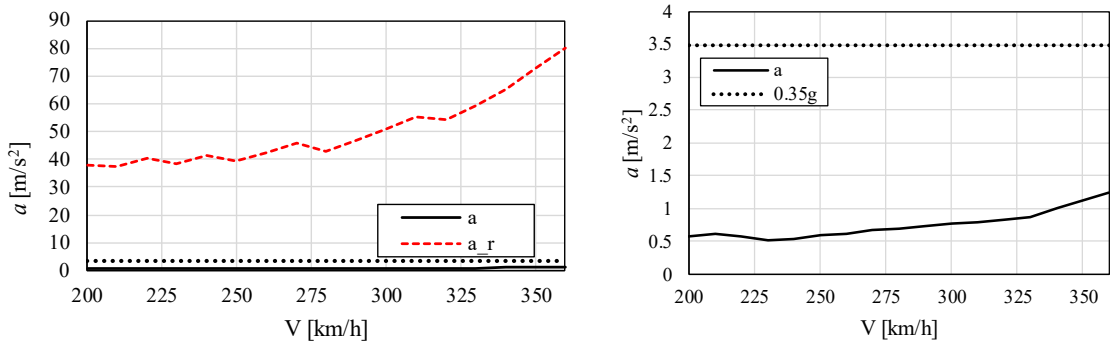

Figure 46. Influence of speed on the midspan acceleration. Short bridge, monolithic slab track, moving point load.

4.3.3.2. Independent slab track

As in Section 4.3.3.1, the first results shown are the vibration modes and the list of natural frequencies exported from the model after a modal analysis. Figure 47 shows the first vibration modes of the bridge along its length. The values of the frequencies are listed in Table 18. It can be seen how the results of the frequencies with the independent slab track configuration are higher than those obtained with the ballasted track model and slightly lower than those obtained in the case with monolithic slab track. For example, the first frequency decreases with respect to the monolithic ballastless track, with values of 5.3 Hz and 5.6 Hz, respectively, while the ballasted track model is 4.9 Hz. The second mode of vibration is 21.1 Hz, while in the previous section the second frequency has a value of 22.3 Hz and in the lower ballasted track it is 10.0 Hz.

The reason for the slight reduction of frequencies with respect to the monolithic ballastless track can be due to smallest stiffness of the complete structure. Also there is some variation of the mass, but the stiffness might be the dominant effect.

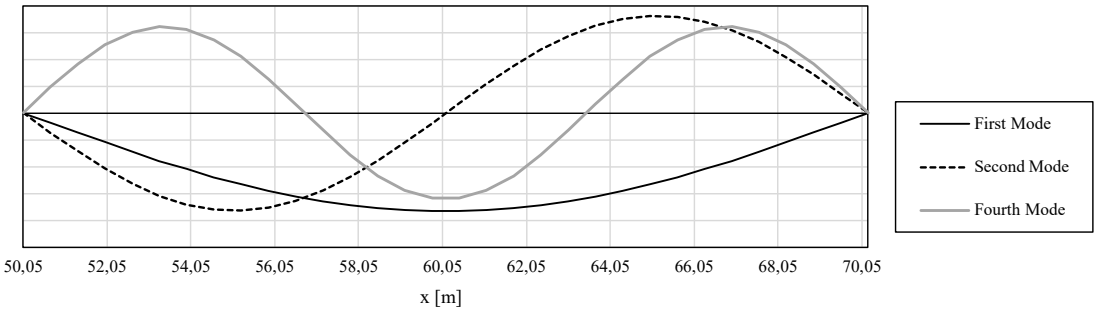

Figure 47. First vertical vibration modes of the bridge model with independent ballastless track.

Figure 48 shows the vibration modes corresponding to the track, including the part on the left lateral embankment (corresponding to $x < 50$ m), the bridge ($50 < x < 70$ m) and the right lateral embankment ($x > 70$ m). A detail of the bridge and the track excitation by the vibration modes is plotted in Figure 49. It is necessary to emphasize that neither in Figure 47 nor in Figure 48 the third vibration mode is represented, because it correspond to the horizontal mode that is outside the study (it is not excited by train loads).

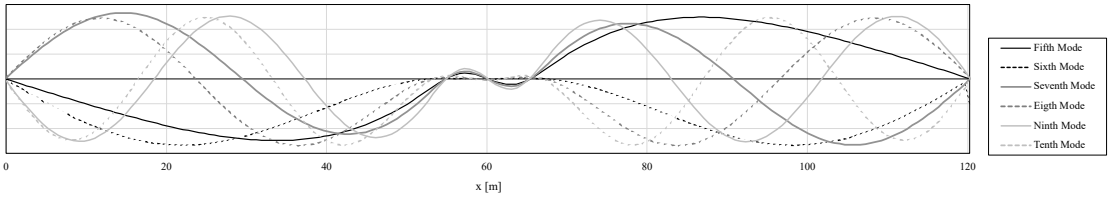

Figure 48. First vertical vibration modes of the rail from the model with independent ballastless track.

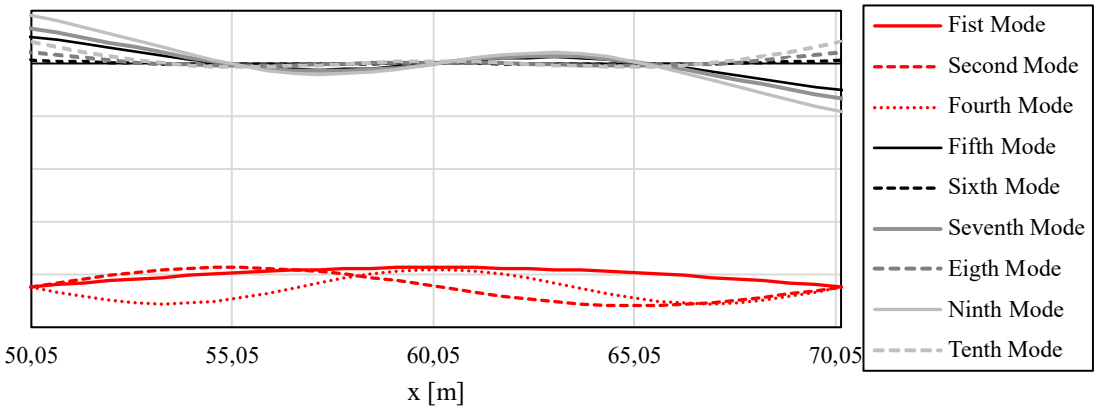

Figure 49. First vertical vibration modes on the rail and bridge deck with independent ballastless track.

Mode	Frequency (Hz)
1	5,33
2	21,15
3	40,86
4	46,06
5	52,59
6	52,60
7	52,60
8	52,60
9	52,60
10	52,61

Table 18. List of first ten frequencies of the bridge model with independent ballastless track.

In a completely analogous way to what was done for the monolithic slab track in section 4.3.3.1, different results have been obtained: vertical displacements and accelerations at midspan as a function of time (Figure 50 and detail of accelerations in Figure 51), vertical displacements and DAF as a function of speed (Figure 52), and accelerations as a function of speed (Figure 53).

In overall, it can be concluded that the independent slab track model indicates a slight reduction of the dynamic effects on the bridge observable by the slightly smaller DAF than in the monolithic slab track. Concerning rail results, somewhat higher accelerations are obtained with the independent ballastless track than with the monolithic slab track and ballasted track.

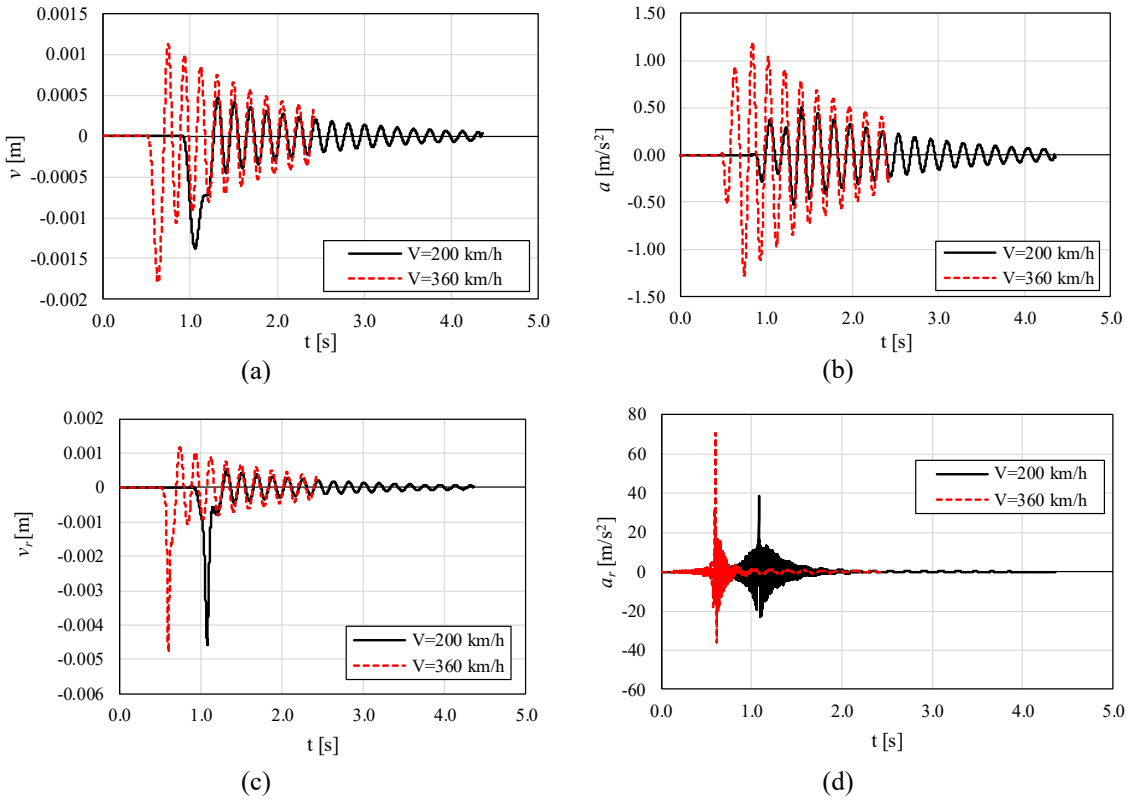

Figure 50. Results at midspan for $V = 200$ km/h and 360 km/h. Short bridge, independent ballastless track, moving point load: (a) Bridge displacement; (b) Bridge acceleration; (c) Rail displacement; (d) Rail acceleration.

The results of Figure 50 show the values of vertical displacements and accelerations over time at speeds 200 and 360 km/h at midspan. Results on the bridge deck and on the rail can be seen at Figure 50 a-b and c-d, respectively. The first peak represents the effect of the moving load at the time when the load crosses the midspan, followed by the free vibration phase. The maximum vertical accelerations on the bridge are 1.23 m/s^2 and 0.58 m/s^2 for 360 km/h and 200 km/h, respectively. The maximum vertical displacements on the deck of the bridge for both speeds are -1.76 mm and -1.33 mm respectively. These results are almost the ones obtained for the monolithic slab track configuration.

With respect to accelerations, maximum values are 90.24 and 44.23 m/s^2, for 360 and 200 km/h respectively, which mean a difference between bridge and rail of approximately 1/4 at the peaks. It is also observed that accelerations at the rail are higher with the independent slab track model than with the monolithic one at 200 km/h the maximum rail accelerations are 79.85 and 37.77 m/s^2.

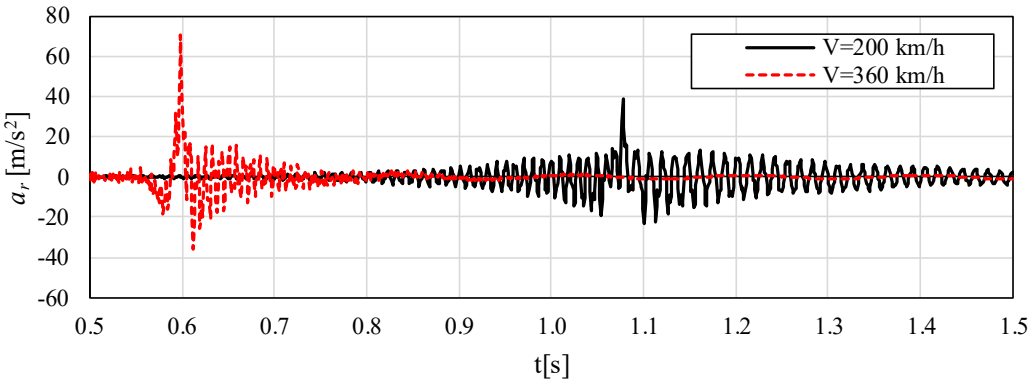

Figure 51. Detail of midspan accelerations at the rails for V = 200 km/h and 360 km/h. Short bridge, independent ballastless track, moving point load.

In Figure 52, the vertical displacement is represented as a function of the speed. As it can be seen again, the vertical displacement at the bridge increases with the speed. Also, the maximum vertical displacement occurs at a different speed at the rail and the deck: at 300 km/h for the rail (the peak is 2.63 mm), and at 360 km/h for the deck. Considering the length of the bridge (L = 20.15 m) the limit of maximum deflection according to IAPF is $L/600$ = 0.0334 m, which is never reached neither at the rail and the bridge. It means that the rail and the bridge meet the requirement of the standard.

The DAF used to analyze the dynamic effects is shown in Figure 52b. It can be observed that the DAF increases with the speed with values from 1.2 to 1.6 at 200 km/h and 360 km/h, respectively.

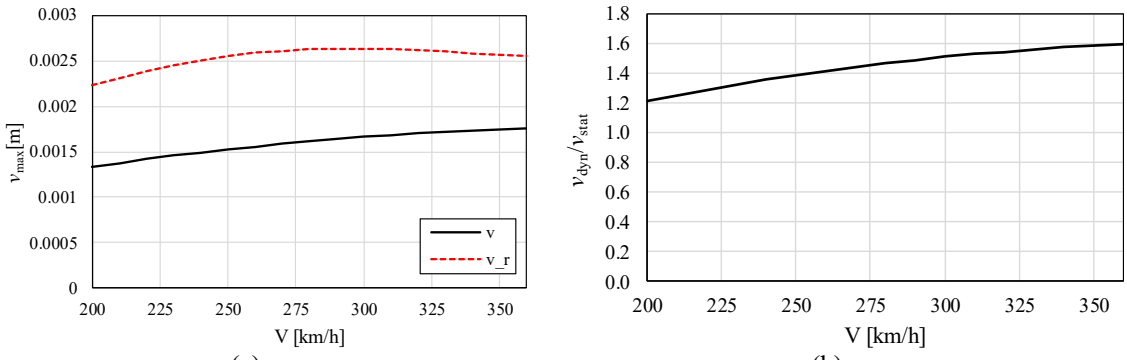

(a) (b)

Figure 52. Influence of speed on the (a) midspan deflection and (b) DAF. Short bridge, independent ballastless track, moving point load.

The two graphs of Figure 53 show the midspan accelerations at speeds from 200 to 360 km/h. The left one represents the results for both the rail and the bridge deck. On the right, a zoom is made to easily observe the results on the bridge. The maximum acceleration increases with the speed and occurs at the speed of 360 km/h, being the values of 1.24 and 90.24 m/s^2 at bridge and rail, respectively.

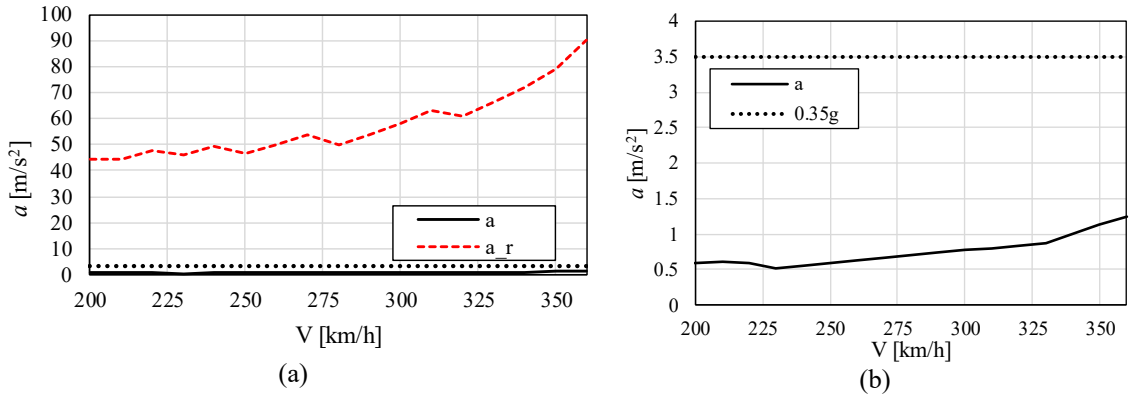

Figure 53. Influence of speed on the midspan acceleration. Short bridge, independent slab track, moving point load.

4.4. Effect of train loads

In this Section, the effect of moving train loads on studied bridges is studied. Two real commercial trains (Talgo and AVE-S101) considered in the standard IAPF have been taken as representative of the rail traffic in Spain. Nevertheless, it has to be noted that in a specific project, model trains HSML (as defined in Section 2.6) should be analyzed. The studied cases are divided as a function of the type of bridge, namely short isostatic bridge and long hyperstatic bridge. In all cases, the three track types considered in the study have been simulated (ballasted track and the two types of ballastless track: monolithic and independent from the bridge girder).

Before going into the details of the results, it is first necessary to discuss the natural frequencies and vibration modes of the bridges. As in the previous Section 4.3 those of the short bridge have been already obtained and analyzed, here the attention is paid at the dynamic properties of the long bridge, for the different track types considered. Thus, the first vertical vibration modes of the long bridge are represented in Figure 54, and the list of natural frequencies is given in Table 19.

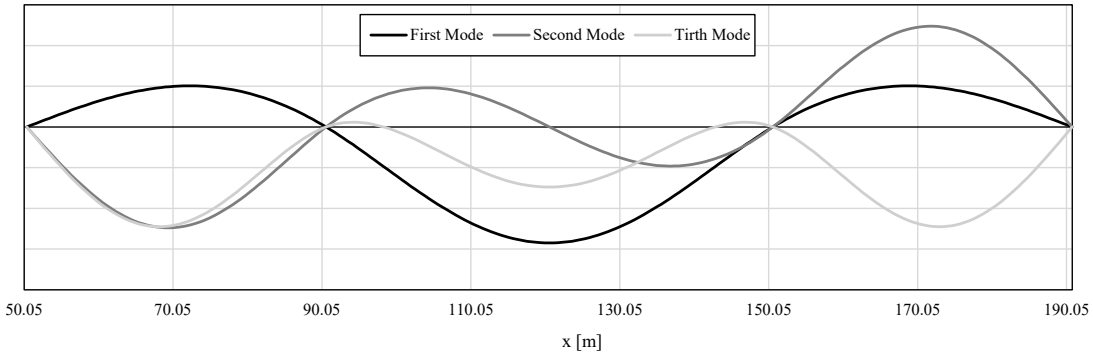

(a)

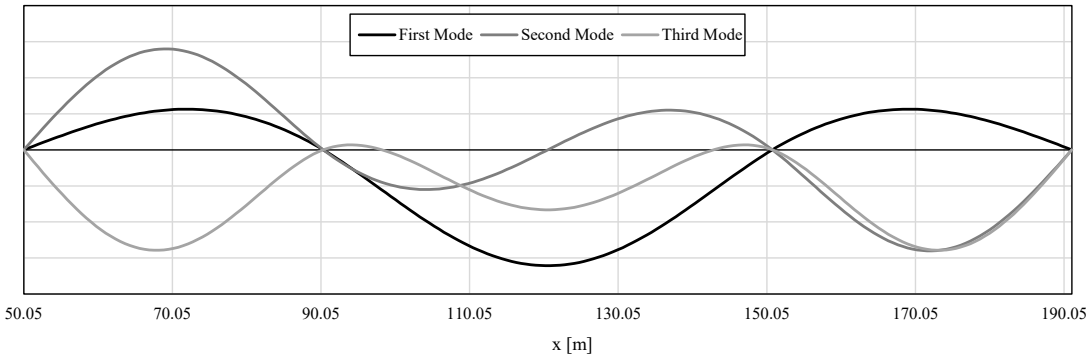

(b)

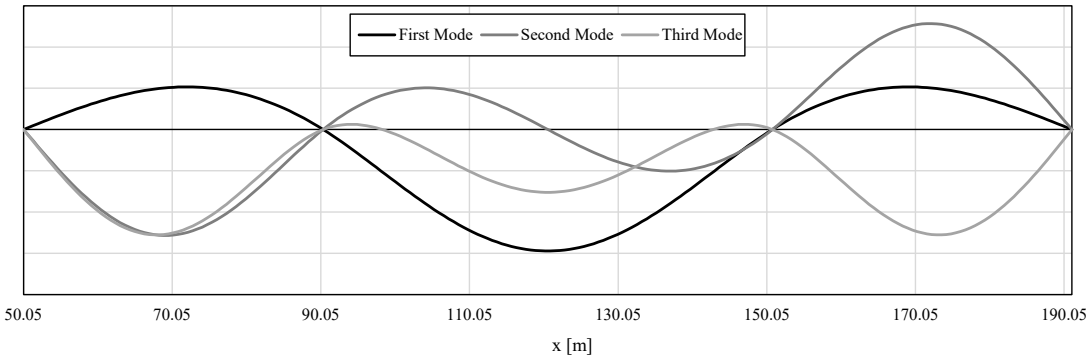

(c)

Figure 54. First vertical vibration modes of the long hyper-static bridge with: (a) ballasted track; (b) monolithic ballastless track; (c) independent ballastless track.

	Frequency (Hz)		
Mode	Ballasted track	Monolithic ballastless track	Independent ballastless track
1	2.25	2.53	2.31
2	4.19	4.75	4.35
3	4.90	5.56	5.10
4	5.71	6.01	5.79
5	8.17	9.29	8.52
6	13.56	15.87	14.57
7	15.13	17.99	16.51
8	17.14	18.02	17.37
9	17.19	20.78	19.07
10	22.75	30.04	28.01

Table 19. List of first ten frequencies of the long bridge model with the three track types.

4.4.1. Short isostatic Bridge

The first type of bridge for which results are presented in terms of deflection and acceleration is the short isostatic bridge with a length of 20 m in all cases. In Chapter 2 the load distributions for the Talgo and AVE cases have been defined, with details of the axle loads and axle spacing.

4.4.1.1. Train TALGO

The results produced by the Talgo train when it crosses the short bridge are represented in terms of the vertical displacement at the midspan section over time in Figure 55, at 200 and 360 km/h. In Figure 55a, the deflections produced by the Talgo are plotted for the three track types. It must be noted that all the axle forces of the Talgo are the same (170 kN), with an axle distance of 13.14 m in the wagons, and shorter distances in the locomotives. The governing axles which lead to the peak displacements are those which correspond to the end of the first composition and the beginning of the second composition (a train consists of two subsequent compositions, refer to Section 2.6). Details of the peak displacements for the two speeds of 200 and 360 km/h are represented in Figure 55b-c.

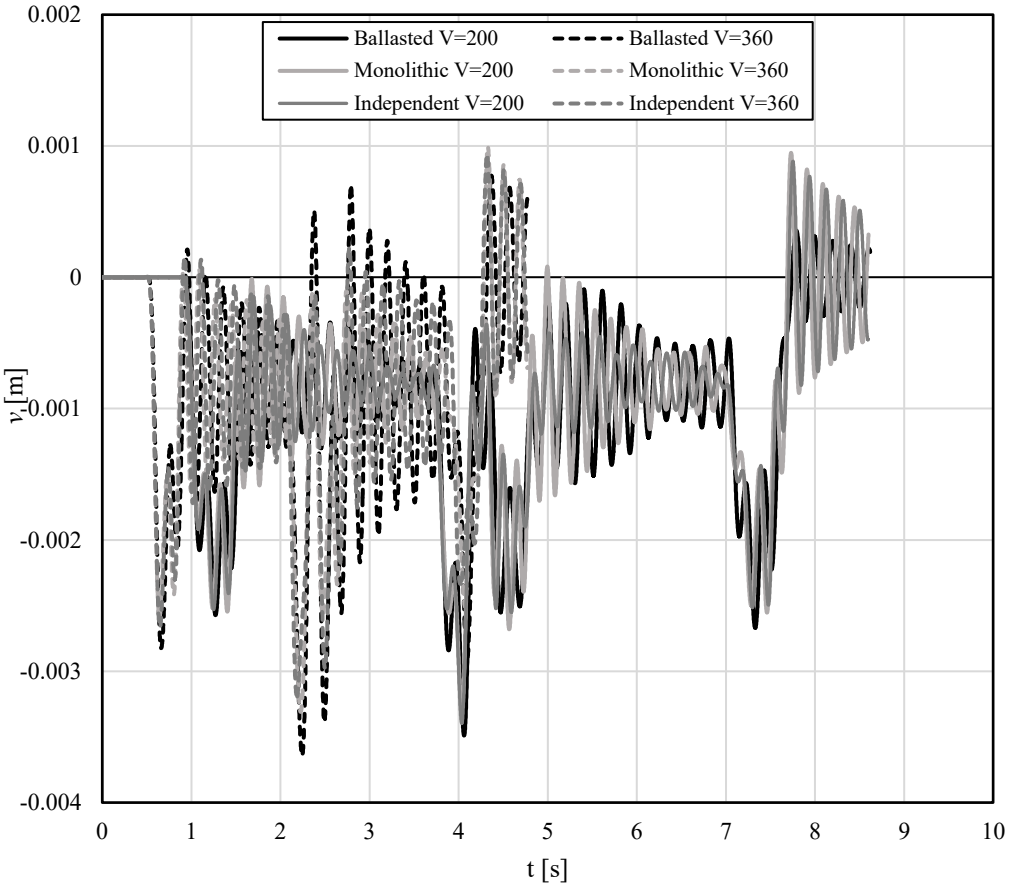

(a)

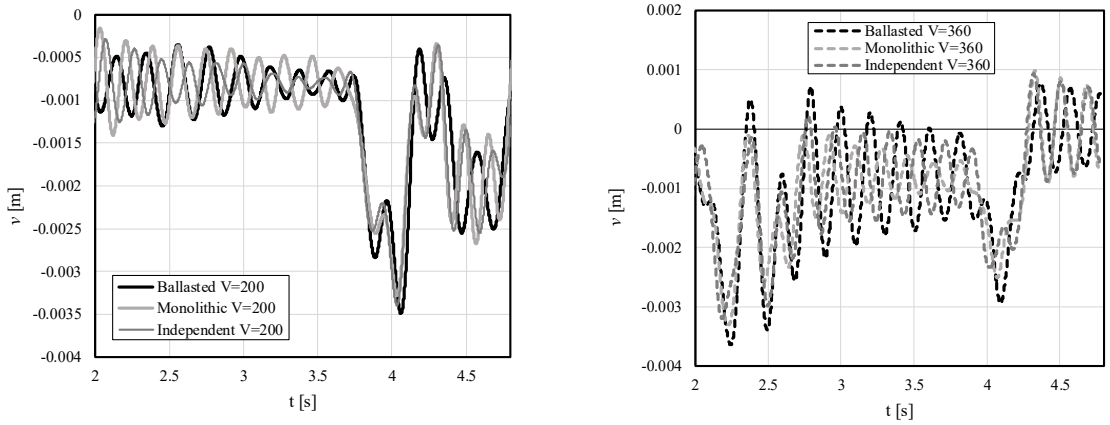

(b) (c)

Figure 55. Results of vertical deflections at midspan of the bridge for V = 200 km/h and 360 km/h. Short bridge, train Talgo for (a) the different track types; (b) detail for 200 km/h; (c) detail for 360 km/h.

The results in terms of accelerations at the midspan of the bridge as a function of time are plotted in Figure 56.

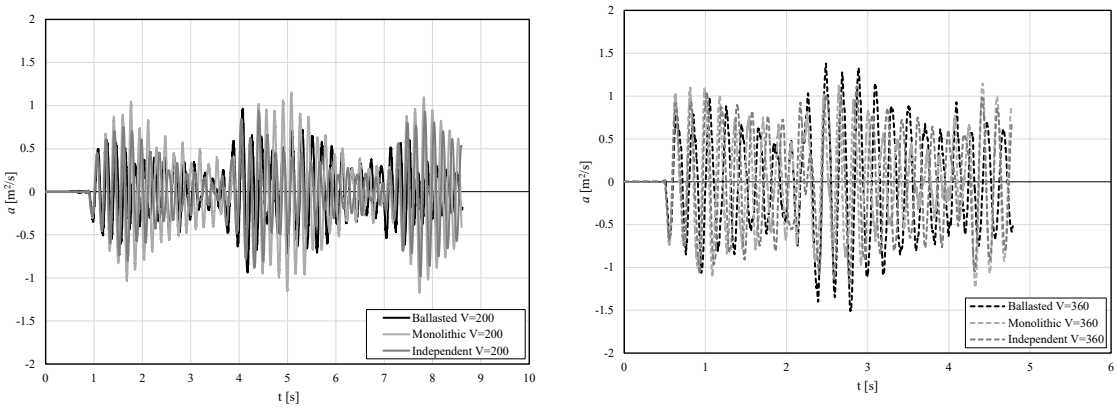

(a) (b)

Figure 56. Results of vertical accelerations at midspan of the bridge. Short bridge, train Talgo: (a) V = 200 km/h; (b) V = 360 km/h.

To understand the influence of the speed on the dynamic behavior of the bridge, the peak vertical displacements and associated DAF are plotted in Figure 57 as a function of the velocity in the range between 200 and 360 km/h. To obtain the reference static deflections that allow calculating the DAF, a static analysis is performed to obtain the maximum vertical displacement by the composition of the Talgo train loads. It must be sought the position of the loads which determine the maximum deflection configuration along the span length of the bridge. To do that, an analysis is firstly made over time to determine which position is the cause of the maximum deflection, which in most cases matches the position of maximum dynamic deflection. Then, a static analysis is done with the train loads statically placed at the obtained positions. In some cases the position of the loads which produce the maximum static deflection and the maximum dynamic deflection do not coincide due to the dynamic phenomena that amplify the maximum vertical displacement of the deck at a time instant corresponding to another position of the train loads.

The process to calculate the maximum static deflection in these cases has been more challenging than expected due to the fact that in order to find the exact position of the train loads which produce the maximum static deflection it was necessary to analyze each position which the train can occupy over time.

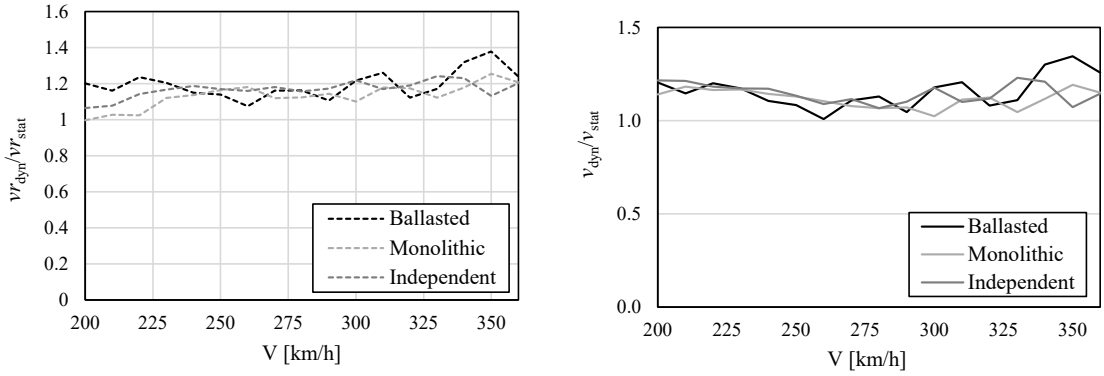

Figure 57. Influence of speed on the DAF of displacements: (a) at the rail; (b) at the bridge. Short bridge, train Talgo.

An interesting result from Figure 57 is that there is no remarked peak of the DAF at the velocity which corresponds to the theoretical resonance frequency. In the Talgo train, the axle distance of the wagons is 13.14 m. As the first natural frequency of the bridge is around 5 Hz, the theoretical resonance velocity is close to 236.5 km/h. The reason why there is not a peak of the DAF at that velocity is that the highest deflection is not governed by the axles of the wagons, but by those of the locomotives of the compositions, where the axle loads are closer to each other. This result can be better explained with the help of Figure 58, where the vertical deflection at the midspan of the bridge is represented as a function of time for a velocity of 236.5 km/h. In order to analyze the eventual resonant effects, this particular calculation has been solved with and without damping (i.e. setting all the damping factors of the components of the model equal to zero). The results of Figure 58 show clearly how the effects of the axles of the intermediate wagons are significantly amplified by dynamic effects (see the periods from t = 1.5 s to 3 s and from t = 4.2 s to 6 s). The static deflection produced by a single axle load of the Talgo (170 kN) is 0.84 mm, which means that the axles of the wagons are having an amplification factor of 1.5 (with damping) and 2.3 (without damping). Nevertheless, the highest deflections are achieved by the closely spaced axles of the heads of the two compositions of the train, which leads to three sets of peaks: 1) at the beginning, when the locomotive of the first composition crosses the bridge, 2) when the end of the first composition and the beginning of the second composition cross the bridge (time from t = 3.2 s to 4 s), 3) at the end, when the ending locomotive of the second composition crosses the bridge.

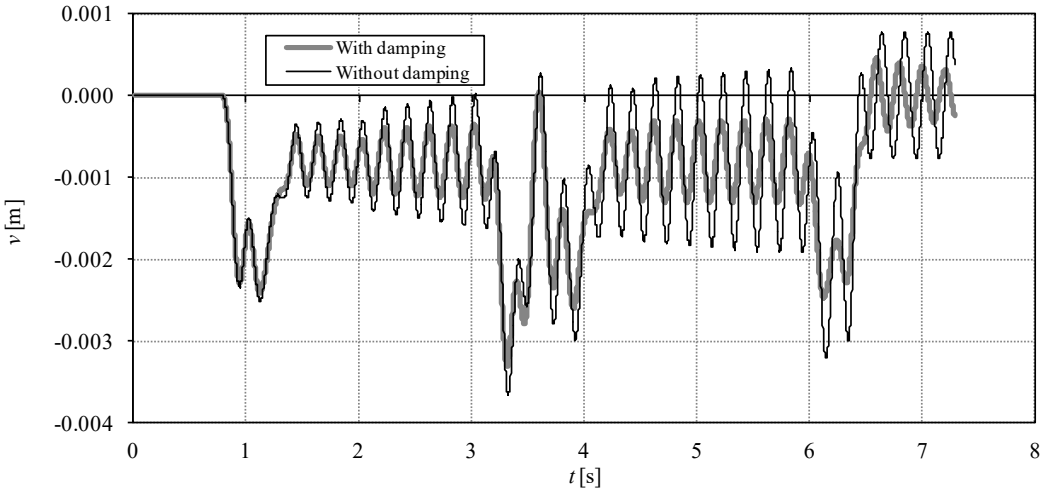

Figure 58. Bridge midspan deflection caused by the Talgo at 236.5 km/h. Short bridge, train Talgo.

The maximum accelerations obtained in the rail and the bridge deck are represented in Figure 59 as a function of the speed of the train. The maximum values at the rail depend on the track type (Figure 59a): the highest rail accelerations are obtained with independent ballastless track (largest acceleration of 80 m/s^2 at a speed of 350 km/h), while the smallest rail accelerations are found with ballasted track (largest value of 38 m/s^2 at a speed of 360 km/h). The rail accelerations with monolithic ballastless track are somewhat smaller than those with independent ballastless track, but larger than those with ballasted track.

Regarding the accelerations at the bridge deck (Figure 59b), it seems that there is a small influence of both the train speed and the track type. Largest accelerations of the order of 1.5 m/s^2 are obtained for the three track types at a speed of 360 km/h. In all cases, the bridge accelerations are below the IAPF limit of 0.35g.

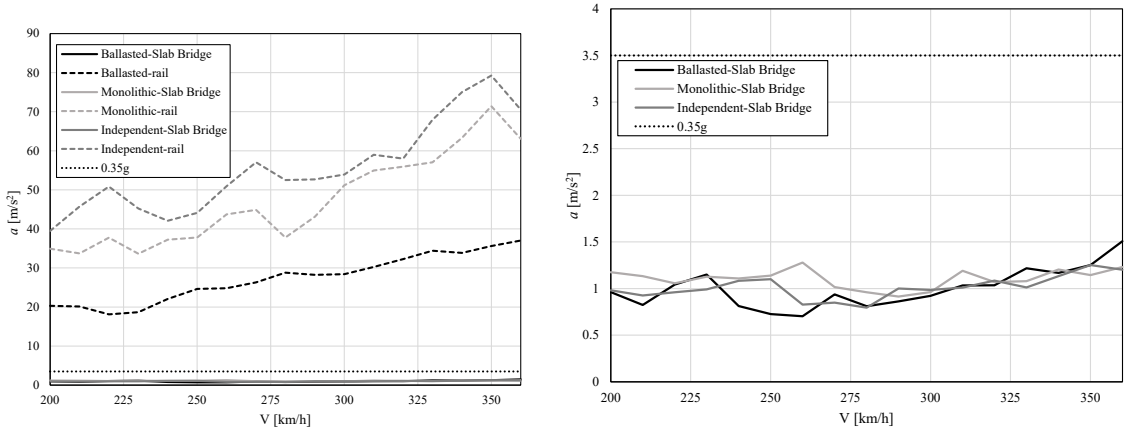

(a) (b)

Figure 59. (a) Influence of speed on the accelerations; (b) detail of bridge accelerations at the bridge. Short bridge, train Talgo.

4.4.1.2. Train AVE

The results of the AVE train crossing the short bridge at speeds of 200 and 360 km/h are shown in Figure 60 in terms of the vertical displacement of the mid-section over time. Figure 60a shows the deflections generated by the AVE for the three track types.

It should be noted that all axle forces on the AVE are not the same and their values range from 131.6 to 172.1 kN, with an axle distance of 11.0 m in the wagons approximately, and shorter distances in the locomotives. The control axis that causes the peak corresponds to the end of the first combination and the start of the second combination (a train sequence consists of two consecutive combinations, see Section 2.6). Figure 60b-c show the details for the two speeds of 200 and 360 km/h.

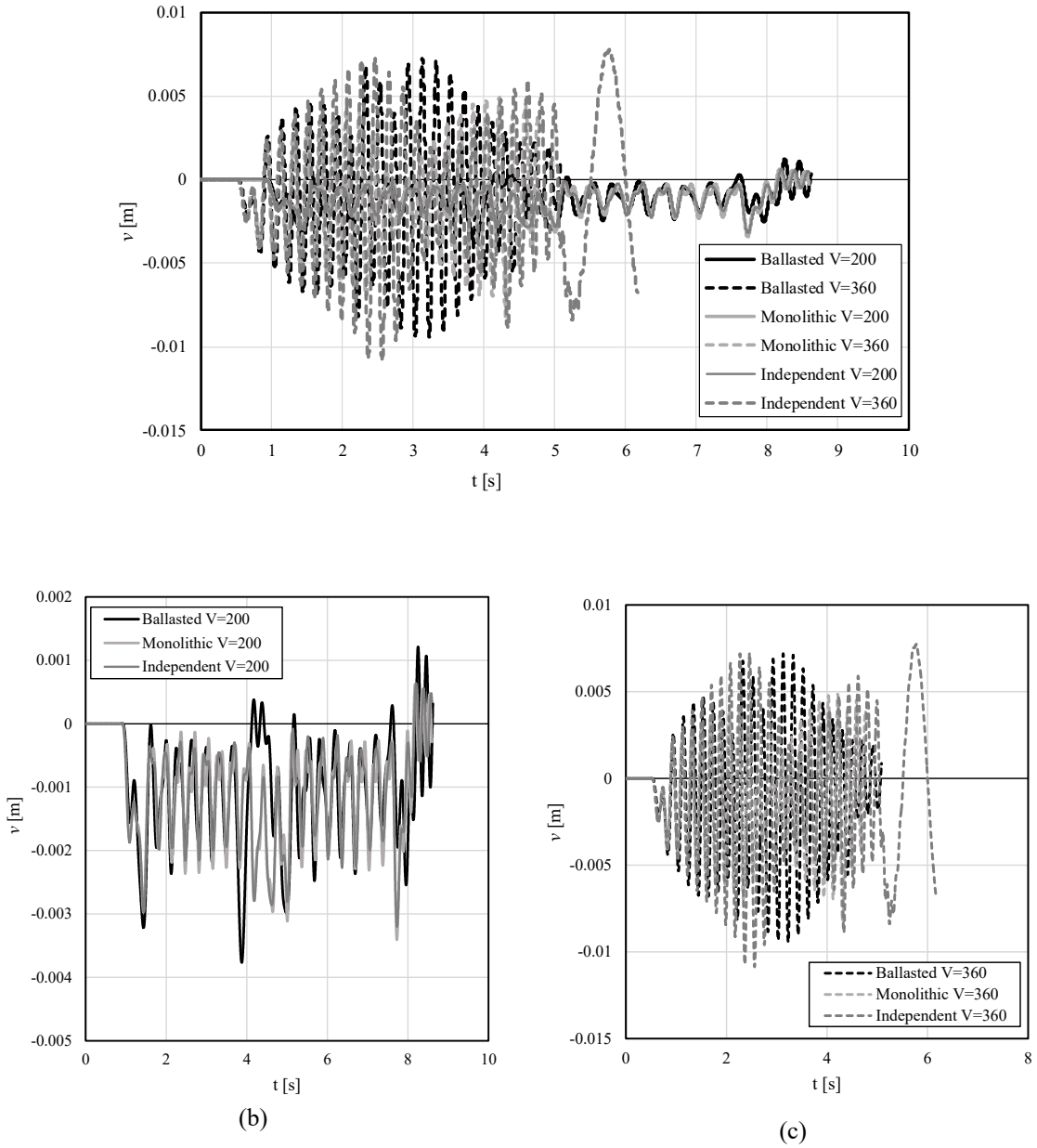

Figure 60. Results of vertical deflections at midspan of the bridge for V = 200 km/h and 360 km/h. Short bridge, train AVE for (a) the different track types; (b) detail for 200 km/h; (c) detail for 360 km/h.

The accelerations obtained as a function of time are shown in Figure 61a-b. Figure 61a shows the results with the different types of tracks for the AVE train travelling at a speed of 200 km/h, while Figure 61b shows the results in the same way for the three types of track, but with the AVE train circulating at 360 km/h.

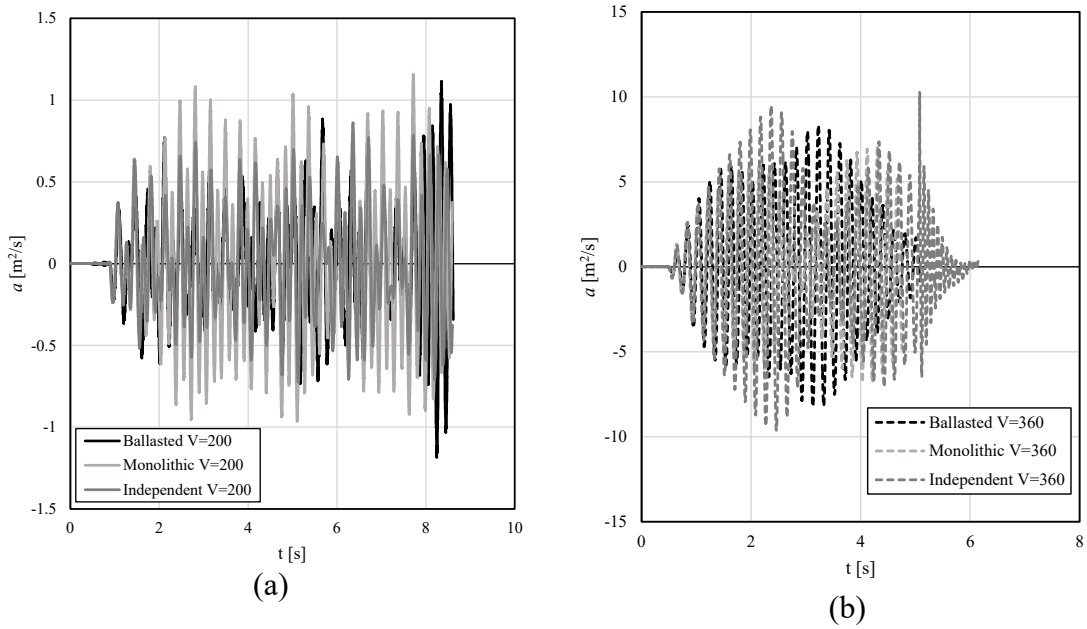

Figure 61. Results of vertical accelerations at midspan of the bridge. Short bridge, train AVE: (a) V = 200 km/h; (b) V = 360 km/h.

As it has been done in Section 4.4.1.1 for the Talgo train in the isostatic bridge, an analysis of the influence of the speed on the dynamic behavior of the bridge has been made with the peak vertical displacements. The associated DAF are plotted in Figure 62 as a function of the velocity in the range between 200 and 360 km/h. To obtain the maximum static deflections, a theoretical calculation is performed for the AVE train loads in an analogue way as it has been explained in Section 4.4.1.1 for the Talgo train. So, it is important to take into account that it is possible that in some cases the position of the loads which lead to the maximum deflection may be modified due to resonant dynamic effects caused by the arrangement of the axle loads of the train. A detail search of the governing position of train loads which results in the maximum vertical deflections has been completed in all cases.

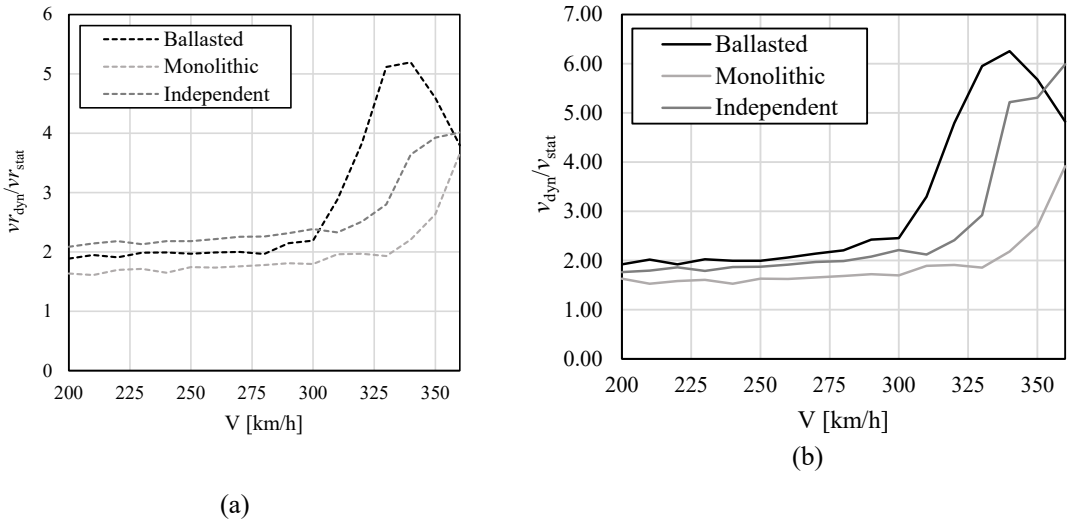

Figure 62. Influence of speed on the DAF of displacements: (a) at the rail; (b) at the bridge. Short bridge, train AVE.

The maximum accelerations obtained in the rail and the bridge deck are represented in Figure 63 as a function of the speed of the train. The maximum values at the rail depend significantly on the track type (Figure 63a): the highest rail accelerations are obtained with independent ballastless track (largest acceleration of 77.68 m/s^2 at a speed of 350 km/h), while the smallest rail accelerations are found with ballasted track (largest value of 40.38 m/s^2 at a speed of 350 km/h). The rail accelerations with monolithic ballastless track are somewhat smaller than those with independent ballastless track, but larger than those with ballasted track.

Regarding the accelerations at the bridge deck (Figure 63b), it seems that there is a high influence of both the train speed and the track type. The largest accelerations are of the order of 10.0 m/s^2 for the three track types at the highest speeds. With the ballasted track the highest acceleration is obtained at 350 km/h an its value is 9.89 m/s^2; thus, the IAPF limit of 0.35g for the deck is exceeded from a speed of 305 km/h. When the monolithic slab track is analyzed, it is observed that the peak acceleration of 7.03 m/s^2 is at 360 km/h and the standard limit is exceeded when the AVE crosses the bridge at speeds higher than 340 km/h. Last, when the independent slab track is studied, the results show that the maximum acceleration is reached at 360 km/h and its value is 10.26 m/s^2; in addition, the 0.35g limit is passed for speeds higher than 330 km/h.

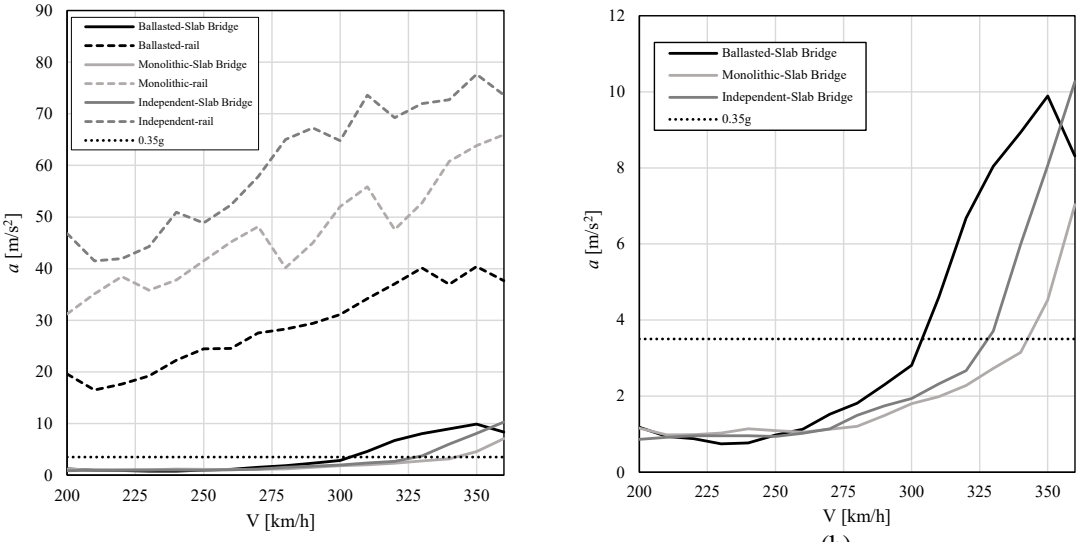

Figure 63. (a) Influence of speed on the accelerations; (b) detail of bridge accelerations at the bridge. Short bridge, train AVE.

4.4.2. Long hyperstatic Bridge

The second type of bridge analyzed is the three-span hyperstatic bridge with 40 + 60 + 40 m span lengths. Once again, both Talgo and Ave trains are considered, with the details of axle loads and axle distance given in Chapter 2. Since the bridge has different spans in the lateral and center spans, the results are analyzed in the mid-sections of both of them.

4.4.2.1. Train TALGO

a) Lateral span

The time-history midspan displacements at the lateral span of the long bridge are represented in Figure 64 for the three track types and the velocities of 200 and 360 km/h due to passage of the Talgo train (which has the same loads on all axles and a constant axle spacing between them). It is observed that the maximum deflection is -1.8 and -1.5 mm, for the speeds of 200 and 360 km/h, respectively. Figure 64b shows the detail when the Talgo train crosses the bridge at 200 km/h with the different types of track, while Figure 64c shows the same results for speeds of 360 km/h.

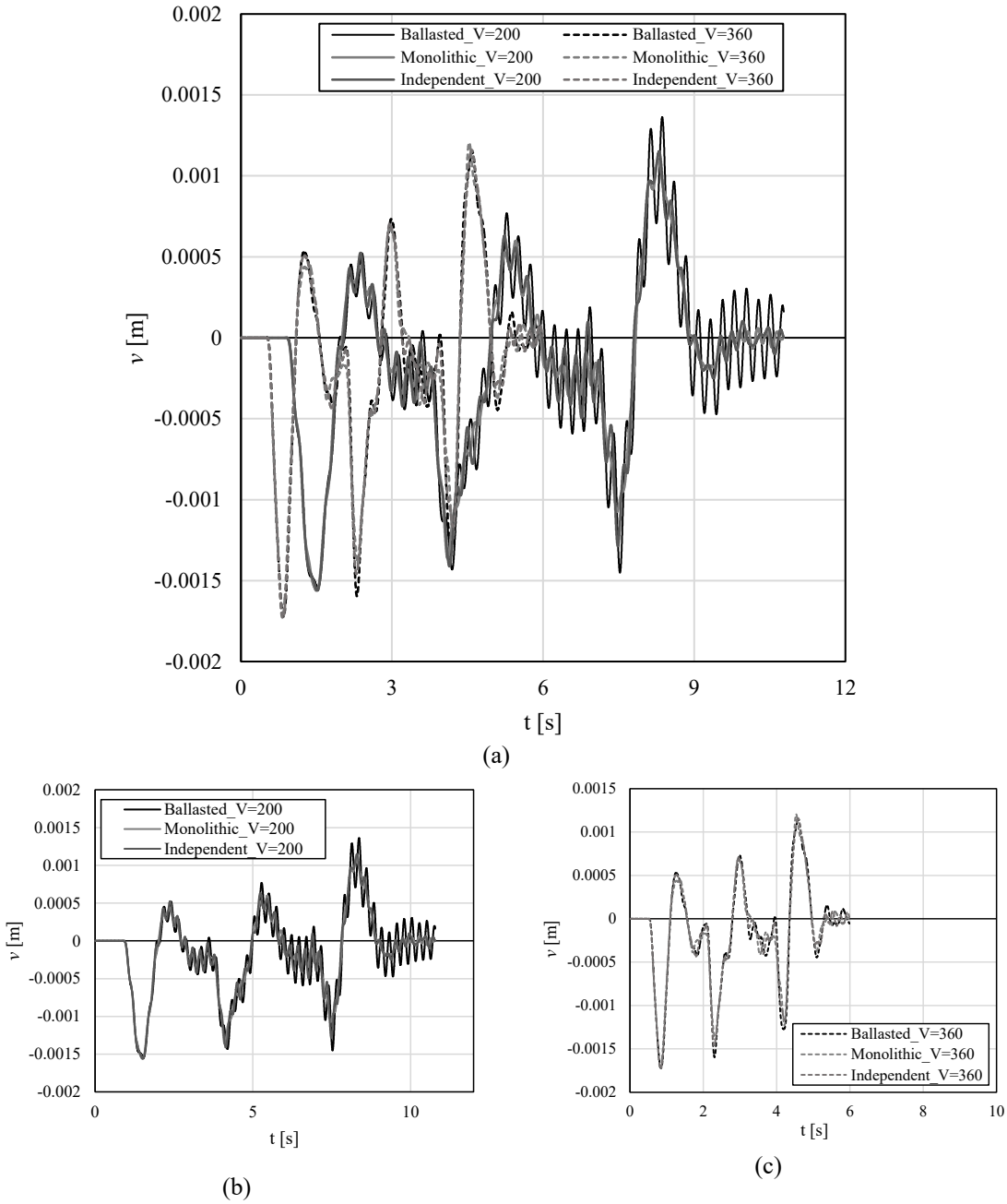

Figure 64. Results of vertical deflections at midsection of the lateral span of the bridge for V = 200 km/h and 360 km/h. Long bridge, lateral span, train Talgo for (a) the different track types; (b) detail for 200 km/h; (c) detail for 360 km/h.

Likewise, the acceleration at the mid-section of the lateral span of the bridge as a function of time can also be observed in Figure 65. Figure 65a shows the results for train passing at a speed of 200 km/h while in Figure 65b the train crosses the bridge at a speed of 360 km/h. The maximum accelerations in both cases are approximately 0.25 m/s^2 and they occur with the monolithic slab track.

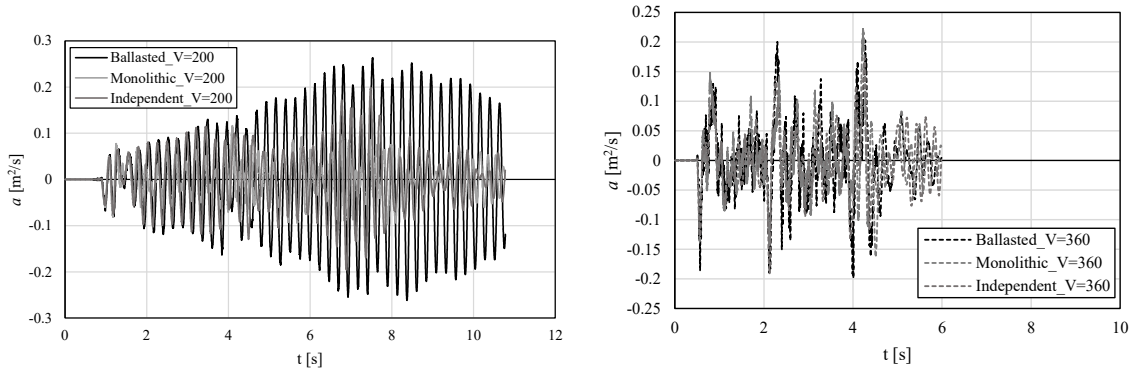

(a) (b)

Figure 65. Results of vertical accelerations at midsection of the lateral span of the bridge. Long bridge, lateral span, train Talgo: (a) V = 200 km/h; (b) V = 360 km/h.

b) Central span

The results of maximum vertical displacements and accelerations at the mid-section of the main span are studied below. Figure 66 shows the results of the maximum deflections when the train travels along the 60 m main span. Figure 66b shows the results when the speed is 200 km/h for the three types of track, obtaining a peak of -4 mm regardless of the type of track, while Figure 66c shows the results with a speed of 360 km/h, with a peak of -4.3 mm.

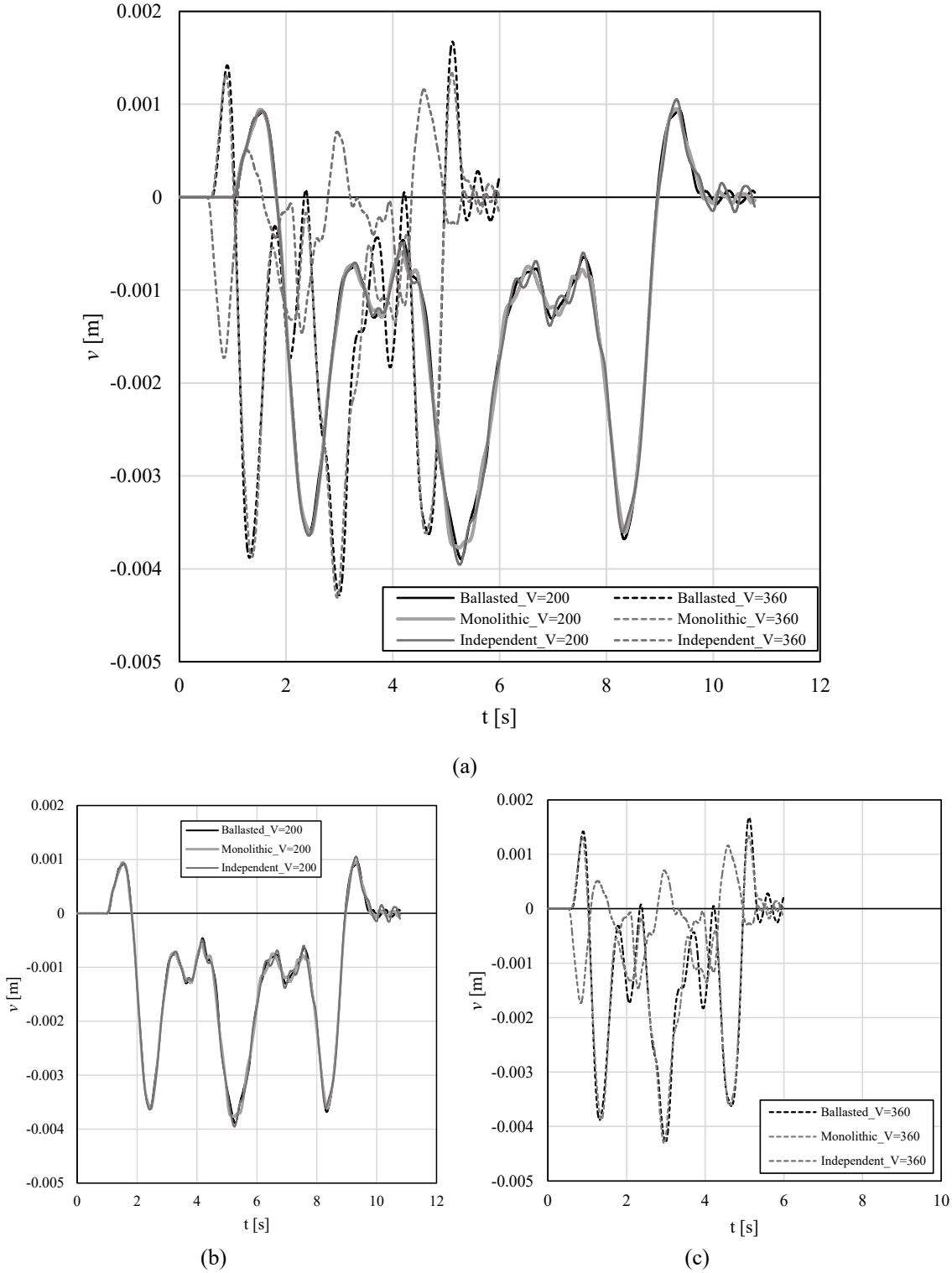

Figure 66. Results of vertical deflections at midsection of the central span of the bridge for V = 200 km/h and 360 km/h. Long bridge, central span, train Talgo for (a) the different track types; (b) detail for 200 km/h; (c) detail for 360 km/h.

In the same way, the accelerations caused by the Talgo train at the center span running at 200 and 360 km/h as a function of time are also studied in Figure 67: in Figure 67a for the speed of 200 km/h and in Figure 67b for the speed of 360 km/h, with peak accelerations of 0.07 and 0.2 m/s^2 respectively.

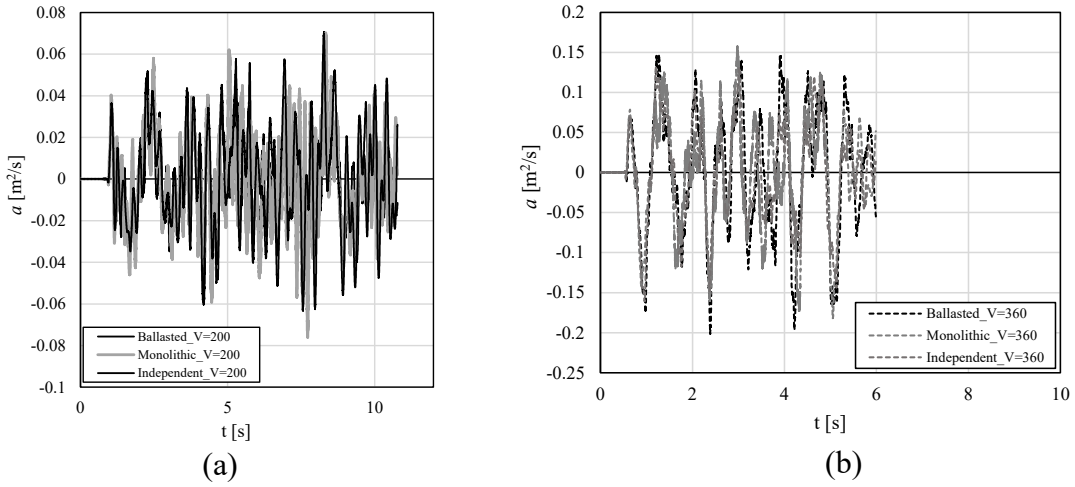

Figure 67. Results of vertical accelerations at midsection of the central span of the bridge. Long bridge, train Talgo: (a) V = 200 km/h; (b) V = 360 km/h.

c) DAF

The study of the DAF has been carried out as in the isostatic short bridge cases, studying the train passage along the long bridge at speeds ranging from 200 to 360 km/h with speed increments of 10 km/h. The maximum results are sought, which are always found at the center of the main span. As mentioned before, the maximum static displacement depends on the configuration of axle loads. Unlike in the case of the short bridge, it must be taken into account that the train can be placed here in other contiguous spans, compensating the maximum vertical displacement by the combination of actions in the three spans. Once the loads are placed on the bridge, the maximum vertical displacement has been obtained and the results are shown in Figure 68a in terms of the DAF. The largest value is 1.18 at a speed of 340 km/h in the case of monolithic ballastless track. In the case of monolithic ballasted track, the maximum of 1.17 is obtained at a speed of 310 km/h, and in the case of independent slab track, the maximum is obtained at 320 km/h with a DAF of 1.17. The results in the bridge, the DAFs are more susceptible to speed and type of track than the results in the rail. Figure 68b shows that the DAF on the rail is rather uniform for all speeds, with maximum values for ballasted track, monolithic slab track and independent slab track of 1.40, 1.33 and 1.89 at speeds of 300, 340 and 310 km/h respectively.

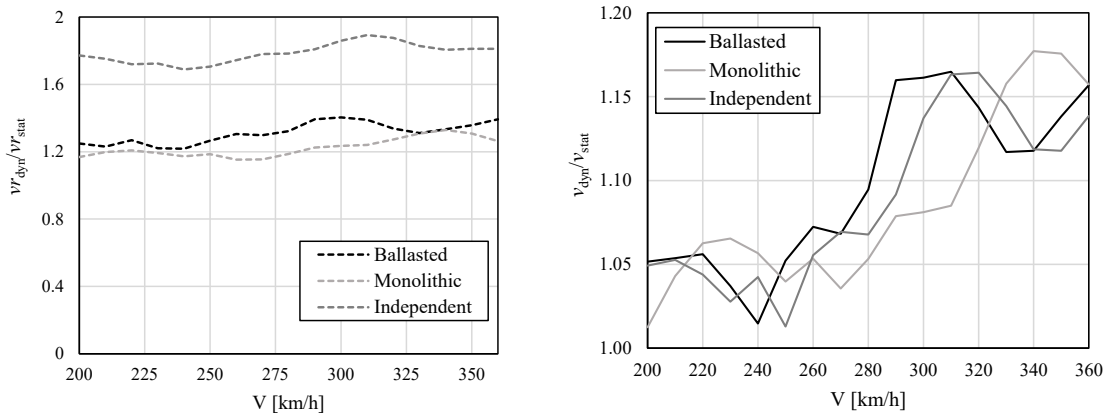

(a) (b)

Figure 68. Influence of speed on the DAF of displacements: (a) at the rail; (b) at the bridge. Long bridge, central span, train Talgo.

The accelerations obtained for the speed range from 200 to 360 km/h are shown in Figure 69. Figure 69a shows the results for all types of tracks, for both the bridge and the rail. The results for the bridge deck are far below the limits established by IAPF. Figure 69b shows only the results at the bridge deck, which are very uniform for all types of tracks throughout the entire speed range of the study. To analyze the results accurately, the maximum values of accelerations in the bridge deck are 0.21 m/s^2 at 290 km/h for ballasted track, 0.26 m/s^2 at 240 km/h for monolithic slab track, and 0.24 m/s^2 at 210 km/h for independent slab track. In all cases, the maximum accelerations are much lower than the limit imposed by the standard of 0.35 g, 14 times lower than the values obtained with respect to the limit, which is due to the beneficial effect of the hyperstatic bridge and also because train loads extend over the three spans, exciting simultaneously many vibration modes (in the short bridge, less modes are excited and the first vertical mode governs the response).

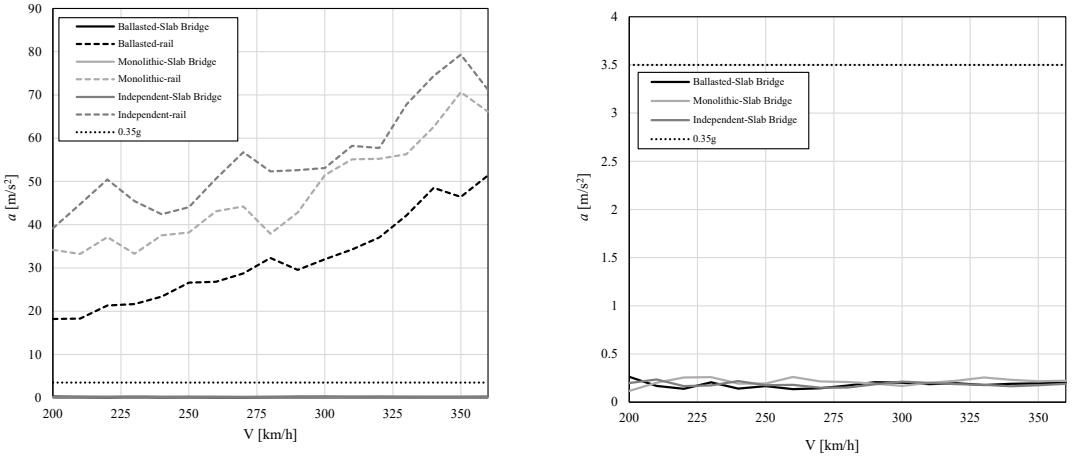

(a) (b)

Figure 69. (a) Influence of speed on the accelerations; (b) detail of bridge accelerations. Long bridge, central span, train Talgo.

4.4.2.2. Train AVE

The study carried out for the Talgo train on the hyperstatic long bridge is analogous to the study carried out for the AVE train.

a) Lateral span

The analysis begins with the time results of vertical displacement and accelerations at the mid-section of the lateral span. Figure 70a shows the deflections obtained for each type of track at speeds of 200 and 360 km/h. To observe the results with clarity, Figure 70b-c shows the details of the vertical displacements obtained when the AVE train travels along the entire length of the bridge. For a speed of 200 km/h, the maximum deflection is approximately -1.5 mm for all types of track, while at speeds of 360 km/h the maximum deflection is -2 mm, also regardless of the type of track on which the train is moving.

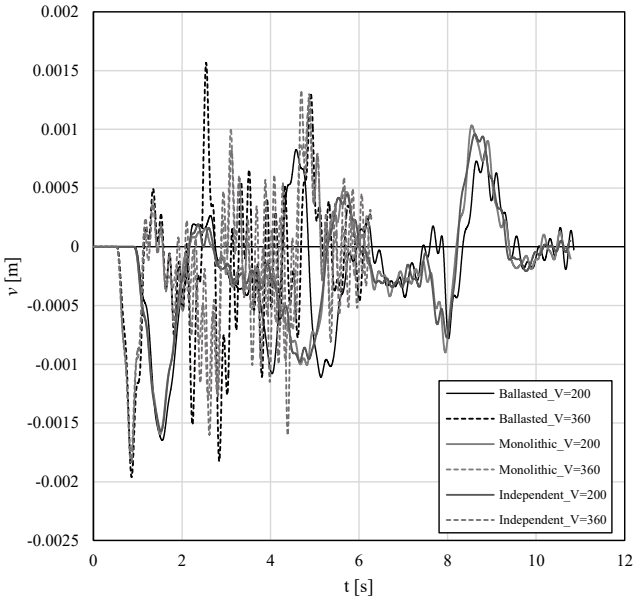

(a)

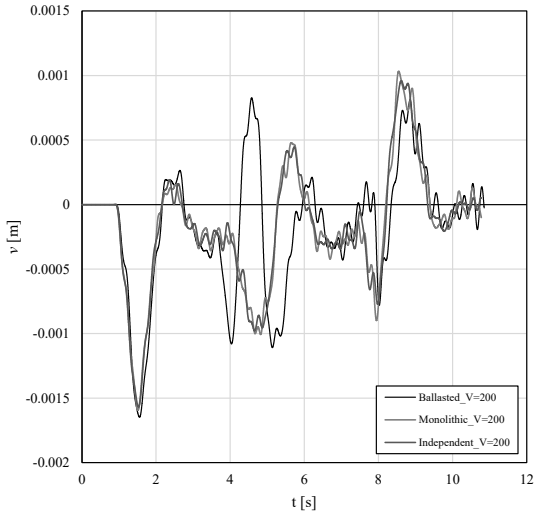

(b)

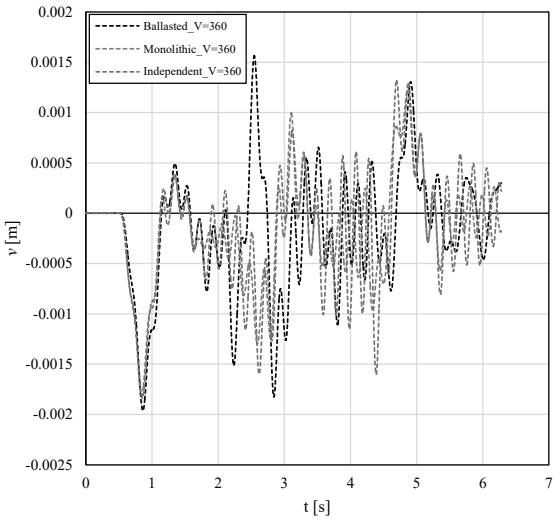

(c)

Figure 70. Results of vertical deflections at midsection of the lateral span of the bridge for V = 200 km/h and 360 km/h. Long bridge, lateral span, train AVE for (a) the different track types; (b) detail for 200 km/h; (c) detail for 360 km/h.

The results of accelerations over time are shown in Figure 71a for speeds of 200 km/h, with maximum values on ballasted track of 0.18 m/s^2, 0.12 m/s^2 on monolithic slab track and 0.08 m/s^{2}on independent slab track of. The maxima for each track type occur at different times once the train has entered the bridge. Figure 71b shows the accelerations for a speed of 360 km/h in which temporary maxima of 0.60, 0.53 and 0.83 m/s^2 are observed for ballasted, slab and independent track, respectively, again at different times.

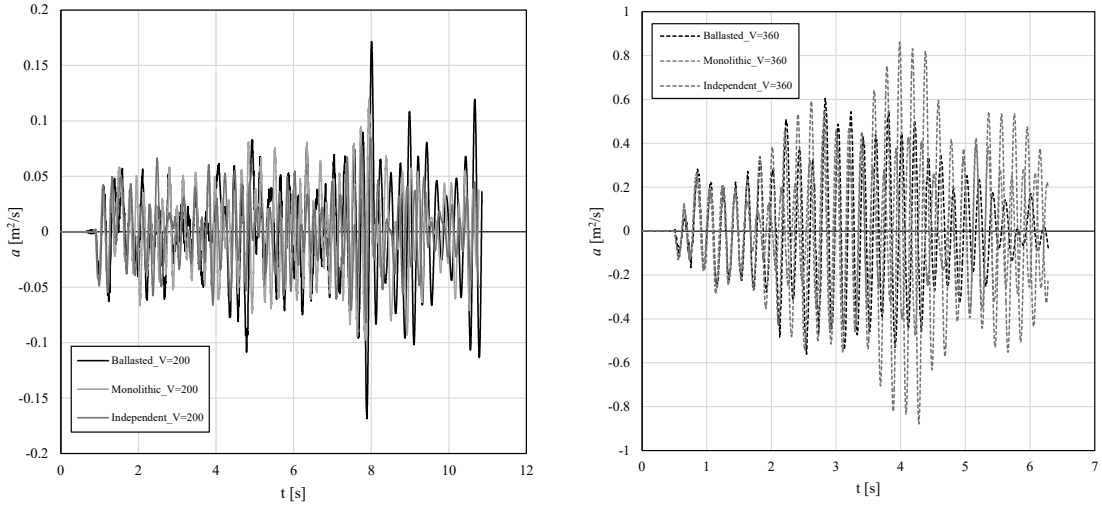

Figure 71. Results of vertical accelerations at midsection of the lateral span of the bridge. Long bridge, lateral span, train AVE: (a) V = 200 km/h; (b) V = 360 km/h.

b) Central span

At the mid-section of the main span, the maximum vertical displacements and accelerations as a function of time are studied, taking into account that the train traveling on the bridge is an AVE whose loads are not equal on all axles, nor are they equidistantly spaced.

Figure 72a shows the deflections obtained for speeds of 200 and 360 km/h for the three types of track. To analyze it in detail, Figure 72b shows the results when the train passes at 200 km/h and from which maximum vertical displacements of -3.40, -4.45 and -4.18 mm are obtained for the cases of ballasted track, monolithic slab track and independent slab track, respectively. In Figure 72c the results for the 360 km/h speed show maximum deflections of -4.48 mm on ballasted track, -4.35 mm on monolithic slab track and -1.6 mm in the case of independent slab track.

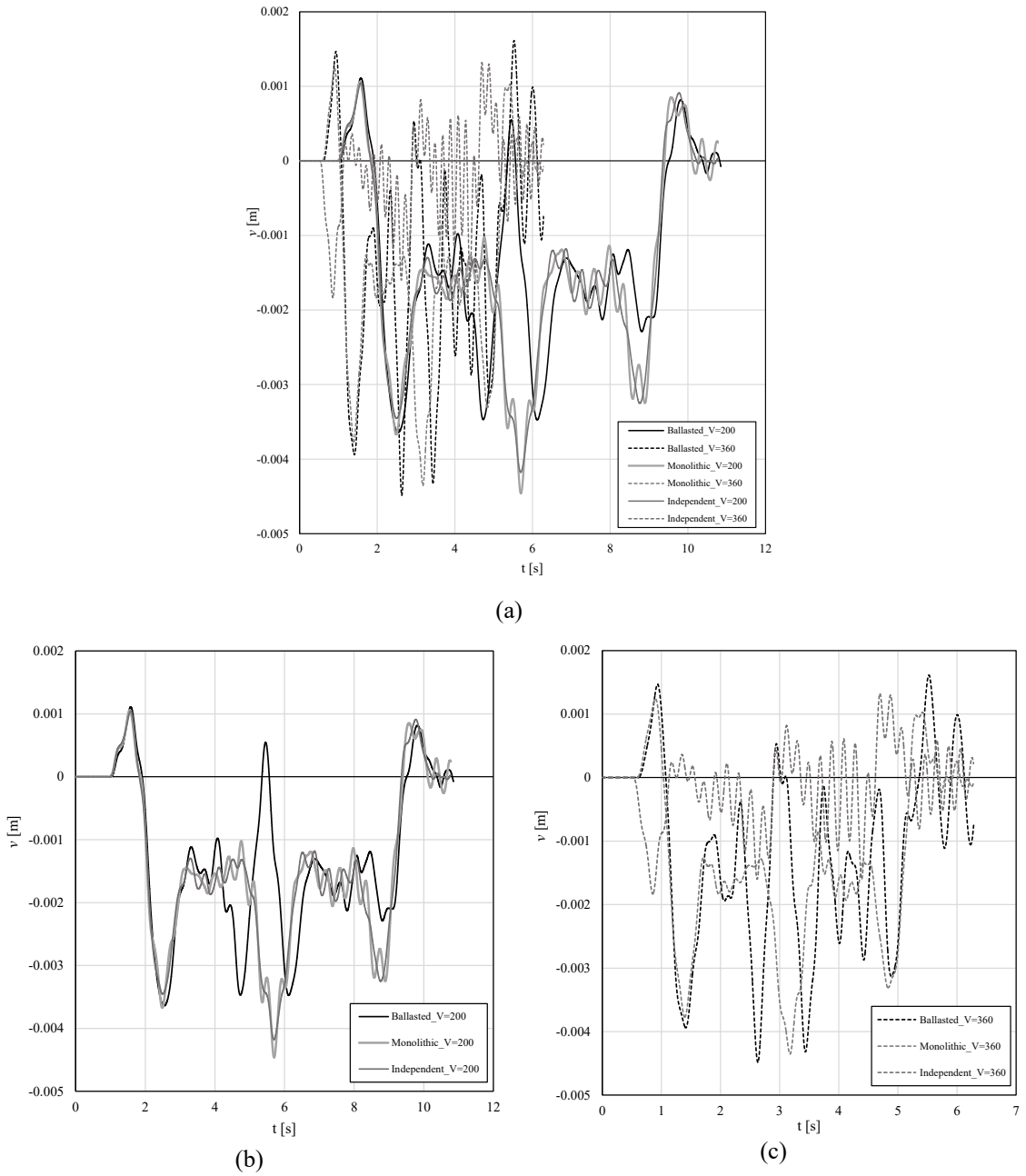

Figure 72. Results of vertical deflections at midsection of the central span of the bridge for $V = 200$ km/h and 360 km/h. Long bridge, central span, train AVE for (a) the different track types; (b) detail for 200 km/h; (c) detail for 360 km/h.

As for the analysis of the results of the accelerations over time, they are shown in Figure 73a for a speed of 200 km/h. Maximum accelerations of 1.18, 1.70 and 0.08 m/s^2 are obtained on ballasted track, on monolithic slab and on independent slab respectively. Similarly, in Figure 73b, the maximum accelerations for a train speed of 360 km/h are 0.46, 0.27 and 0.43 m/s^2 also for ballasted track, on monolithic slab and on independent slab respectively.

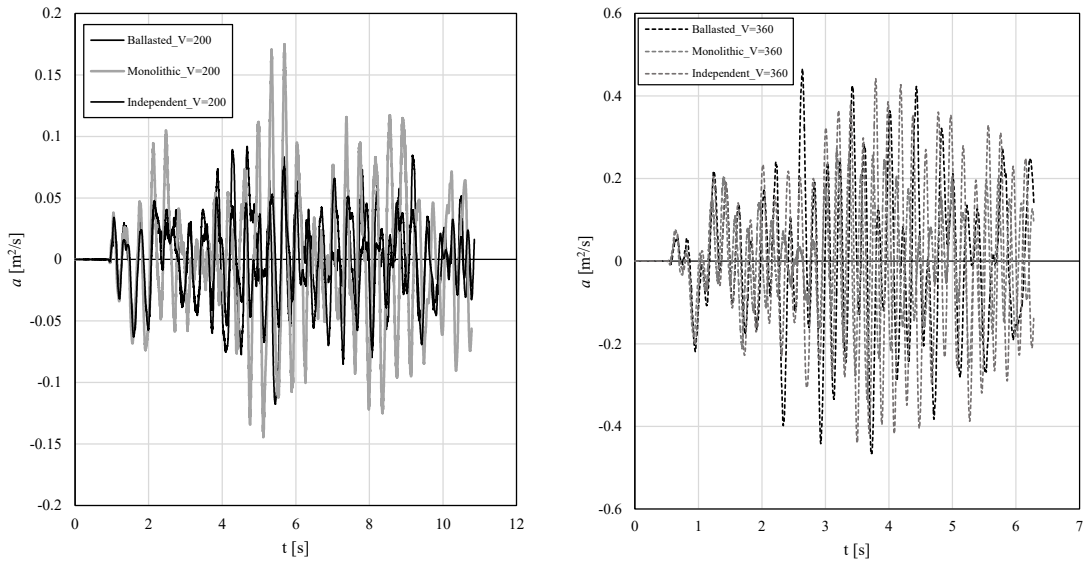

(a) (b)

Figure 73. Results of vertical accelerations at midsection of the central span of the bridge. Long bridge, central span, train AVE: (a) V = 200 km/h; (b) V = 360 km/h.

a) DAF

Finally, the study of the DAF for the hyperstatic bridge caused by the AVE train is carried out in a similar way to the previous cases. Firstly, Figure 74a shows the results for the bridge deck for the three types of track, i.e. on ballast, on monolithic slab and on independent slab, resulting in 1.18, 1.13 and 1.16 at speeds of 360, 360 and 350 km/h respectively. Figure 74b shows the DAF at the rail. Maximum results obtained are 1.41, 1.29 and 1.13 at speeds of 350, 360 and 350 km/h, respectively, for the aforementioned types of track. The DAF results in both figures are practically uniform, almost completely straight lines with a slight increase with increasing speed.

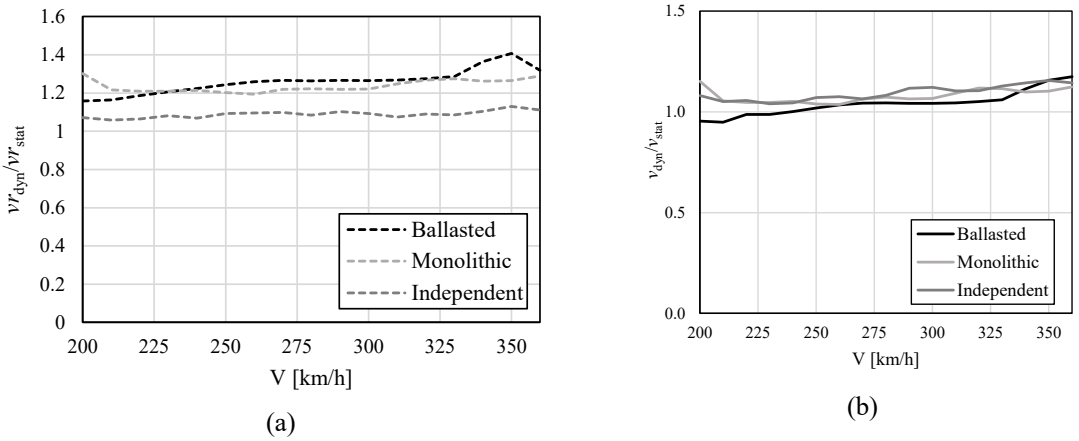

(a) (b)

Figure 74. Influence of speed on the DAF of displacements: (a) at the rail; (b) at the bridge. Long bridge, central span, train AVE.

The study of accelerations throughout the TFM has been of great importance, so once again it is verified that the maximum accelerations in the studied speed range (from 200 to 360 km/h), do not exceed the limit of most limiting value of 0.35g imposed by the standard. Figure 75a shows the maximum accelerations at the rail and the bridge, the latter being much lower than the former; therefore, Figure 75b focuses on the maximum accelerations at the bridge deck. For ballasted track a peak of 0.8 m/s^2 is reached at a speed of 350 km/h; in the case of monolithic slab track, the maximum value is 0.6 m/s2 at a speed of 330 km/h; finally, in the case of independent slab track, the maximum acceleration is 0.88 m/s2 and it is reached at 360 km/h. All these results are lower than the worst limit of 0.35g established by the IAPF, around 4.5 times less.

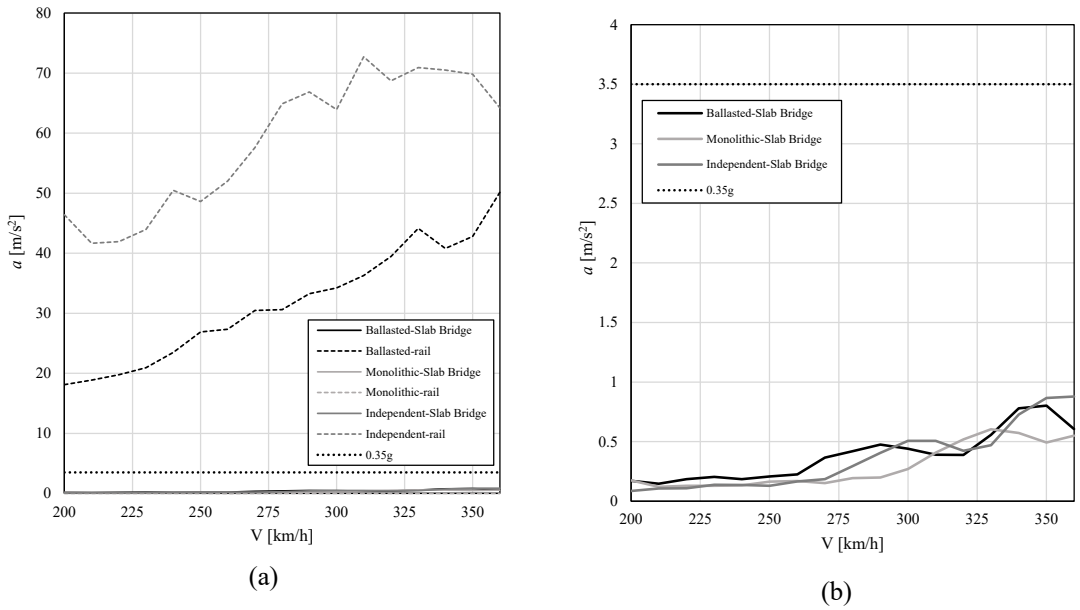

Figure 75. (a) Influence of speed on the accelerations; (b) detail of bridge accelerations. Long bridge, central span, train AVE.

Chapter 5

Discussion of results

5.1. Introduction

In this chapter, the influence of the track type on the most important results defining the dynamic response of studied bridges is discussed. Such results are the dynamic amplification factor (DAF) and the acceleration at the midspan of the bridge. The results are taken from the simulations explained in the previous chapter and they are put together in order to understand the influence of the track typology and the eventual beneficial effects produced by the installation of ballastless track systems with respect to ballasted track on high-speed railway bridges.

5.2. Effect of single moving loads

The dynamic effects produced by a single moving load as a function of the type of track and its speed has been taken as a departure point for the discussion of the results. For this study, as described in Section 4.3, the structure is an isostatic bridge of 20 m span length.

Figure 76 shows the comparison of the results of the DAFs for the three cases, the first one on ballasted track, the second one on monolithic slab track and the third one on independent slab track. It can be seen how the results obtained for the ballasted track are slightly higher than the two cases of ballastless track, although practically parallel. The results obtained in the cases of monolithic and independent slab track are the approximately coincident regardless of the speed. In all three cases, the maximum DAF is obtained when the moving load crosses the bridge at 360 km/h speed. In ballasted track the maximum value obtained is 1.7 while in slab track it is 1.6, which means that a slight reduction of the dynamic amplification produced by single running loads can be achieved if ballastless track is installed instead of ballasted track.

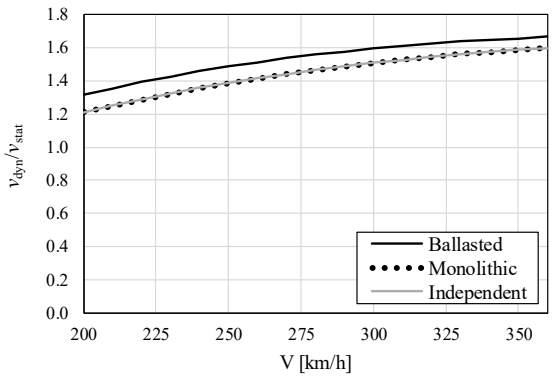

Figure 76. Comparison of DAF. Short bridge, moving point load.

5.3. Effect of train loads

5.3.1. Short single-span bridge

In order to ease the analysis of the influence of the track type on the dynamic effects induced by train loads in the studied short bridge (L = 20 m), a comparison of the results is presented in Figure 77 in terms of the DAF and the acceleration, both at the midspan section of the bridge.

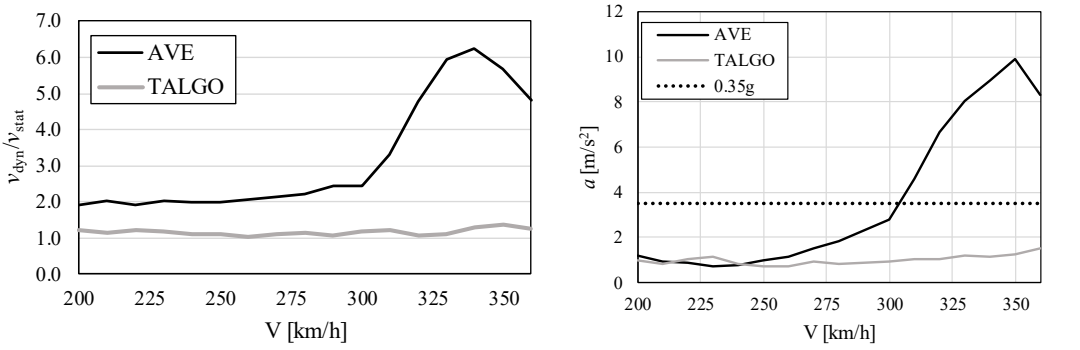

(a)

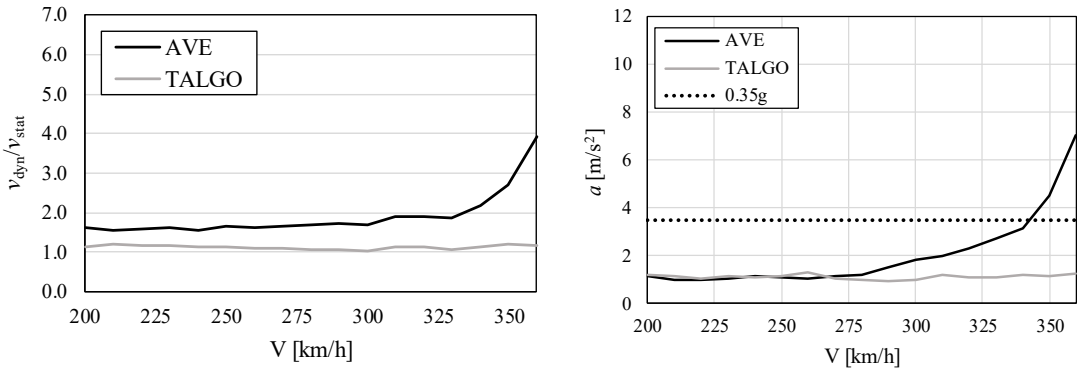

(b)

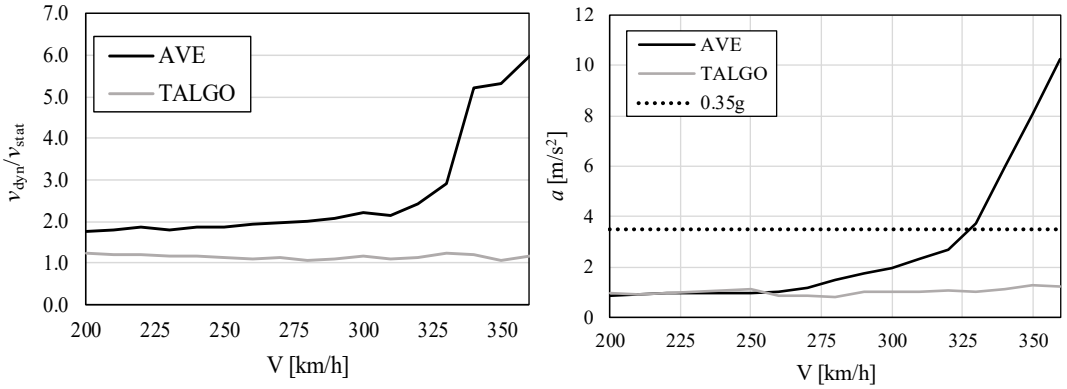

(c)

Figure 77. Comparison of DAF and midspan acceleration at the bridge. Short bridge. (a) Ballasted track; (b) Monolithic ballastless track; (c) Independent ballastless track.

With regard to the DAF (graphs in the left column of Figure 77), it is clearly observed that the AVE produces greater dynamic amplifications than the Talgo. In the case of both monolithic and independent ballastless track, the DAF produced by the AVE increases with speed, as obtained by Goicolea for ballastless track on embankment (Figure 15). In the case of ballast, no uniform trend is obtained, but the highest DAFs are obtained for intermediate speeds (this is also consistent with what Goicolea obtained for embankment, Figure 14). For AVE trains on ballasted track, the peak is around 330-340 km/h and for Talgo trains no remarkable peak is obtained. This last result is also in analogy with Goicolea's results on embankments, no uniform trend of DAF with speed is obtained (he obtains the peak at 360 km/h for D1 irregularities and 240 km/h for D2 irregularities, as defined in section 2.4.2).

The dynamic amplifications are especially high for speeds above 300 km/h for the AVE train, while for the Talgo the results are more moderate, and its maximum DAFs are found for intermediate speeds. If it is considered that the axle distance of the Talgo wagons is 13.14 m, and that the natural frequency of the bridge is approximately 5 Hz, the speed at which the greatest dynamic amplification would appear would be 236.5 km/h. The locomotive wheelbases (2.65 m and 8.35 m) would result in critical speeds below 200 km/h (outside the high-speed range). As discussed in Section 4.4.1.1, no appreciable peak is produced by the Talgo at the theoretical resonance velocity (236.5 km/h) because the highest deflections and accelerations are not caused by the axles of the wagons, but by the closely spaced axles of the locomotives. It has to be noted that the peak at the theoretical resonant velocity was not also detected in the dynamic analysis of an isostatic high-speed viaduct with ballasted track included in Monograph No. 15 (ACHE 2015).

On the other hand, the axle distance of the AVE cars is 15.7 m (extreme wheelbase) or 18.7 m (distance between bogie centers), so that the most problematic speeds would be between 283 and 340 km/h, which is consistent with Figure 77.

As for the accelerations, the graphs in the right column of Figure 77 indicate that the peaks occur at approximately the same speeds as the DAF maxima discussed in the previous paragraph. The results indicate that the Talgo would always produce accelerations below the more stringent 0.35g limit of the IAPF. However, the AVE

would exceed that limit, and even the 0.5g limit imposed by the IAPF for slab track, for the higher speeds. Therefore, there could be a loss of users' comfort for speeds higher than 305 km/h on ballasted track. If independent ballastless track is used, the loss of comfort occurs at speeds above 335 km/h (considering the 0.5g limit). Finally, the monolithic ballastless track achieves the best result, as the loss of comfort would occur for speeds higher than 350 km/h. This interesting result indicates that the use of ballastless track can be beneficial to reduce accelerations on the bridge due to the dynamic effects associated with the passage of high-speed trains.

5.3.2. Long hyperstatic bridge

Analogously to what was concluded with the results of the isostatic short bridge in the previous section, the analysis of those corresponding to the hyperstatic long bridge is discussed here, taking into account that the comparative analysis is carried out according to the types of trains operating on the bridge and the types of track.

Figure 78 shows the results of DAF and maximum accelerations for the different types of tracks. Figure 78a represents the results for ballasted track. On the left, the DAF obtained on this type of track for the Talgo and AVE trains indicates that the DAF of the former is slightly higher than that of the later, except for the highest velocities from 330 km/h onwards, where, although they are practically similar, the DAF of the AVE is higher. The maximum values obtained in both cases are 1.19 at a speed of 360 km/h. The graph on the right shows the maximum accelerations on the bridge deck for each type of train and it can be concluded that they comply with the limit established by the IAPF standard of not exceeding accelerations of 0.35 g. The maximum accelerations of the deck appear when the AVE train runs at 330 km/h and produces a value of 0.6 m/s^2, while the accelerations caused by the Talgo are practically uniform as a function of the running speed and reach the maximum of 0.35 m/s^2 at a speed of 330 km/h. Thus, the established limit is 6 times higher than the bridge accelerations in the case of the AVE train and 10 times higher in the case of the Talgo.

In the same way, the analysis of the results on the long bridge with monolithic slab track are shown in Figure 78b, in which the DAF is practically the same for the two studied trains, AVE and Talgo. The difference is that the maxima are obtained when the first train travels at 200 km/h and its value is 1.8, while that of the second train is 1.9 at 340 km/h. The accelerations are again much lower than the limit of 0.35 g: in the case of the AVE about 6 times lower because it reaches its peak at 330 km/h and its value is 0.6 m/s^2, while the Talgo produces more uniform accelerations as a function of the velocity, being the maximum of 0.3 m/s^2 at 260 km/h.

The last results are those corresponding to the independent slab track, which are shown in Figure 78c. The maximum DAF appears for the AVE train when it runs at 350 km/h and reaches a maximum value of 1.18, while the Talgo attains the maximum of 1.17 when it travels at 310 km/h. In this case it can be seen that the requirement of not exceeding the acceleration limit of 0.35g is always fulfilled. As it can be seen, the maximum acceleration of the deck is 0.98 m/s^2 when the AVE train travels at a speed of 350 km/h and 0.25 m/s^2 in the case of the Talgo at 230 km/h. This means that in the first case the maximum obtained is 3.6 times lower than the limit and in the second case 10 times lower.

Once analyzed what occurs on all types of track depending on the type of train traveling on the bridge at different speeds, it can be seen how in all cases the values of the DAF and the accelerations obtained in the long hyperstatic bridge are much lower than those obtained when the same trains on a short isostatic train. The dynamic response is lower in this case since the degree of hyperstatism reduces the critical dynamic response and more modes of vibration are excited in the long bridge than in the short one (in the short bridge, the dynamic response is mainly governed by the first mode of vibration).

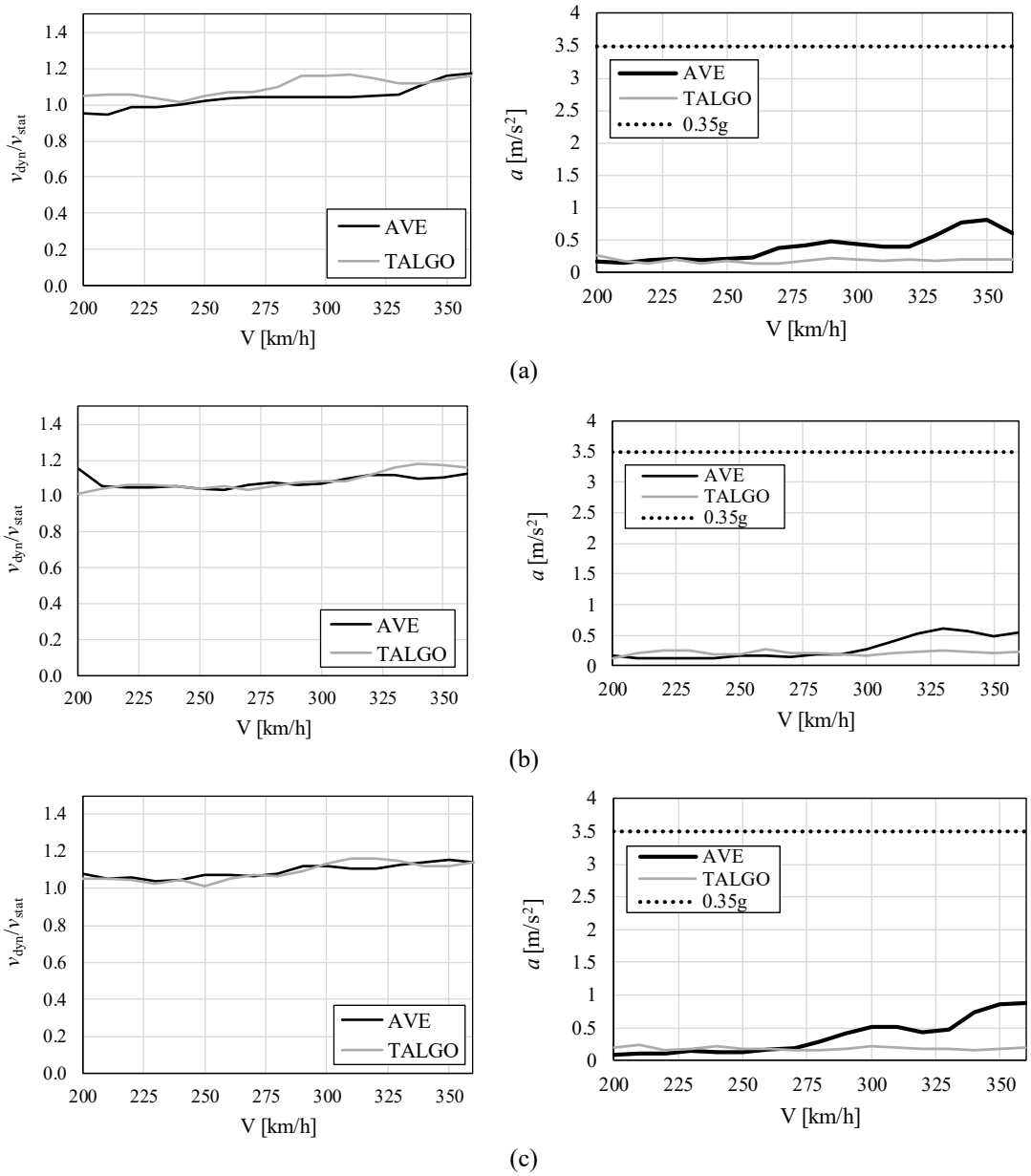

Figure 78. Comparison of DAF and midspan acceleration at the central span of the bridge. Long bridge. (a) Ballasted track; (b) Monolithic ballastless track; (c) Independent ballastless track.

In all the above cases it must be highlighted that the results are based on models with track-bridge interaction, but without considering the track irregularities. As explained in Chapter 2, such irregularities might induce additional dynamic effects. Nevertheless, for railway bridges of high-speed lines, the amount of dynamic amplification due to irregularities is much smaller than the effects produced by moving loads, which are studied in the present TFM. The former can be justified by a doing a rough estimation of the effects of the track irregularities with the help of the formulation of the IAPF. According to Appendix B of IAPF, the total dynamic amplification factor in a railway bridge can be expressed by $1 + \varphi' + r\varphi''$, where $r\varphi''$ is the amplification factor due to track irregularities, as follows:

$$\varphi'' = a\left[0.56e^{-\left(\frac{L_\Phi}{10}\right)^2} + 0.50\left(\frac{f_0 L_\Phi}{80} - 1\right)e^{-\left(\frac{L_\Phi}{20}\right)^2}\right];\ a = \min\left(\frac{V}{22}, 1\right) \tag{15}$$

In the above equation, L_Φ is the span length, f_0 is the first natural frequency and V is the train speed (in m/s). For high-speed lines (well maintained), $r = 0.5$. Therefore, for the short single-span bridge studied in the present TFM (L_Φ = 20 m, $f_0 \approx 5$ Hz), the amplification due to track irregularities for a speed of 360 km/h yields the rather moderate value of 0.061 (it is reminded that φ' is the DAF obtained from the dynamic analysis without irregularities). Therefore, it is justified to skip it in the numerical models (explicit modeling of the vehicle or the axles would be otherwise required).

Chapter 6

Conclusions

6.1. Introduction

In this chapter, the main conclusions and future research lines are highlighted. As in other research works, the results of the present TFM lead to interesting concluding remarks, which are detailed in Section 6.2. Also like in all researches, the results open the gate for further detailed analyses and other lines for future works which are listed in Section 6.3.

6.2. Conclusions

From the results obtained in this TFM, the following concluding remarks may be drawn:

- The first conclusion is extracted from the cases of short, isostatic bridges. It has been proven that the influence of the type of track is very significant for the highest speed range, especially when the train running is the AVE. In such cases, a rather high DAF is obtained and the accelerations overcome the IAPF limit of 0.35g. For the studied short bidge:

    a) Maximum accelerations of 10 m/s^2 are reached when the speed of the AVE train is 350 km/h runing on ballasted track, which are over the limit of 0.35g. Likewise, the servicebaility limit is exceeded in the case that the track is a monolithic ballastless system when the AVE train runs at speeds higher than 340 km/h (a peak of 7 m/s^2 is reached at a speed of 360 km/h). Finally, in the case of independent slab track, the limit of 0.35g is exceeded from speeds of 300 km/h, reaching a maximum acceleration of 10.5 m/s^2 at 360 km/h.

    b) The dynamic amplification produced by the Talgo train is much lower than the one caused by the AVE train due to the fact that the equidistant axle loads of the wagons do not govern the structural response, but the highest deflections and accelerations are produced by the axles of the locomotives (heads) of the train composition.

- The most relevant conclusions for the cases of the long hyperstatic bridge are that the maximum acceleration limits imposed by the IAPF standard are never exceeded. Moreover, the results in terms of deflections, DAF and accelerations are much lower than those of the short bridge for the two types of commercial trains studied, Talgo and AVE. This is due to the beneficial effect of the hyperstatic structure as the trains mobilize many vibration modes when the loads are simultaneously located in all the spans, while the the dynamic response of the short bridge is characterized by the mobilization of mainly the first vibration mode.

6.3. Future work

Besides the aspects that have been dealt with throughout this TFM, it can be considered that the work can be extended in the future with the following investigation lines.

- Perform an analysis of the influence of other types of commercial trains as well as HSML train models since the second group of trains are the most conservative envelope of all existing train types in Europe, not only in Spain. The analysis with all possible train combinations require much more computaional time than the one available for a TFM.

- Carry out a detailed study of the most critical situations of bridges, which according to the tendences observed in the present TFM might correspond to very short bridges, in particular those with a span length of less than 15 m.

- Study the influence of the dynamic effects produced by heavy trains, which despite traveling at speeds slower than 200 km/h could produce significant dynamic effects in the case that the load distribution is coupled to the structure's natural frequencies. Moreover, the track irregularirites could be also an issue in freight traffic lines, as the level of maintenance migh be lower than that of high-speed lines.

- Special typologies such as suspension bridges, arch bridges and also old bridges built with masonry materials, whose dynamic behavior is also of interest. For this type of bridges, a specific particular analysis should be carried out in each case.

Bibliography

ADIF. 2021. «NAV 7-1-0.7.»

Albajar Molera, Luis, y Carlos Zanuy Sánchez . 2007. «2.3 Caracterización del deterioro de losa y elementos de vía en placa.» En *Estudio del comportamiento a medio y largo plazo de las estructuras ferroviarias de balasto y placa*, de Jose Maria Goicolea, Manuel Cuadrado, Jordi Viñolas, Pedro Galvin y Ángel Mateos, 30-36.

2013. ANSYS Version 15.

Barkhordari, Pegah, Roberto Galeazzi, Alejandro de Miguel, y Ilmar Santos. 2019. *Identification of Behavioural Models for Railway Turnouts Monitoring.* Denmark. https://www.researchgate.net/figure/Railway-track-cross-section-with-highlighted-components_fig2_336552261.

Chopra, Anil K. 2007. *Dynamics of structures.* Pearson Education.

Claisse, Peter, y Calla Calla. 2006. «Rail ballast: Conclusions from a historical perspective.» *Proceedings of the ICE - Transport (P I CIVIL ENG-TRANSP)* 159 (2): 69-74. http://dx.doi.org/10.1680/tran.2006.159.2.69.

Clough , Ray , y Joseph Penzien . 2010. *Dynamics of structures.* McGraw-Hill Education.

Dominguez Barbero, Jaime. 2001. *Dinámica de puentes de ferrocarril para alta velocidad: métodos de cálculo y estudio de la resonancia* . Tesis doctoral, Universidad Politécnica de Madrid.

EN 1991-2: EUROCODE 1, European Committee for Standardization. 2002. «Action on structures.» *Traffic loads on bridges.*

ERRI, European Rail Research Institute. 2002. «Utilisation de convois universels pour le dimensionnement dynamique de ponts-rails.» Cap. ERRI D214.2 RP1.

Esveld, Coenraad. 2001. *Modern Railway Track.* Delft: MRT-Productions. www.esveld.com.

FCH, Fundación Caminos de Hierro. 2006. *Proyecto PT-2006-024-19CCPM.* Informe final del proyecto de investigación.

Goicolea , José María. 2011. “Acciones dinámicas debidas al tráfico ferroviario en viaductos de alta velocidad.”. Actas del Seminario Torroja 2011, Madrid, España.

Goicolea Ruigómez, José Maria, Luis Albajar Molera , Pablo de la Fuente Martín, Felipe Gabaldón Castillo, Khanh Nguyen, Carlos Zanuy Sánchez , Mario Bermejo Castro, and Cecilia Vale. 2007. “2.2 Caracterización mecánica y evaluación de las acciones dinámicas transmitidas por tráficos a la losa y plataforma de las vías.” In *Estudio del comportamiento a medio y largo plazo de las estructuras ferroviarias de balasto y placa*, by José Maria Goicolea , Manuel Cuadrado, Jordi Viñolas, Pedro Galvin and Ángeles Mateos, 18-30.

Goicolea Ruigómez, Jose Mª. 2007. "La consideración de los fenómenos dinámicos en el proyecto de puentes ferroviarios." https://w3.mecanica.upm.es/papers/cordoba_JMGoicolea.pdf.

González Rodríguez , Óscar. 2010. "Interacción Vía estructura en puentes de ferrocarril". Trabajo de Fin de Máster, Universidad Politécnica de Madrid.

Humar, Jagmohan L. 2005. *Dynamics of structures* . The Netherlands: Balkema Publishers.

IAPF, MOF. 2007. «Instrucción sobre las acciones a considerar en el proyecto de puentes de ferrocarril, IAPF-07.»

INECO. 2018. «Estudio Informativo del Proyecto de la Línea de Alta Velocidad Palencia-Alar del Rey.»

Martín de Soto Aláez , Alfonso. 2020. *Interacción longitudinal vía - estructura en puentes de ferrocarril con plataforma de vía en placa.* Trabajo Fin de Máster, Universidad Politécnica de Madrid.

Michas, Georgios. 2012. «Slab Track Systems for High-Speed Railways.» Masters Degree Project , KTH - Royal Institute Of Technology.

Tayabji, Shiraz. 2000. «Concrete slab track for freight and high speed service applications.» *Transportation Research Record Journal of the Transportation Research Board.*

UIC, Union Internationale des Chemins de Fer. 1979. *Charges a prendre en considération dans le calcul des ponts-rails.*

Zhai, W, K Wang , Z Chen, S Zhu, C Cai, y G Liu. 2020. «Full-scale multi-functional test platform for investigating mechanical performance of track–subgrade systems of high-speed railways.» *Railway Engineering Science* 28: 213-231.

Annex I

Practical Application

1. Memory

The practical application is focused on a 30 m viaduct with a single span of slab track over the Huerna river, in the Pajares-AV bypass in Pola de Lena, which belongs to the León-Asturias high speed line and belongs to the La Robla-Campomanes section.

The type of slab track that has been considered in this practical application for this viaduct is a monolithic slab track, consisting of a reinforced concrete slab in which bi-block sleepers are embedded.

The cross-section consists of a double trough beam with a B355-W60M concrete slab spaced 60 cm apart. This eliminates the joint between slab and trough concrete, which in the medium term leads to cracks and durability problems, and reduces the construction height. Thanks to the bi-block sleeper, which is connected by lattice reinforcement, the contact surface between the slab concrete and the sleeper, which could be one of the weak points of the system under dynamic effects, is minimized. In addition, the contact surface of the reinforcement with the slab concrete is increased.

2. Economic valuation

The following is a summary of the budget for the 30 m long viaduct over the Huerna River based on the materials and measurements obtained from the Revit model.

RESUMEN DE PRESUPUESTO

Viaducto sobre el Huerna para AV

CAPÍTULO	RESUMEN	IMPORTE	%
2001263	Plataformas	203 545.55	30.41
2001300	Cimentación estructural	173 835.19	25.97
2000700	Materiales	142 039.89	21.22
2001320	Armazón estructural	43 320.33	6.47
2000032	Suelos	20 085.24	3.00
2000126	Barandillas	85 470.31	12.77
2008044	Tuberías	446.96	0.07
2000151	Modelos genéricos	538.16	0.08
	PRESUPUESTO DE EJECUCIÓN MATERIAL	**669 281.63**	
	21% IVA	140 549.14	
	PRESUPUESTO BASE DE LICITACIÓN	**809 830.77**	

Asciende el presupuesto a la expresada cantidad de OCHOCIENTOS NUEVE MIL OCHOCIENTOS TREINTA con SETENTA Y SIETE CÉNTIMOS

3. Construction Plan

First of all, the yields of each of the works described above will be determined in the economic valuation, represented below in the yield summary and according to the phases of the work.
Figure 79 below shows a series of views of the model from which the yields have been extracted, the optimum work plan and the measurements for the budget summarized in the previous section.

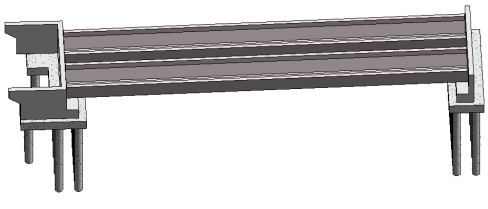

(a)

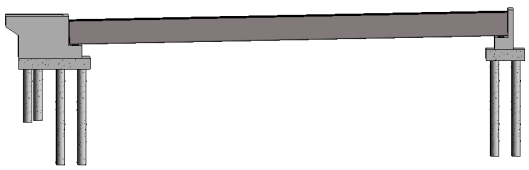

(b)

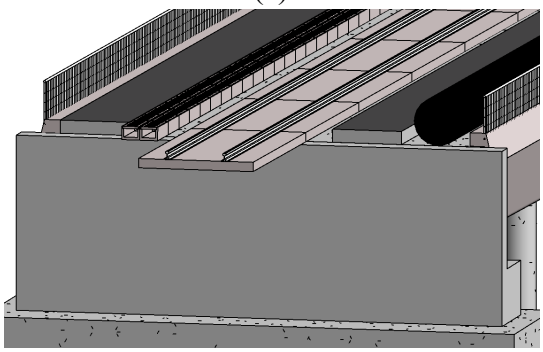

(c)

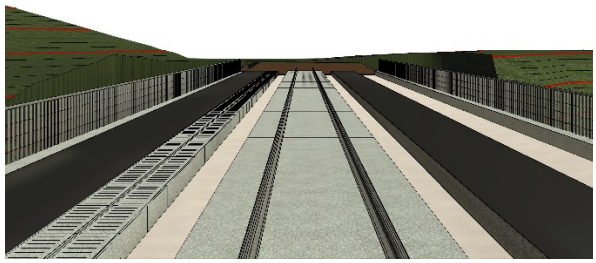

(d)

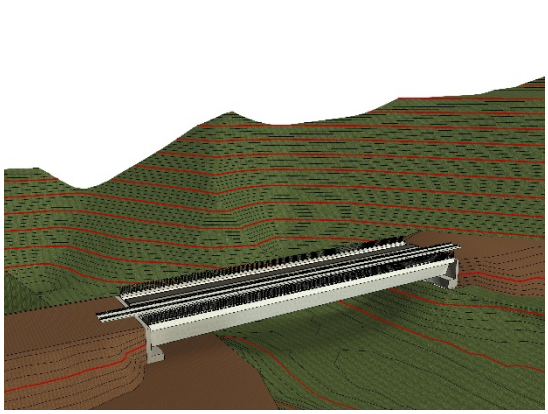

(d)

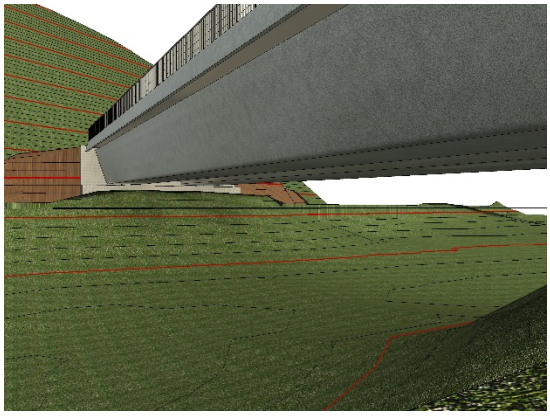

(e)

Figure 79. Bridge over Huerna river. a) View of the viaduct in perspective, b) profile of the viaduct, c) detail of the track slab and UIC-60 rails, d) view of the track section over the viaduct, d) location of the viaduct, e) detail of the trough beam below.

The construction phases and their critical path are shown in the attached Gant Diagram. The first phase consists of preliminary actions, followed by the execution of the foundations, the structure, the laying of the slab track and finally the finishing work, all within a period of seven months.

CUADRO DE RENDIMIENTOS

UD	ACTIVIDAD	MEDICIONES Y RENDIMIENTOS					DURACIÓ			
		Med.	Rto teórico	Coef. Clima	Coef. Corr.	Rdto. Real	Total dias	HORARIO	TURNOS	Nº EQ.
	FASE 1: CIMENTACIÓN									
m3	Pilotes E1	126.670	4.00	0.890	0.850	3.00	42.22	**DIURNO**	**1**	1
m3	Encepado E1	41.760	8.00	0.800	0.850	5.00	8.35	**DIURNO**	**1**	1
m3	Encepado E2	58.720	8.00	0.800	0.850	5.00	11.74	**DIURNO**	**1**	1
m3	Estribo E1	35.470	6.00	0.800	0.850	4.00	8.87	**DIURNO**	**1**	1
m3	Estribo E2	54.080	6.00	0.800	0.850	4.00	13.52	**DIURNO**	**1**	1
	FASE 2: ESTRUCTURA									**1**
ud	Colocacion neoprenos	4.000	10.00	0.800	0.850	7.00	0.57	**DIURNO**	**1**	1
m3	Viga artesa 1 (forma en U)	61.500	80.00	0.893	0.850	61.00	1.01	**DIURNO**	**1**	1
m3	Viga artesa 2 (forma en U)	61.500	80.00	0.893	0.850	61.00	1.01	**DIURNO**	**1**	1
m3	Losa hormigón	193.500	20.00	0.800	0.850	14.00	13.82	**DIURNO**	**1**	1
m3	Bases barandillas	6.174	7.00	0.800	0.850	5.00	1.23	**DIURNO**	**1**	1
m	Barandillas	100.000	50.00	0.800	0.850	34.00	2.94	**DIURNO**	**1**	1
	FASE 3 : VÍA EN PLACA									**1**
m2	Losas prefabricadas	793.040	800.00	0.800	0.850	544.00	1.46	**DIURNO**	**1**	1
m	Rieles	100.006	90.00	0.800	0.850	61.00	1.64	**DIURNO**	**1**	1
	FASE 4 : ACABADOS									
ud	Aceras	61.500	20.00	0.800	0.850	14.00	4.39	**DIURNO**	**1**	1
m3	Canaletas	3.460	3.00	0.800	0.800	2.00	1.73	**DIURNO**	**1**	1
m	Tapa canaletas	50.000	80.00	0.800	0.800	51.00	0.98	**DIURNO**	**1**	1
m	Tuberia drenaje	50.000	500.00	0.800	0.800	320.00	0.16	**DIURNO**	**1**	1

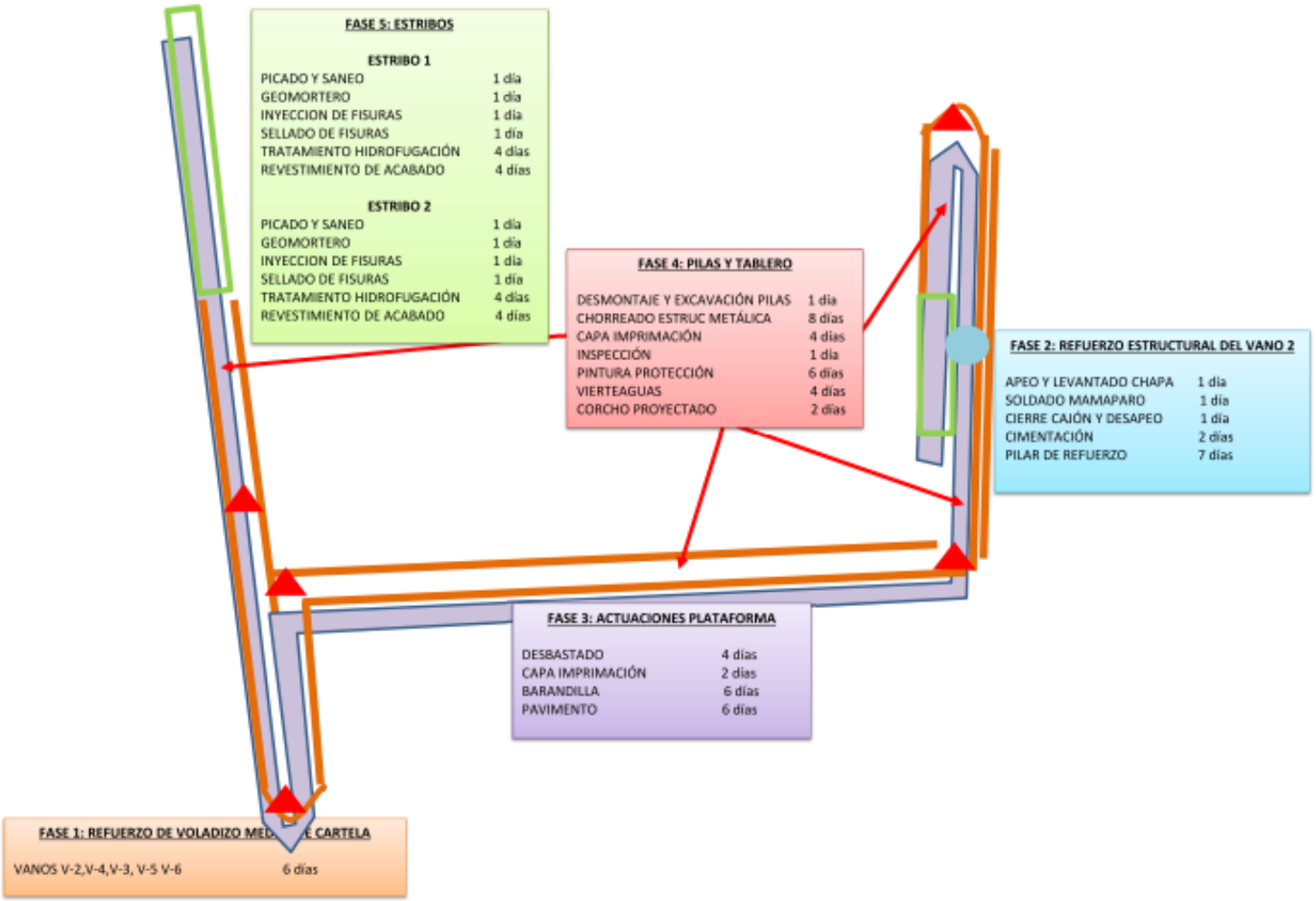
FASE 5: ESTRIBOS
ESTRIBO 1
PICADO Y SANEO 1 día
GEOMORTERO 1 día
INYECCION DE FISURAS 1 día
SELLADO DE FISURAS 1 día
TRATAMIENTO HIDROFUGACIÓN 4 días
REVESTIMIENTO DE ACABADO 4 días
ESTRIBO 2
PICADO Y SANEO 1 día
GEOMORTERO 1 día
INYECCION DE FISURAS 1 día
SELLADO DE FISURAS 1 día
TRATAMIENTO HIDROFUGACIÓN 4 días
REVESTIMIENTO DE ACABADO 4 días
FASE 4: PILAS Y TABLERO
DESMONTAJE Y EXCAVACIÓN PILAS 1 día
CHORREADO ESTRUC METÁLICA 8 días
CAPA IMPRIMACIÓN 4 días
INSPECCIÓN 1 día
PINTURA PROTECCIÓN 6 días
VIERTEAGUAS 4 días
CORCHO PROYECTADO 2 días
FASE 2: REFUERZO ESTRUCTURAL DEL VANO 2
APEO Y LEVANTADO CHAPA 1 día
SOLDADO MAMAPARO 1 día
CIERRE CAJÓN Y DESAPEO 1 día
CIMENTACIÓN 2 días
PILAR DE REFUERZO 7 días
FASE 3: ACTUACIONES PLATAFORMA
DESBASTADO 4 días
CAPA IMPRIMACIÓN 2 días
BARANDILLA 6 días
PAVIMENTO 6 días
FASE 1: REFUERZO DE VOLADIZO MED E CARTELA
VANOS V-2,V-4,V-3, V-5 V-6 6 días

DIAGRAMA DE GANTT

Id	Nombre de tarea	Duración	Comienzo	Fin
1	Viaducto sobre el río Huerna	145 días	lun 02/08/21	mar 22/02/22
2	INICIO DE LAS OBRAS	0 días	lun 02/08/21	lun 02/08/21
3	GESTIONES PREVIAS	145 días	lun 02/08/21	mar 22/02/22
4	Acta de replanteo	1 día	lun 02/08/21	lun 02/08/21
5	Aprobación de plan de seguridad y salud	1 día	lun 02/08/21	lun 02/08/21
6	Localización de servicios afectados	1 día	mar 03/08/21	mar 03/08/21
7	Encargo de elementos prefabricdos	30 días	mar 03/08/21	lun 13/09/21
8	Instalaciones auxiliares (casetas)	4 días	mar 03/08/21	vie 06/08/21
9	FASE 1: CIMENTACIÓN	106 días	lun 09/08/21	mié 05/01/22
10	Pilotes	43 días	lun 09/08/21	mié 06/10/21
11	Encepado E1	9 días	jue 07/10/21	mié 20/10/21
12	Encepado E2	12 días	jue 21/10/21	lun 08/11/21
13	Movimiento de tierras	20 días	mar 09/11/21	lun 06/12/21
14	Estribo E1	8 días	mar 07/12/21	jue 16/12/21
15	Estribo E2	14 días	vie 17/12/21	mié 05/01/22
16	FASE 2: ESTRUCTURA	15 días	jue 06/01/22	mié 26/01/22
17	Colocacion neoprenos	1 día	jue 06/01/22	jue 06/01/22
18	Viga artesa 1 (forma en U)	1 día	vie 07/01/22	vie 07/01/22
19	Viga artesa 2 (forma en U)	1 día	vie 07/01/22	vie 07/01/22
20	Losa hormigón	8 días	lun 10/01/22	mié 19/01/22
21	Bases barandillas	2 días	jue 20/01/22	vie 21/01/22
22	Barandillas	3 días	lun 24/01/22	mié 26/01/22
23	FASE 3:VÍA EN PLACA	10 días	jue 27/01/22	mié 09/02/22
24	Losas prefabricada 1	2 días	jue 27/01/22	vie 28/01/22
25	Losas prefabricada 2	2 días	lun 31/01/22	mar 01/02/22
26	Losas prefabricada 3	2 días	mié 02/02/22	jue 03/02/22
27	Losas prefabricada 4	2 días	vie 04/02/22	lun 07/02/22
28	Rieles	2 días	mar 08/02/22	mié 09/02/22
29	FASE 4: ACABADOS	5 días	jue 10/02/22	mié 16/02/22
30	Aceras	5 días	jue 10/02/22	mié 16/02/22
31	Canaletas	2 días	jue 10/02/22	vie 11/02/22
32	Tapa canaletas	1 día	lun 14/02/22	lun 14/02/22
33	Tubería drenaje	1 día	jue 10/02/22	jue 10/02/22
34	LIMPIEZA OBRA	4 días	jue 17/02/22	mar 22/02/22
35	SEGURIDAD Y SALUD	145 días	lun 02/08/21	mar 22/02/22
36	GESTIÓN DE RESIDUOS	145 días	lun 02/08/21	mar 22/02/22
37	CONTROL DE CALIDAD	145 días	lun 02/08/21	mar 22/02/22
38	FIN DE OBRA	0 días	mar 22/02/22	mar 22/02/22

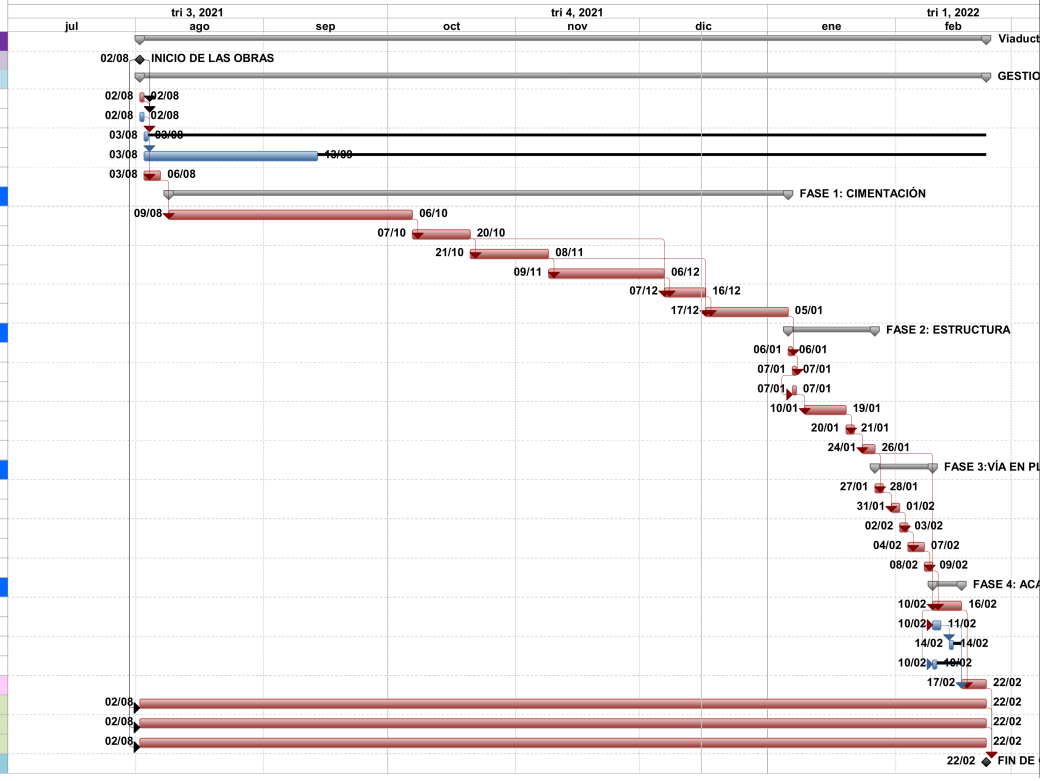

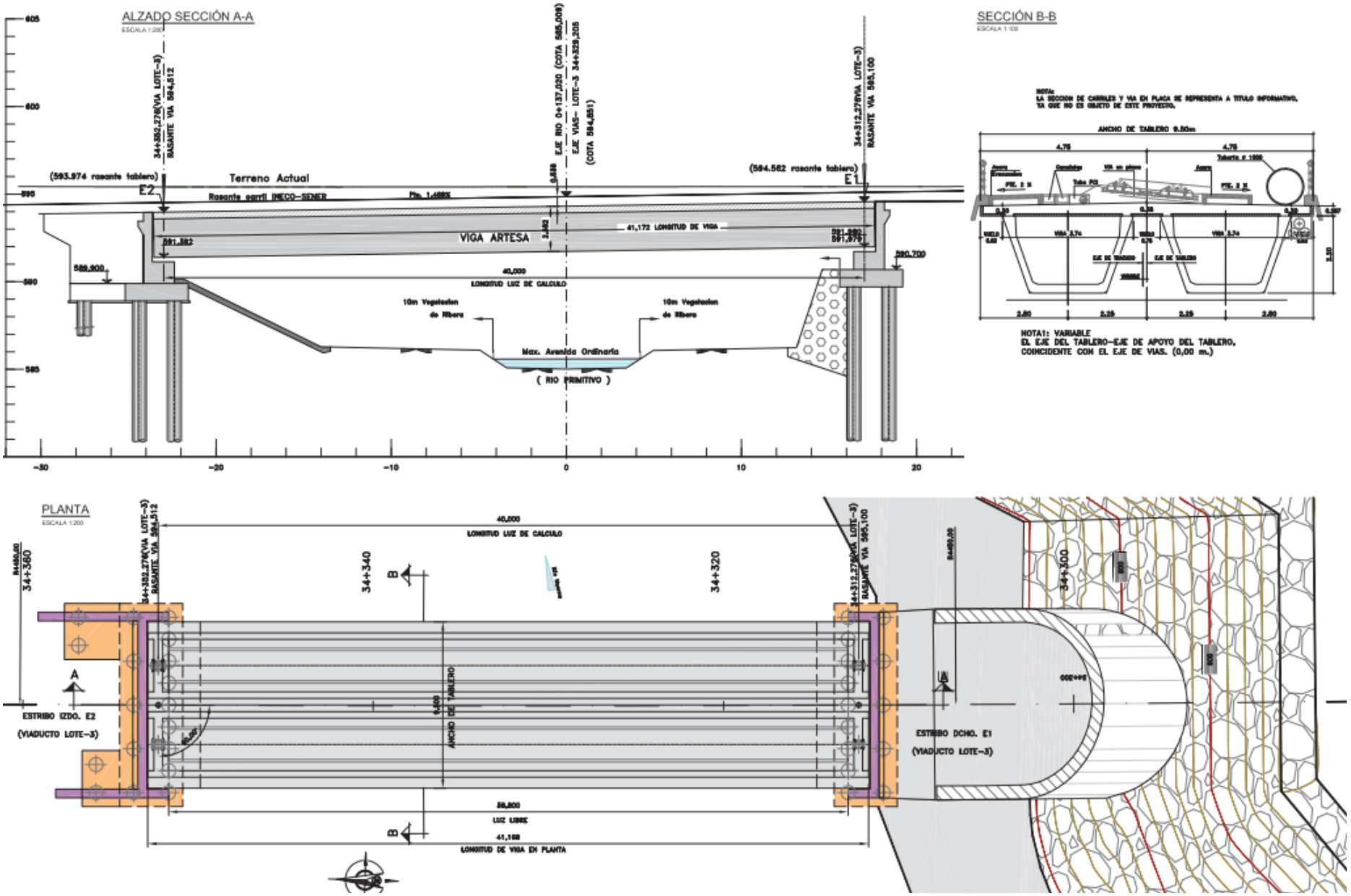
ALZADO SECCIÓN A-A
ESCALA 1:200
SECCIÓN B-B
ESCALA 1:100
PLANTA
ESCALA 1:200
Terreno Actual
Rasante carril INECO–SENER
VIGA ARTESA
41,172 LONGITUD DE VIGA
40,000
LONGITUD LUZ DE CALCULO
10m Vegetacion de Ribera
10m Vegetacion de Ribera
Max. Avenida Ordinaria
(RIO PRIMITIVO)
(593.974 rasante tablero)
(594.562 rasante tablero)
E2
E1
34+352.276(VIA LOTE–3) RASANTE VIA 594.512
34+312.276VIA LOTE–3) RASANTE VIA 595.100
EJE RIO 0+137.020 (COTA 585.009)
EJE VIAS– LOTE–3 34+329.205 (COTA 594.851)
589.900
590.700
591.582
591.970
ANCHO DE TABLERO 9.50m
NOTA1: VARIABLE
EL EJE DEL TABLERO–EJE DE APOYO DEL TABLERO, COINCIDENTE CON EL EJE DE VIAS. (0,00 m.)
34+360
34+340
34+320
34+300
ESTRIBO IZDO. E2
(VIADUCTO LOTE–3)
ESTRIBO DCHO. E1
(VIADUCTO LOTE–3)
ANCHO DE TABLERO
38,800
LUZ LIBRE
41,188
LONGITUD DE VIGA EN PLANTA